Magnetic Resonance Characterization of Hepatocellular Carcinoma in the Woodchuck Model of Chronic Viral Hepatitis

Eilean J. McKenzie

A Thesis submitted to the Faculty of Graduate Studies of

The University of Manitoba

In partial fulfilment of the requirements of the degree of

Doctor of Philosophy

Department of Medical Microbiology

University of Manitoba

Winnipeg, Manitoba Canada

Table of Contents

List of Abbreviations iv

Abstract vii

Acknowledgements ix

List of Figures and Illustrations x

1. Introduction 1

    1.1 Global Epidemic of Hepatitis B Infection 1

    1.2 Woodchuck Hepatitis Virus 3

    1.3 The Woodchucks as an Animal Model of Hepatocellular Carcinoma 7

    1.4 Development of Hepatocellular Carcinoma Due to Chronic Hepatitis 13

    1.5 Magnetic Resonance Imaging 16

    1.6 Magnetic Resonance Spectroscopy 23

    1.7 Choline and Cancer 46

    1.8 Current Clinical Diagnostic Criteria 47

    1.9 Statement of Objectives 49

2. Establishing the Method for Chronic Care and Repeated MR Imaging of Woodchucks 51

3. ^{31}P-MRS of uninfected and chronically infected woodchuck livers 90

4. *Ex vivo* analysis of uninfected and HCC tissue determines elevated PC confirms tumour growth using ^{31}P-NMR 109

5. Tumour growth continues despite positive immune response elicited by vaccinia-derived immunostimulant in the woodchuck model of hepatocellular carcinoma 120

6. Discussion 143

7. Future Directions 151

References 154

List of Abbreviations:

2D-CSI	TWO DIMENSIONAL CHEMICAL SHIFT IMAGING
AH	ACUTE HEPATITIS
ALT	ALANINE AMINOTRANSFERASE
AST	ASPARTATE AMINOTRANSFERASE
CCAC	CANADIAN COUCIL OF ANIMAL CARE
CH	CHRONIC HEPATITIS
CTL	CYTOTOXIC T LYMPHOCYTES
DNA	DEOXYRIBONUCLEIC ACID
ELISA	ENZYME LINKED IMMUNOSORBANT ASSAY
FID	FREE INDUCTION DECAY
FLASH	FAST LOW ANGLE SHOT
GEFI	GRADIENT ECHO FAST IMAGING
GGT	γ-GLUTAMYLTRANSFERASE
GPC	GLYCEROPHOSPHOCHOLINE
GPE	GLYCEROPHOSPHOETHANOLAMINE
HCC	HEPATOCELLULAR CARCINOMA
HCl	HYDROCHLORIC ACID
HSP	HEAT SHOCK PROTEIN
IFN-γ	INTERFERON GAMMA
IU/L	INTERNATIONAL UNITS / LITRE
KOH	POTASSIUM HYDROXIDE

MRI	MAGNETIC RESONANCE IMAGING
MRS	MAGNETIC RESONANCE SPECTROSCOPY
MVA	MODIFIED VACCINIA VIRUS ANKRA
NMR	NUCLEAR MAGNETIC RESONANCE
α-NTP	ALPHA NUCLEOTIDE TRIPHOSPHATE
β-NTP	BETA NUCLEOTIDE TRIPHOSPHATE
γ-NTP	GAMMA NUCLEOTIDE TRIPHOSPHATE
PC	PHOSPHOCHOLINE
PCA	PERCHLORIC ACID
PCR	POLYMERASE CHAIN REACTION
PDE	PHOSPHODIESTER
PE	PHOSPHOETHANOLAMINE
Pi	INORGANIC PHOSPHATE
PME	PHOSPHOMONOESTER
PPA	PHENYL PHOSPHATE
RF	RADIO FREQUENCY
RT-PCR	REAL TIME POLYMERASE CHAIN REACTION
RNA	RIBONUCLEIC ACID
SNR	SIGNAL TO NOISE RATIO
T_1	SPIN-LATTIC RELAXATION
T_2	SPIN-SPIN RELAXATION
TE	ECHO TIME
TNF-α	TISSUE NECROSIS FACTOR ALPHA

TotP	SUM TOTAL OF ALL PHOSPHORUS RESONANCES
TR	REPETITION TIME
WHcAg	WOODCHUCK HEPATITIS VIRUS CORE ANTIGEN
WHsAg	WOODCHUCK HEPATITIS VIRUS SURFACE ANTIGEN
WHV	WOODCHUCK HEPATITIS VIRUS

Abstract:

Woodchucks are the preferred animal model to study chronic viral hepatitis and the development of hepatocellular carcinoma (HCC), which occurs as a result of infection with woodchuck hepatitis virus (WHV). This project was divided into three main components: phase 1 – establishing the model and *in vivo* phosphorus spectroscopy study; phase 2 – *ex vivo* ^{31}P nuclear magnetic resonance analysis of tissues; phase 3– vaccinia trials. In Phase 1, tumour growth in the livers of chronically infected woodchucks (n=5) was followed using magnetic resonance imaging (MRI) and *in vivo* phosphorus spectroscopy (^{31}P-MRS) and compared to spectra obtained from the livers of uninfected woodchucks (n=5). It was determined that significant elevations in the phosphomonoester (PME) peak in the *in vivo* ^{31}P-MRS spectrum correlated to the presence of HCC. Serology indicated significant elevations in γ-glutamyl transaminase (GGT) and aspartate aminotransferase (AST) indicative of hepatocyte injury due to tumour growth. In Phase 2, perchloric acid extracts of frozen samples of HCC from infected woodchucks (n=9) were compared to noncancerous tissues from uninfected control woodchuck livers (n=5). Samples were prepared in triplicate from all woodchucks and analyzed with ^{31}P-NMR. The PME resonance detected *in vivo* is composed of resonances from two molecules: phosphocholine (PC) and phosphoethanolamine (PE). It was found that HCC tissue had significantly elevated concentrations of PC compared to uninfected control tissues, confirming that the elevation of PME is specific to the tumour's growth. Finally, in Phase 3, a recombinant vaccinia virus was constructed to express a fusion protein of hepatitis virus core antigen and *Mycobacterium tuberculosis* heat shock protein 70, stimulating the immune systems of infected woodchucks against

cells expressing core antigens. The immune stimulation should have delayed the onset of HCC because cells expressing core antigen would be destroyed via a Th1 mediated immune response. Despite reductions in surface antigen expression and viral load, elevations in serum GGT and the PME in ^{31}P-MRS indicated that there was tumour growth in treated woodchucks (n=3). Results were compared to the uninfected woodchucks from phase 1 (n=5). In conclusion, the PME peak represents a potential biomarker of cancerous growth when used in conjunction with serological tests to detect HCC in the liver due to chronic hepatitis virus infection.

c) Acknowledgements

I'd like to thank my amazing supervisor Dr. Marco Gruwel for his encouragement, suggestions, patience, and sense of humour throughout this project. I've learned so much from Marco and realized that even after all this, I still know less than a fraction of a percent of what he does! I'd like to thank Dr Coombs and Dr Hegmann their advice throughout this project. I'd also like to thank all the staff at the National Research Council – Institute for Biodiagnostics for their support, especially Allan Turner, Lori Gregorash, Lauralee Quinn, and the rest of Animal/Surgical Services, Jiankang Sun and Omkar Ijare for teaching me how to operate the 7T and the NMR and learning zen of shimming, Dr. Mike Jackson for initiating the project, and everyone in Biosystems for helping out when I needed it. I'd like to thank Dr. Jingxin Cao, Yvon Deschambault and the staff at the Canadian Science Centre for Human and Animal Health for performing the viral load assays, Dr. Thomas Michalak and Norma Churchill at Memorial University for performing the WHsAg and anti-WHc ELISAs, and Drs. N Pettigrew, K. Kaita, and Klein for reviewing the histological slides and answering my questions on liver cancer pathology, Dr. Goodridge and the staff at the Toronto Zoo for helping when my chucks were sick. Special thanks to Liane, Kathy, and Sasha for being great friends through all this, especially when I don't listen to their advice. Finally, the biggest thank you goes to my parents and Brendon for their love, unwavering belief in me, endless support in the tough times, and their optimism for my future.

List of Figures and Illustrations

Figure		Page
1	Larmor frequency and the relationship between ΔE and B_0	19
2A	Difference amount of energy required for two different atoms to change nuclear spin	26
2B	Two different nuclei appear as two peaks on an NMR spectra	26
3A	Molecular structure of phosphocholine	31
3B	Molecular structure of phosphoethanolamine	31
3C	Molecular structure of adenosine triphosphate	31
3D	Molecular structure of inorganic phosphate	31
3E	Molecular structure of glycerophosphocholine	31
3F	Molecular structure of glycerophosphoethanolamine	31
4	^{31}P-MRS of other liver disorders	36
5A	Representation of two dimensional chemical shifting imaging (2D-CSI)	39
5B	^{31}P-MR spectrum of liver tissue	39
5C	Metabolite map of PME	39
6	GEFI coronal section demonstrating triangular shape of liver	42
7	Phosphorus spectrum of gall bladder	44
8A	Photograph of group housing facility for up to five woodchucks	55
8B	Photograph of individual woodchucks	62
9	Photograph of woodchuck prepared for imaging	67
10A	Photomicrograph of HCC	67

10B	8x magnification of HCC	67
10C	20x magnification of early HCC	68
11A	Photomicrograph of control tissue	70
11B	8x magnification of control tissue	70
12A	Radiograph of tumour growth over time compared to control	73
12B	Coronal GEFI image of large HCC in infected woodchuck	74
12C	T_2-weighted axial image of woodchuck with HCC	75
13	Graph of the change of weight over time in infected and uninfected woodchucks	78
14	Graph of the change of viral load over time	81
15	Graph of the change of GGT over time	84
16	T_2-weighted axial image of the liver of a woodchuck with HCC	88
17	Sagittal FLASH image of a woodchuck	92
18	Axial FLASH image of a woodchuck liver	95
19	2D-CSI of a control and HCC woodchucks	98
20	Changes in PME over time	102
21	Difference in phosphorus-containing compounds between HCC and control	104
22	*Ex vivo* ^{31}P-NMR spectrum of control and HCC tissue	113
23	Difference in phosphorus-containing compounds between HCC and control	116
24	Changes in viral load over time after vaccinia treatment	126
25	Changes in WHsAg over time after vaccinia treatment	129

26	Changes in GGT over time after vaccinia treatment	132
27	Changes in PME over time after vaccinia treatment	135
28	Difference in phosphorus-containing compounds between HCC and control	137
29	Photo of an HCC at necropsy	140

Introduction

1.1 Global Epidemic of Hepatitis B Infection

Approximately 2 billion people world-wide have been exposed to human hepatitis B virus (HBV), resulting in 350 million people developing chronic HBV infection and causing 1.2 million deaths per year due to terminal liver diseases (World Health Organization2008). Chronically infected individuals are 100 times more likely to develop progressive liver diseases such as cirrhosis and terminal hepatocellular carcinoma (HCC) than uninfected people, with men more likely to develop HCC than women (Beasley *et al*., 1981; Chang *et al*., 1997b; El-Serag *et al*., 1999; Pisani *et al*., 1999). HCC is now the fourth most common cancer worldwide, causing an estimated 427,000 deaths in 1999 and 600,000 by 2008, most of which were in developing countries (Pisani *et al*., 1999; World Health Organization2008).

Transmission of the virus occurs from exposure to contaminated blood and body fluids including reusing tattoo and piercing needles, sharing syringes, razors, or toothbrushes, via contaminated blood transfusions, or through transmission between infected mothers to newborn (World Health Organization2008). Rates of HCC due to chronic HBV infection have been declining with the introduction of HBV vaccines Energix™, Twinrix™ and Recombivax™, and with screening of donated blood and blood products (Alter,1999; Chang *et al*., 1997a). For example, between 15-20% of the population of Taiwan are chronic carriers of HBV (3.4-4.5 million people) but after a universal vaccination program was instituted for all infants born after 1984, the incidence of chronic infection has decreased from 9.8% of children younger than 15years old, to

0.7% (Ni *et al*., 2001). Along with the decreased prevalence of HBV in the population, a concurrent decrease in the rate of childhood HCC has been seen, from 0.52 per 100,000 to 0.13 per 100,000 (Chang *et al*., 1997b; Ni *et al*., 2001). Regions where HBV is not endemic and a universal childhood vaccination program has not been implemented have seen increases in the rates of HCC diagnosis, but this may also be due to increased immigration from countries where HBV is endemic. In the United States, for example, where it is estimated that 1 – 1.25million people are chronically infected with HBV, three times more men than woman are diagnosed with HCC (El-Serag *et al*., 1999). Rates of HCC have increased from 4.0 per 100,000 to 6.1 per 100,000 among men of African descent, and from 1.7 per 100,000 to 2.8 per 100,000 in men of Caucasian descent, between 1976 and 1995 (El-Serag *et al*., 1999).

Current commercial HBV vaccines use the surface protein (HBsAg) as an immunological target to induce protective anti-HBs antibodies. However, between 5-10% of immunized people fail to develop protective antibodies, increasing their risk of developing a chronic infection (Lu *et al*., 1999). Chronic hepatitis B infection results from a failure of the host immune system to recognize and eliminate the virus, leading to immune tolerance or immune system fatigue (Menne *et al*., 2007). Characteristic features of a chronic infection include: persistent levels of infectious virus circulating in the blood and within hepatocytes, low levels of neutralizing antibodies to surface, core and envelope antigens, and low levels of HBV-specific cytotoxic T lymphocytes (CTLs). Even with current treatment strategies reducing the viral load to undetectable levels effectively, low levels of non-replicating virus remain dormant within a variety of non-liver tissues and can re-emerge during times of immunosuppression, such as during organ

transplant or co-infection with other viruses (Coffin *et al*., 2004; Michalak,1998; Michalak,2000). People with infections are at a higher risk of developing HCC later in life than either people who have resolved an acute infection or people who have never been exposed to the virus.

1.2 Woodchuck Hepatitis Virus

HBV is a member of the virus family *Orthohepadnaviridae* in the family Hepadnaviridae (Menne *et al*., 2007; Michalak,1998; Tennant,2001). The name of the viral family is derived from the viruses' hepatotropism (specificity for hepatocytes) and the DNA-based genome; therefore, Hepa-DNA-virus. Other members in this viral family, aside from HBV, include woodchuck (WHV), ground squirrel (*Spermophilus beecheyi*) (GSHV), arctic ground squirrel (*Spermophilus parryi*), duck (*Anas domesticus*), and grey heron (*Ardea cinerea*) hepatitis viruses (Buendia,1994; Tennant,2001). All of these viruses cause liver inflammation (hepatitis) but only mammalian hepatitis viruses cause chronic infection and HCC. Rates of HCC development in the ground squirrel are significantly lower than in humans or woodchucks, and take longer to develop than in woodchucks.

The infectious virion measures only 45nm or 42nm for WHV and HBV respectively, making Hepadnaviruses some of the smallest DNA viruses known (Menne *et al*., 2007; Michalak,1998; Tennant,2001). The genome of Hepadnaviruses is unique in that it contains both double- and single-stranded portions of DNA. The full-length negative-sense strand contains all of the genetic information necessary for viral functions. The complementary plus-sense strand is incomplete and is therefore shorter than than the

negative-sense strand (Buendia,1994; Michalak,1998; Zhang *et al*., 2006). The virus initiates the infection by binding to an unknown receptor on the surface of the hepatocyte (Menne *et al*., 2007). The genome and the polymerase enzyme are enclosed within a 27nm icosahedral nucleocapsid that is composed of core (WHcAg) proteins (Michalak,1998). After entry into the cell, the virus uncoats, and the genome travels to the nucleus where viral polymerase enzymes complete the missing portions of the plus-sense DNA strand (Menne *et al*., 2007; Michalak,1998). Once the genome is completed, the DNA can remain as a complementary closed circular DNA (cccDNA) in the cytoplasm as persistent episomes that can trigger re-infection during times of immunosuppression (Menne *et al*., 2007). WHV is unlike HBV in that WHV cccDNA is found in the cytoplasm of infected hepatocytes whereas HBV cccDNA is found in the nucleus (Menne *et al*., 2007). The cccDNA acts as a template from which RNA is transcribed (Ganem *et. al*., 2001).

During replication, host RNA polymerase II enzymes use the negative strand of cccDNA as a template to create plus-sense pregenomic RNA (Ganem *et. al*., 2001; Michalak,1998). Viral polymerase has a reverse transcriptase function that can synthesize single-stranded negative sense DNA from the pregenomic RNA templates, and an RNAase function to degrade the plus-sense RNA template (Menne *et al*., 2007; Michalak,1998). As the complementary plus-sense strand is being synthesized by viral polymerase, it and the polymerase enzyme associate with core particles. Core particles self-assemble and create the nucleocapsid, terminating further synthesis of the plus-sense DNA when the nucleocapsid encloses the genome, cutting off the supply of nucleotides (Michalak,1998). The nucleocapsid buds through the endoplasmic reticulum and Golgi

apparatus, where surface proteins (WHsAg) were translated and some underwent post-translational modifications (i.e. glycosylation) (Michalak,1998). The infectious viruses are released without cytopathic effects to the hepatocyte (Menne *et al*., 2007; Michalak,1998).

The genome encodes for seven proteins from four overlapping open reading frames: X, Core, Surface and Polymerase (Michalak,1998; Zhang *et al*., 2006). The S gene can be further subdivided into S, pre-S1 and pre-S2 regions that encode for three different sized proteins: small (S gene), medium (S + pre-S2 genes) and large (S + pre-S2 + pre-S1 genes). All surface proteins share a common C-terminal end but have different N-terminal regions. The surface proteins can be either glycosylated or not, resulting in potentially six different surface proteins with different weights depending on glycosylation (Michalak,1998). WHsAg can self-assemble into empty spherical or filamentous particles which can remain within the hepatocyte's cytoplasm or be released to circulate throughout the bloodstream during chronic infection (Michalak,1998). Empty particles that remain in the hepatocyte are typically composed of medium sized WHsAg, whereas circulating particles are composed of equal amounts of small and medium WHsAg (Michalak,1998). Particles that remain in the cytoplasm associate with other WHsAg particles in densely packed groups (Li *et al*., 2002). Because these particles do not contain any genetic material, they are not infectious. It is speculated that these 20-25nm circulating particles act as immunological decoys and induce immune system fatigue because the host's immune system is constantly exposed and mounts immune responses against these surface antigens (Michalak,1998). WHsAg particles are found in the plasma of exposed woodchucks within the first 6 weeks of an infection, followed by

WHcAg (Michalak,1998). A reduction in WHsAg and the appearance of anti-WHs and anti-WHc antibodies are indications of a recovery from an acute infection (Michalak,1998; Zhang *et al*., 2006). Persistent levels of WHsAg after 6 months indicate the development of chronic infection (Michalak,1998; Wang *et al*., 2003).

The core antigen (WHcAg) is encoded by the C gene and is a strongly immunogenic peptide that induces both B and T cell responses (Schodel *et al*., 1993; Zhang *et al*., 2006). Two core antigen polypeptides associate and create an α-helical dimmer. Two dimers self-assemble into spikes on the outer surface of the nucleocapsid (Billaud *et al*., 2005; Vejchapipat *et al*., 2002). The external loop region of these spikes form B-cell epitopes and the distance between two spikes is similar to the distance between two immunoglobulin receptors on B-cells, allowing for cross-linking as a T-cell independent antigen (Billaud *et al*., 2005; Vejchapipat *et al*., 2002). Activated B-cells act as primary antigen-presenting cells to stimulate a Th2 immune response (Billaud *et al*., 2005; Vejchapipat *et al*., 2002). Anti-WHc antibodies are non-neutralizing and do not limit the infection (Lu *et al*., 1999). WHcAg is highly immunogenic and immunizations with plasmids expressing selected dominant epitopes of WHcAg can protect woodchucks from a viral challenge (Billaud *et al*., 2005; Lu *et al*., 1999; Zhang *et al*., 2006). However, due to WHcAg's encapsulation beneath host-derived membrane, the epitopes of WHcAg are not typically visible to the woodchuck's immune system (Schodel *et al*., 1993; Zhang *et al*., 2006). Only an effective CD8+ cytotoxic T lymphocyte mediated response targeting WHcAg can limit the spread of the virus and prevent the development of a chronic infection by killing those hepatocytes that express WHcAg on the major histocompatibility complex (MHC-I) (Menne *et al*., 1997; Zhang *et al*., 2006).

Individuals that have recovered from an acute infection have a robust, multi-specific T-cell repertoire against WHcAg, unlike those with chronic infections that have a weak to non-existent T-cell response (Wang *et al*., 2003). Woodchucks that develop a chronic infection also have significantly lower expressions of interferon gamma (IFN-γ) and tumour necrosis factor alpha (TNF-α), cytokines released by a virally infected cell that act as a messenger for neighbouring cells, warning of the viral infection (Wang *et al*., 2003). This diminished response to the virus can be detected as early as 8-14 weeks post-infection and can be used to predict infection outcome (Wang *et al*., 2003).

WHcAg has 70% homology to human HBcAg (Zhang *et al*., 2006). Specific regions of WHcAg are cross-reactive to B cell epitopes of HBcAg and HBcAg has been used for immunostaining of woodchuck liver tissues, but HBcAg can not be used for other, more sensitive methods of detection (e.g. ELISA, EIA) of WHcAg (Billaud *et al*., 2005; Schodel *et al*., 1993; Zhang *et al*., 2006).

1.3 The Woodchuck as an Animal Model of HCC

Woodchucks (*Marmota monax*) are large burrowing rodents also known as chucks, whistle pigs and groundhogs (Bellezza *et. al*., 2002). Their geographical range covers southern Alaska, Canada, the Midwestern and Northeastern United States, extending as far south as Georgia, Okalahoma and Alabama (Bellezza *et. al*., 2002; Bezuidenhout *et.al*.,2005; Tennant,2001). Adult woodchucks are 40-65cm long and 28-40cm in girth (McKenzie *et al*., 2006). Body weight increases between 25-100% during spring/summer months, and decreases 15-50% during fall/winter months (1.4kg-2.5kg in the winter, and 2.2-4.2kg in the summer) (Bellezza *et. al*., 2002). The woodchuck's

weight varies with gender; males tending to weigh more than females (Bellezza *et. al*., 2002; McKenzie *et al*., 2006). In captivity, an uninfected woodchuck can live up to 10-14 years (Bellezza *et. al*., 2002). Due to predation, availability of food, and infection, the life expectancy in the wild is reduced usually to less than 7 years (Bellezza *et. al*., 2002). In the wild, woodchucks hibernate during the winter months where all body functions are reduced to minimal levels including heart rate and core body temperature. Food intake and waste excretion are nearly absent (Bellezza *et. al*., 2002; Tennant,2001). Woodchucks survive hibernation by metabolizing fat in the liver and around organs which was accumulated during the summer (Bellezza *et. al*., 2002). Woodchucks in an animal facility do not go into a full hibernation, in spite of maintaining constant levels of humidity, light, and temperature. The woodchuck's weight, body temperature, respiratory rate and food intake decrease significantly during winter months, but it is not the same as hibernation seen in the wild (Bellezza *et. al*., 2002; McKenzie *et al*., 2006).

The woodchuck has been the preferred animal model of chronic viral hepatitis since 1979 with the discovery that a significant number of captive woodchucks at the Penrose Research Centre in Philadelphia, PA developed HCC. (Bellezza *et. al*., 2002; Tennant,1999). Within the population at Penrose, 23% developed HCC and 15% had evidence of an active viral replication (Tennant,1999). These woodchucks had not been exposed to hepatotoxins such as aflatoxin B1 or carbon tetrachloride; rather, they had been infected with woodchuck hepatitis virus (WHV), a previously unknown DNA virus with significant homology to HBV (Buendia,1994; Michalak,1998). Epidemiological studies show that approximately 59% of wild-caught woodchucks in Pennsylvania, New Jersey and Maryland have serological evidence of exposure to WHV, while wild-caught

woodchucks in the Northeastern United States and Canada have rates of exposure less than 2% of the tested population (Tennant,2001). In the wild, exposure to WHV is due to vertical transmission from an infected dam to her pups, or through exposure to infected fluids between fighting adults (Buendia,1994; Coffin *et al*., 1999). In addition to immunological studies for both acute and chronic infection by Hepadnavirus, woodchucks have been used to test novel anti-viral drugs currently used in treatment of human viral infections including: 3-azido-3-deoxythymidine (AZT), acyclovir, 1-(2-fluoro-5-methyl-beta, L-arabinofuranosyl) uracil (Clevudine), (-)β-L-2,3-dideoxy-3-thiacytidine (lamivudine) and interferon-α (INF-α) (Korba *et al*., 2000; Menne *et al*., 2007; Peek *et al*., 2001; Tennant,1999), for novel gene therapy (Putzer *et al*., 2001), for imaging studies using ultrasound (Lisi *et al*., 2003; Nada *et al*., 1997), positron emission tomography (Salem *et al*., 2007), magnetic resonance imaging (MRI) and spectroscopy (MRS) (McKenzie *et al*., 2005; McKenzie *et al*., 2006; Ohtomo *et al*., 1991; Putzer *et al*., 2001; Tennant *et al*., 2004).

The pathogenesis of chronic infection in woodchucks has been studied extensively to better understand the mechanisms that determine infection outcome: acute, resolved or chronic infection. As with human exposure, the younger that an individual woodchuck is exposed to the virus, the more likely that a chronic infection will develop (Chang,2000; McMahon *et al*., 1985). Ninety-five percent of human children exposed at birth to infected mothers will develop asymptomatic chronic infections, while children who are exposed to HBV before five years old have a 30% chance of developing a chronic infection (Lee,1997; McMahon *et al*., 1985; World Health Organization2008). Between 3-5% of adults exposed to HBV will develop a chronic infection (Alter,1999;

Chang,2000; Lee,1997; McMahon *et al*., 1985; Tassopoulos *et al*., 1987). Lab-adapted strains of WHV such as WHV7P1 used by Cornell University have greater rates of chronic infection than wild strains due to greater genetic homology within the breeding population, greater control of the timing and the concentration of viral inoculation, and lab selection of viral strains with the most predictable results (Bruni *et al*., 2006; Buendia,1994; Menne *et al*., 2007). WHV7P1 produces chronic hepatitis in 60-75% of woodchucks if they are inoculated within 7-10 days after birth, less than 10% become chronically infected if inoculated within two months after birth, and less than 5% as adults (Menne *et al*., 2007; Tennant,1999). This infection rate in woodchucks is significantly lower than in humans, where 90% of infants exposed to HBV at birth will develop chronic hepatitis.

Neonatal woodchucks inoculated with $5x10^6$ WID_{50} of WHV7P1 three days after birth have been used to create a predictable model of infection (Cote *et al*., 2000; Wang *et al*., 2003; Wang *et al*., 2004). Serial blood samples and liver biopsies were taken at regular intervals for the first 15 months and the woodchucks were followed to determine significant differences that would correlate to the development of an acute resolving infection or chronic infection that leads to HCC. At 8 weeks post-infection, the "early acute phase" of the infection, all woodchucks have detectable levels of WHV mRNA in their livers, equal viral loads (serum concentrations of WHV DNA), and histology has shown little evidence of inflammation or necrosis. Histology did demonstrate elevated concentration of lymphocytes and some bile duct proliferation (Cote *et al*., 2000). Expression of mRNA of FasL and perforin, mediators of apoptosis and necrosis, were the same as in uninfected woodchucks (Wang *et al*., 2004). At two months post-exposure,

there was little difference between the immune responses of woodchucks that developed chronic infection and woodchucks that resolved their infections (Cote *et al*., 2000; Wang *et al*., 2004).

By ten weeks post-exposure, woodchucks that would eventually develop chronic infection (CH) had 4.3 times higher serum concentration of WHV DNA and a 6 times greater serum concentration of WHsAg than did woodchucks that would resolve their infection (AH) (Wang *et al*., 2004). Significant elevations in serum aspartate aminotransferase (AST), alanine aminotransferase (ALT) and sorbitol dehydrogenase, liver enzymes that are indicators of liver injury, as well as FasL and perforin mRNA, indicators of apoptosis due to a Th1 response, were found in AH but not CH. This confirms that in woodchucks with AH, the immune system is stimulated more effectively and there is greater immune-mediated killing of infected hepatocytes than in the CH woodchucks (Wang *et al*., 2004).

By 12 weeks post-infection, AH woodchucks have reached their peak viremia, with the maximum viral load they will experience (Wang *et al*., 2004). The outcome of an infection, whether the woodchuck will develop chronic or acute infection, can be accurately predicted based on serum analysis at week 14 (Cote *et al*., 2000; Wang *et al*., 2003; Wang *et al*., 2004). At week 14, the "incubation phase" of the infection, WHV DNA in AH woodchucks has begun to decline while it is still increasing in CH woodchucks. This increase in viral load is due to CH woodchucks having a defective Th1, or cytotoxic T cell-mediated immune response to the virus (Wang *et al*., 2003; Wang *et al*., 2004). AH woodchucks have higher concentrations of CD8+, IFN-γ and

TNF-α, all mediators of Th1 immune response, as well as significantly higher concentrations of CD4+ and IL-10, mediators of Th2 or antibody mediated immune response (Wang *et al*., 2003). The higher concentrations of IFN-γ and TNF-α correlate to a reduction in WHV cccDNA within the hepatocytes, however the reduction in WHV cccDNA may also be due to an increased hepatocyte turn-over and not exclusively due to IFN-γ or TNF-α directly inhibiting viral replication (Wang *et al*., 2003). AH woodchucks have peaked their serum concentrations of ALT, AST and sorbitol dehydrogenase, demonstrating that there is a two week delay between the immune response (evidenced by a decrease in viral load) and liver injury (evidenced by increased liver enzymes) (Wang *et al*., 2003; Wang *et al*., 2004). At 14 weeks post-infection, 50-85% of infected hepatocytes have been eliminated and replaced with healthy uninfected cells (Wang *et al*., 2003). From 14 weeks onward, AH woodchucks have undetectable serum concentrations of WHsAg and liver enzymes similar to uninfected woodchucks of the same age (Cote *et al*., 2000; Wang *et al*., 2004). AH woodchucks have developed anti-WHc antibodies and by week 14, have begun to develop anti-WHs antibodies which protects from future infections (Lu *et al*., 1999; Wang *et al*., 2004). In CH woodchucks, IFN-γ and TNF-α are three times greater than in age-matched uninfected woodchucks, but are still significantly lower than AH woodchucks at the same time point (Wang *et al*., 2003). Histological examination of tissue obtained from CH woodchucks indicates bile duct proliferation, regions of necrosis and degenerating hepatocytes, and lower levels of inflammation than in AH (Cote *et al*., 2000). Human tissue would be scored as having "moderate hepatitis" if it were examined at this point in the infection (Cote *et al*., 2000).

At fifteen months post-infection, CH woodchucks have significant concentrations of WHV DNA and WHsAg in the blood and liver tissue (Wang *et al*., 2003). They continue to have mild and persistent inflammation in the liver, detectable by slight elevations in ALT and sorbitol dehydrogenase (Wang *et al*., 2003). IFN-γ and TNF-α are not significantly different than in uninfected woodchucks (Wang *et al*., 2003). The infection will persist in chronically infected woodchucks until their eventual death at approximately 2.5-3 years post-infection due to irreversible liver damage and HCC. Woodchucks that are chronically infected with WHV have nearly a 100% chance of developing HCC within 29-56 months post-infection (Buendia,1994; Menne *et al*., 2007; Tennant,1999). Infected woodchucks that have an acute infection and develop both protective neutralizing antibodies and specific T lymphocytes have an 80% survival rate greater than 60 months (Tennant,1999).

A chronic infection is due primarily to a deficient Th1 response to the virus (Wang *et al*., 2003). An appropriate immune response should have created multi-specific Th1 cytotoxic T-lymphocytes towards many different viral antigens, especially against WHc, as well as stimulated a Th2 immune response that would have created neutralizing antibodies. Anti-WHc antibodies develop early in AH, well before the protective neutralizing anti-WHs antibodies do (Lu *et al*., 1999). Although CH woodchucks do develop some antibody response to WHV, they are non-neutralizing and do not stop viral replication and proliferation.

1.4 Development of Hepatocellular Carcinoma Due To Chronic Hepatitis

HCC development is a multi-step process requiring many years of persistent infection. The severity of the disease and the development of HCC also depends on the strain of HBV that an individual is infected with (Liu *et al*., 2005). Rates of HCC are higher in countries where HBV is endemic and the number of individuals with chronic hepatitis is significantly higher (Chang *et al*., 1997b; Ni *et al*., 2001; Pisani *et al*., 1999). Of the eight strains of HBV, named genotypes A-H, adults chronically infected with HBV genotype C (typically found in Taiwan and parts of Asia) are more likely to develop cirrhosis and HCC compared to adults infected with genotype B. In Europe and North America, those infected with genotype A typically develop chronic hepatitis while those exposed to genotype D have acute hepatitis, although the opposite is true in India (Liu *et al*., 2005). The relative risk of developing HCC with chronic infection is 100 times greater than without infection (Beasley *et al*., 1981; Hann *et al*., 2004; Tennant,2001).

Unlike human HCC, woodchuck HCC is not metastatic and not associated with cirrhosis (Bruni *et al*., 2006; Buendia,1994). In humans, HCC develops more in males than in females, whereas in woodchucks, there is no sex preference (El-Serag *et al*., 1999; Michalak,1998; Pisani *et al*., 1999). Similar to human HCC, non-tumour tissue has higher levels of viral protein expression than do hepatocytes found within HCC (Jacob *et al*., 2004; Michalak,1998; Wong *et al*., 2006). Using immunohistological staining for WHsAg, surrounding parenchyma has a greater stain density for the WHsAg than does the tumour (Li *et al*., 2002; Michalak,1998; Radaeva *et al*., 2000). The tumours that develop in woodchucks are well differentiated from surrounding liver parenchyma by fibrotic connective tissue (Buendia,1994; Michalak,1998; Tennant,2001). The tumours

can range in size from 1-10 cm and begin to develop from foci of a few altered hepatocytes after the first year of active hepatitis (Bellezza *et. al*., 2002; Buendia,1994; Michalak,1998). Within the tumour are regions of necrosis, low levels of WHV protein expression, inflammation, and bile duct proliferation (Buendia,1994; Michalak,1998; Tennant,2001).

The mechanism of carcinogenesis is unknown as WHV does not contain any known oncogenes, nor is integration into the host genome required for the viral replication (Buendia,1994; Michalak,1998; Tennant,2001). Integration has been shown to occur; however, it is usually truncated and involves rearranging sections of WHV genes, rather than the complete genome (Buendia,1994; Menne *et al*., 2007; Tennant,2001). If integration does occur, it is normally at multiple random sites within the host genome rather than at particular "hot spots" of integration (Jacob *et al*., 2004; Tennant,2001). It is speculated that carcinogenesis may result from integration of a viral genomic section that upregulate the expression of the hepatocyte's regulatory genes, especially in the *c-myc* and *N-myc2* genes of woodchucks (Bruni *et al*., 2006; Jacob *et al*., 2004; Radaeva *et al*., 2000). Integration of WHV upstream of the *N-myc2* genes and rearrangements of *N-myc2* genes have been documented in some HCC of lab-raised woodchucks, however the integration and activation of these genes are lower in wild-caught woodchucks (Buendia,1994; Jacob *et al*., 2004; Bruni *et al*., 2006). This difference may be due to the specific strain of virus used or the similar host genetics of lab-raised woodchucks (Bruni *et al*., 2006). Increased expression of *c-myc* is only found in 10% of HCC whereas upregulation of *N-myc2* genes can be found in more than 60% of HCC in woodchucks (Tennant,2001). *N-myc2* is typically expressed in woodchuck brains, not in the liver, and

is not found in humans (Buendia,1994; Jacob *et al*., 2004). Transgenic mice carrying *N-myc2* genes with WHV transcriptional regulators spontaneously develop HCC, indicating that the increased gene expression may play a role in carcinogenesis (Jacob *et al*., 2004; Tennant,2001).

Mutations within the *p53* "anti-cancer" gene can occur and inhibit the apoptotic pathway of hepatocytes with chromosomal abnormalities that would normally trigger a cell's suicide (Fabregat *et al*., 2007). These genetically unstable hepatocytes continue to survive and proliferate because they are either resistant to pro-apoptotic signalling pathways or downregulate the expression of this pathway (Fabregat *et al*., 2007). The X protein encoded by the hepatitis virus is known to associate with p53 proteins to reduce their function. Additionally, alterations to the rate of cell cycle, increasing telomere length, and increased hepatocyte turn-over to replace infected hepatocytes destroyed by CTLs increases the probability of spontaneous mutations in progeny daughter cells (Tennant,2001). The severity of liver disease due to chronic infection is also determined by the extent of inflammation due to host response to the disease. A more aggressive immune response to the virus correlates to greater liver damage and increases the potential for tumourgenesis.

1.5 Magnetic Resonance Imaging

Magnetic resonance is a technique that utilizes the magnetic properties of atoms when exposed to an external magnetic field. Atoms with an even number of protons and neutrons have no net spin so can not be studied using MR. Atoms with an odd number of proton and an even number of neutrons (^{1}H, ^{15}N, and ^{31}P), or an even number of proton

and an odd number of neutrons (^{3}He, ^{17}O), or both an odd number of protons and odd number of neutrons (^{2}H, ^{14}N) have a non-zero net spin and are MR susceptible. The most commonly used atom for magnetic resonance is hydrogen due to its high natural abundance and its relatively short relaxation time. Carbon (^{13}C), fluorine (^{19}F), and phosphorus (^{31}P) are also useful for magnetic resonance spectroscopy (MRS) of biological materials. Other odd-numbered atoms (Na, Rb) can be used; however their low natural abundance limits their usefulness for biological studies (Chakeres *et.al*.,1992; Chavhan,2007).

Magnetic resonance can be performed using any magnetic field. The Earth's magnetic field is approximately 0.3-0.7Gauss; a small fridge magnet is approximately 100G (Schild,1990). A permanent magnet has a magnet field strength of 0.3Tesla or 3,000G, while a superconducting magnet cooled with liquid helium and nitrogen can have field strengths between 1T (10,000G) to 12T (120,000G) (McRobbie *et.al*.,2003; Schild,1990).

The nucleus can have a magnetic moment with angular momentum, called its nuclear spin, which can interact with an external magnetic field and cause the spinning nucleus to precess about the direction of the external magnetic field. The rate at which the nucleus of an atom precesses (spins) within an applied external magnetic field is called its Larmor frequency, and is measured in Hertz (Hz). The Larmor frequency is unique to each element and changes depending on the field strength (B_0) of the applied magnetic field the nucleus is placed in. The Larmor frequency can be calculated by:

Equation 1. $\nu = \gamma B_0$

Where ν is the Larmor frequency, γ is the gyromagnetic ratio of the atom, and B_0 is the strength of the magnet.

Nuclei with spin (I) equal to ½, such as ^{1}H and ^{31}P, can occupy one of two discrete energy states when placed in an external magnetic field; they can orient themself in parallel (I=+1/2) to or anti-parallel (I=-1/2) to the applied magnetic field (B_0) usually labelled the z-axis. Nuclei that are in parallel to z are in low-energy state, whereas nuclei anti-parallel to z are in the high-energy state. At thermal equilibrium, more nuclei are found in the lower energy state versus the higher energy state based on Boltzmann's distribution; therefore the net magnetization is positive and parallel to the z-axis (Chavhan,2007). This is the sample's net longitudinal magnetization (Chakeres *et.al*.,1992; Chavhan,2007). To excite a nucleus from the low-energy state to the high-energy state, the nucleus must absorb a photon of energy equal to the difference between the low- and high-energy levels.

Equation 2. $\Delta E = h \nu$

Where ΔE is the energy difference between the two states, h is Planck's constant (6.626×10^{-34} Js), and ν is the Larmor frequency described in equation 1.

Equation 2 can be combined with Equation 1 and rewritten as:

Equation 3. $\Delta E = h \gamma B_0$

Therefore in a stronger magnetic field, more energy is required to re-orient a nucleus from a low-energy state to a high-energy state (Figure 1).

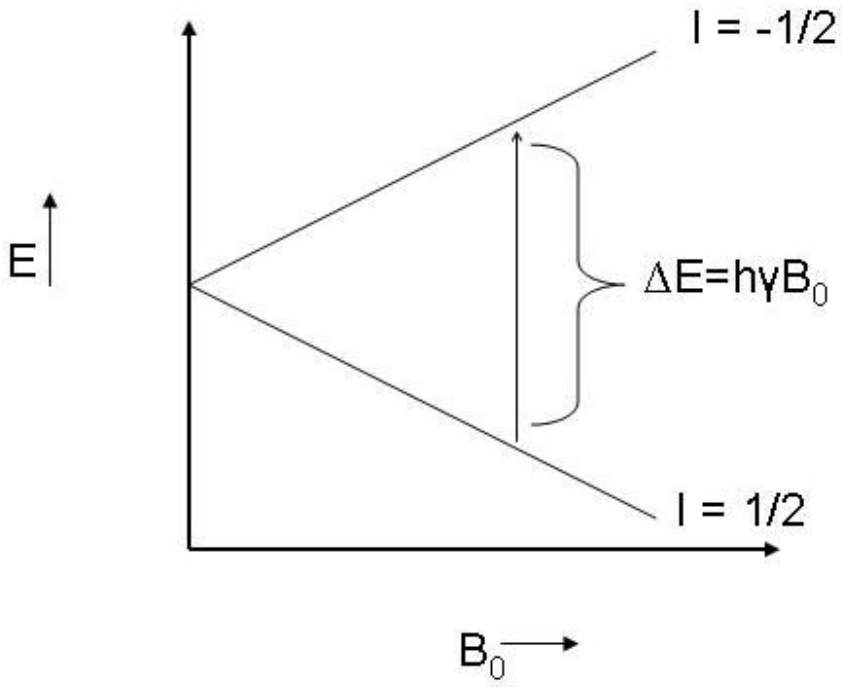
I = -1/2
E
ΔE=hγB0
I = 1/2
B0

Figure 1. This diagram shows that the amount of energy required to change a nucleus' spin from parallel (low energy) to anti-parallel (high energy) to the z-axis is directly proportional to the strength of the applied magnetic field (B_0). (Chakeres *et.al.*,1992)

During magnetic resonance experiments, energy from a radio frequency (RF) pulse is absorbed and re-orients the net magnetization into the x,y plane. The longitudinal magnetization is reduced while transverse magnetization increases. After the RF pulse, the net magnetization recovers or "relaxes" back to equilibrium via two different relaxation mechanisms. The first method is Spin-Lattice relaxation, which is the amount of time for net magnetization to return to being in parallel to the external field by releasing energy into the surroundings, the sample's lattice (Chakeres *et.al.*,1992; Chavhan,2007; Schild,1990). Spin-Lattice relaxation is an exponential process. The time required for 63% of the longitudinal magnetization to return to its original value is a sample's characteristic T_1 constant (Chakeres *et.al.*,1992; Chavhan,2007; McRobbie *et.al.*,2003; Schild,1990). Large molecules whose motion is restricted have a short T_1 while small, highly mobile molecules have a long T_1.

During the RF pulse, all spins have phase coherence; all nuclei are precessing together. Spin-Spin relaxation is the exponential rate of decay at which transverse magnetization loses phase coherence after the RF pulse (Chakeres *et.al.*,1992; Chavhan,2007; McRobbie *et.al.*,2003). Spin-Spin relaxation depends on inhomogeneities in the local and external magnetic fields. It's time constant, T_2, is the time required for the transverse magnetization to reduce to 37% of its original value (Chakeres *et.al.*,1992; Chavhan,2007; McRobbie *et.al.*,2003). Small, highly mobile molecules move quickly and changes to local magnetic fields cancel each other out. Consequently, these molecules have a long T_2. Large molecules move much slower and lose phase coherence quickly, thus they have a short T_2 (Schild,1990). T_1 and T_2 are independent processes of

each other; usually T_2 is shorter than T_1 (Schild,1990). These two rates of relaxation are the main source of contrast for MR imaging (Schild,1990).

Magnetic resonance images are created with an RF pulse, usually 90° or less, tipping the nuclei into the x,y plane, and acquiring the signal after a given time (τ). T_1-weighted images are created by preventing complete T_1 relaxation between RF pulses. Signals from molecules with a short T_1 are enhanced (brighter) compared to molecules with long T_1's. Therefore, fat appears bright because fat has a shorter T_1, while fluids (synovial, cerebral spinal) appear dark because they have a longer T_1 (Chakeres *et.al*.,1992; Chavhan,2007; McRobbie *et.al*.,2003).

T_2-weighted images are typically created by applying spin-echo sequence. An initial 90° RF pulse establishes transverse magnetization. The nuclei lose phase coherence after the RF pulse is stopped, reducing net transverse magnetization. After a given time (τ), a second RF (180°) pulse is applied to re-focus transverse magnetization and an echo occurs without any degradation due to field inhomogeneity (Schild,1990). The shorter the echo time (TE), the stronger the signal strength will be thereby improving image quality by increasing the signal to noise ratio (SNR). A long TE usually creates better contrast between two tissue types; however the signal strength will be small so the image quality will suffer. Changing the TE changes the amount of T_2-weighting and can be adjusted to get the best contrast between two tissues. Large molecules like fat lose phase coherence quickly because of its short T_2. Water molecules appear bright because of the long T_2 value(Chakeres *et.al*.,1992; Chavhan,2007; McRobbie *et.al*.,2003). Therefore, fat appears dark in T_2-weighted images while fluids appear bright (Schild,1990).

To improve image quality, repeating spin echo sequences and averaging the results can help. The time between spin echo sequences is the repetition time (TR). Faster imaging means that more images can be acquired, averaged, and better images created (higher SNR) thereby improving the diagnostic capability of MRI. All of the transverse magnetization must be relaxed before another 90° pulse can be applied. If a 90° pulse is applied while there is still transverse magnetization, the sample will contain a combination of longitudinal and transverse magnetization, giving rise to a combination of echoes and free induction decays and causing artifacts. Typically, TR should be three times the T_1 of the sample in order to observe complete T_1 relaxation. To dephase the spins faster and therefore shorten the TR, gradient fields can be applied that create larger field inhomogeneities within a sample (Chakeres *et.al.*,1992; McRobbie *et.al.*,2003; Schild,1990). Rather than using a 90° pulse, smaller flip angles between 10° and 35° can be used to speed up signal acquisition. The smaller flip angle allows TR to be reduced, further reducing the duration of the experiment. Flip angle and TR are usually determined experimentally. Gradient echo images (e.g. GEFI, FLASH) experiments are faster, but usually have lower SNR. However, gradient echo images can be acquired quickly and can be used as "scout" images, or images that can give information about the position of the sample without being as diagnostically useful as T_1-weighted or T_2-weighted images(Chakeres *et.al.*,1992; McRobbie *et.al.*,2003).

1.6 Magnetic resonance spectroscopy

While magnetic resonance imaging looks at the distribution of water molecules in a tissue, magnetic resonance spectroscopy (MRS) looks at the biochemistry of the tissues

using the same principles as MRI to create an image. MRS simultaneously characterizes all of the molecules and their relative proportions within a sample (Cox *et al*., 2006; Khan *et al*., 2005). Like MRI, MRS can be performed on any nucleus with spin I= ½, like ^{1}H, ^{31}P, ^{14}N, ^{19}F and ^{13}C; however, to study biological processes, hydrogen and phosphorus are most widely used due to their presence in most biological tissues and metabolic pathways. As with MRI, a sample is positioned within an applied external magnetic field. The homogeneity of the MR field is improved by dynamic shimming on the sample (Chakeres *et.al*.,1992; Macomber,1988). By making slight adjustments to the primary (x,y,z), secondary, and higher order shims (x^2-y^2, z^2, z^3, etc.) the field homogeneity is improved, thereby improving the spectral resolution (resonance line width is narrowed) and the precision of the data acquired because slight distortions in the magnetic field are corrected for (Chakeres *et.al*.,1992; Macomber,1988). Shimming is typically performed on the nucleus with the highest signal strength. For ^{31}P-MRS (*in vivo*), shimming was performed on the proton signal since protons are more abundant than phosphorus nuclei. The larger proton signal was used to improve the homogeneity of the MR field. For ^{31}P-NMR (*ex vivo*), shimming was performed on an internal reference of deuterium oxide (D_2O) and water in a capillary tube. D_2O was used as a reference for signal locking to ensure that minor drifting in the magnetic field is corrected for during data acquisition.

Similar to the MRI, an RF pulse excites the net magnetization of the sample in the external magnetic field. The coil detects changes in the voltage of the sample over time as T_2 relaxation occurs. The result is an oscillating wave that decays over time; called the Free Induction Decay (FID). To convert this data from the time domain to the frequency

domain, the FID is processed using Fourier Transformation (Cox *et al*., 2006; Khan *et al*., 2005; Macomber,1988). The position of a signal in the NMR spectrum relative to a known standard is referred to as its chemical shift. A nucleus' chemical shift is unique to each molecule because chemical shift depends on the local magnetic field experienced by the nucleus as a result of the atoms that compose the molecule, what other molecules are present in the sample, coupling between two MR sensitive molecules (e.g. ^{1}H and ^{31}P), shielding, the type of bonds, pH, temperature, and the state of the molecules (dissolved in a solution versus solid) (Cox *et al*., 2006; Khan *et al*., 2005; Macomber,1988). Two different nuclei experience two different local magnetic fields, and therefore appear as two distinct peaks in the spectrum . If identical samples were analyzed on two magnets of significantly different field strengths, the spectrum acquired on the more powerful magnet would have better resolution than spectrum from a weaker magnet (Figure 2). Chemical shifts are reported as either Hertz (Hz) or parts per million (ppm). The latter is a relative scale that allows results to be compared between two magnets of different field strengths. This allows for standardization of results between different MR systems.

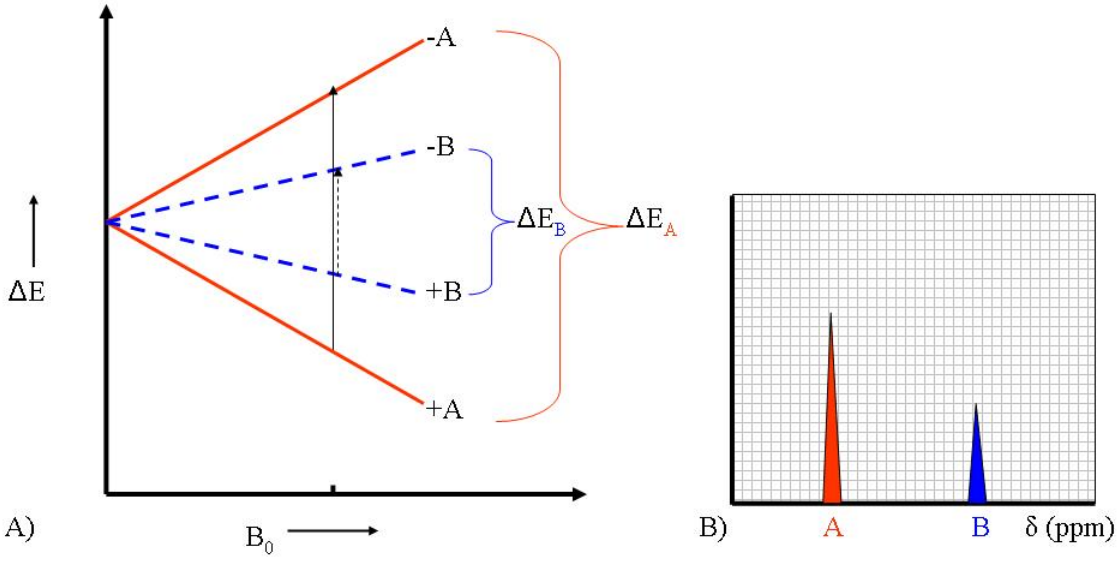
-A
-B
+B
+A
ΔE
ΔE_B
ΔE_A
A)
B_0
B)
A
B
δ (ppm)

Figure 2A) Two nuclei (A and B) in the same external magnetic field (B_0) require different amounts of energy (ΔE_A and ΔE_B) to transition from low-energy (+) to high-energy (-) states. The amount of energy required to transition is proportional to the field strength (B_0); more energy at higher frequency is required at higher field strengths. Consequently, the two nuclei appear as two distinct peaks on the NMR spectrum (Figure 2B). The integral of the peak is proportional to the concentration of the nuclei contributing to the peak. Typically, the chemical shift and the relative concentrations of each nuclei is calculated with respect to a known reference.

Resolution measures how clearly two peaks from different molecules are individually detected. Resolution is proportional to the magnetic field strength; at a lower field strength, two peaks can appear close enough together that one peak resembles a "shoulder" on a larger peak, whereas at higher field strengths, the two peaks are clearly differentiated (Figure 2). Resolution is also inversely proportional to the acquisition time (Macomber,1988). The longer the acquisition time, the greater the resolution, however it also means the longer the experiment. Using shorter acquisition times and averaging repeated measurements can improve resolution without causing significantly longer experiments (Macomber,1988). For *in vivo* experiments, improvements in the resolution of the data requires longer anaesthesia time for the woodchucks. However, the longer that the woodchuck is anaesthetized, the greater the risk that the woodchuck may not recover from the anaesthesia and may die in the MR system. *In vivo* experiments are a compromise between spectral resolution and acquisition time. With a shorter acquisition time and fewer repeats, the resolution of the data is poorer, thus making it harder to differentiate between peaks and detect differences between signals. The voxel size and number of repeats was chosen as a necessary balance between the quality of information contained within the phosphorus spectrum and the ability of the woodchuck to recover without incident to be imaged again the following month.

Signal intensity is proportional to the number of nuclei providing that signal (Macomber,1988). To calculate the proportion of a particular molecule within the sample, the area under the peak was integrated. If an external reference with a known concentration of a compound is included within the sample, the relative concentrations of molecules can be calculated with respect to the standard. An external reference should

have a similar concentration to the sample being measured for more accurate measurements of the integrals of the peak heights. As well, the external reference should have a resonance that is far enough up or down field from the sample's resonances that the reference's resonance does not interfere with the sample. If an external reference can not be included with the sample, as with *in vivo* spectroscopy, ratios of peak integrals within the spectrum are used to determine relative amounts and differences are reported. Ratios can also be used to look at patterns within the tissue. For example, phosphomonoester (PME) is a marker of cell membrane proliferation while phosphodiester (PDE) is a marker of cellular necrosis (Cox *et al*., 1992a; Thomas *et al*., 1994). The ratio of PME/PDE therefore is a measure of cellular turnover and can be used to compare cellular behaviour in cancerous versus non-cancerous tissues (Cox *et al*., 1992a; Thomas *et al*., 1994), cirrhosis (Lim *et al*., 2003; Menon *et al*., 1995), and alcoholic and diffuse liver disorders (Lim *et al*., 2007; Schlemmer *et al*., 2005). Ratios of PME to the sum of the total phosphate signal (TotP) have been used to monitor liver transplant (Chu *et al*., 2005), detect hepatocellular carcinoma, while the ratio of PME to ATP measures the rate of cellular proliferation as a function of tissue energetics (Kiyono *et al*., 1998; McKenzie *et al*., 2005; Meyerhoff *et al*., 1992; Taylor-Robinson *et al*., 1998).

The advantage of phosphorus spectroscopy is that the spectrum is significantly less complicated than proton spectroscopy because it only describes those molecules that contain phosphorus. Protons are abundant within the body, whereas phosphorylated molecules are not. Typical biomolecules found in a phosphorus spectrum of liver tissue include phosphocholine (PC), phosphoethanolamine (PE), inorganic phosphate (Pi),

glycerophosphocholine (GPC), glycerophosphoethanolamine (GPE), and three peaks of nucleotide triphosphate (NTP) that represent the α-, β- and γ- phosphates (Figure 3 A-F).

A)

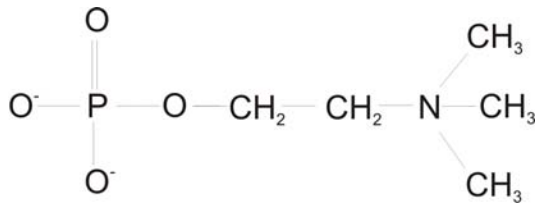

B)

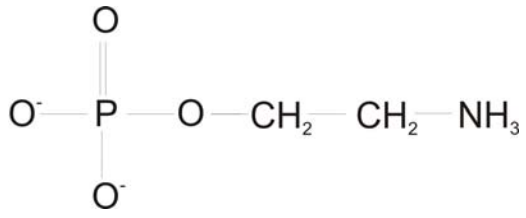

C)

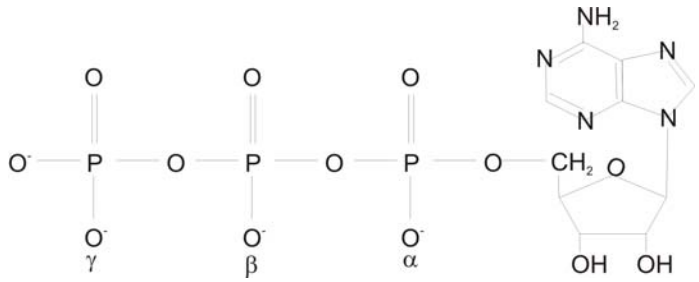

D)

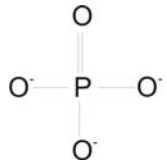

E)

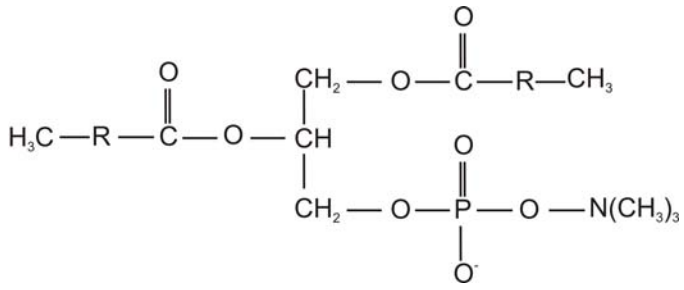

F)

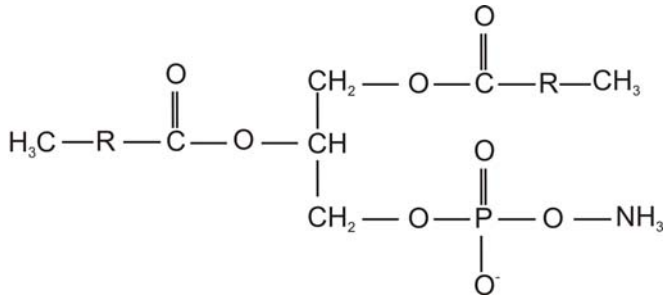

Figure 3A) Molecular structure of phosphocholine (PC). ^{31}P-NMR and MRS detect the phosphorus nuclei at the α-position on the molecule at 7.5ppm.

Figure 3B) Molecular structure of phosphoethanolamine (PE). Similar to PC, the phosphorus molecule on the α-position of the molecule is detected, but due to the ammonium group at the Ω position, the chemical shift of PE is upfield of PC at 8.0pp,.

Figure 3C) Molecular structure of ATP, one of three nucleotide triphosphate molecules used in cells as a high energy source. Hydrolysis of the γ phosphate releases inorganic phosphate (Pi, Figure 3D), generating nucleotide diphosphate. Further hydrolysis of the β-NTP released a second inorganic phosphate molecule and generates nucleotide monophosphate. α-, β- and γ-phosphates of NTP appear as distinct peaks in the phosphorus spectrum at -7.5ppm, -16ppm, -1ppm respectively

Figure 3D) Molecular structure of Pi. Once source of Pi is due to the hydrolysis of NTP as energy for cellular replication. Its chemical shift is at 5ppm.

Figure 3E) Molecular structure of GPC, a by-product of cellular degradation. Resonances from GPC are found at 2ppm.

Figure 3F) Molecular structure of GPE, also a result of cellular degradation but due to the ammonium group, GPE appears as a different resonance than GPC at 2ppm.

Spectra from tissues other than the liver would also include phosphocreatine (PCr) however this molecule is not present in the liver because it lacks creatine kinases. PC and PE contribute to the phosphomonoester (PME) resonance detected *in vivo* while GPC and GPE contribute to the phosphodiester (PDE) peak. Due to motion artifacts from breathing and the large sample size of the woodchuck, the resolution of the *in vivo* spectra is not high enough to differentiate the signals of PC from PE, and GPC from GPE. PME, therefore, appears as a broad peak from 7.5-8.0 ppm. PDE appears as a broad peak from 2.5-4.0 ppm. *Ex vivo* ^{31}P-NMR analysis can differentiate between PC and PE, and GPE from GPC. The total phosphorus resonance (TotP) is calculated as the sum of the resonances of PME, Pi, PDE, α-, β-, and γ-NTP. To detect the differences between normal and cancerous tissues, the ratio of each phosphorus-containing molecule was calculated relative to the total phosphorus resonance (PME/TotP, Pi/TotP etc.). Other molecules can be detected using ^{31}P-spectroscopy, like NADPH and diphosphodiesters, however they are typically in such low concentrations and are found on the spectrum at resonances already represented by other molecules at higher concentrations. Subsequently, these molecules contribute only slightly to a particular resonance and cannot easily be differentiated from the other more abundant phosphorus-containing molecules. For example, diphosphodiesters are found at –7.75 ppm while α-NTP is found at –7.5 ppm. Diphosphodiesters would appear as a shoulder in the α-NTP peak in a phosphorus spectrum *in vivo*. Diphosphodiesters and α-NTP signals can be differentiated if the spectrum is acquired in a high field magnet with smaller sample volume and good shimming. The PME resonance also contains contributions from α-glycerophosphate and

adenosine monophosphate, but these can only be detected *ex vivo* with high resolution systems and their contributions are negligible compared to PC and PE.

^{31}P-MRS has been used to study humans with a variety of different liver disorders to better characterize biochemical changes in the liver for each of the diseases. Of particular interest is hepatitis, or inflammation of the liver, and cirrhosis, the development of fibrous scar tissue, which eventually leads to liver failure. Healthy livers and livers with active hepatitis and cirrhosis, show distinct spectroscopic patterns that can be used to differentiate diseased livers from healthy (Figure 4). Primary biliary cirrhosis typically have significantly elevated PME/NTP, Pi/NTP and PME/PDE ratios and significantly lower PDE/NTP ratios compared to healthy livers (Menon *et al*., 1995; Schiller *et al*., 2002; Taylor-Robinson *et al*., 1997). Chronic active hepatitis and alcohol induced cirrhosis have PME/ATP and Pi/ATP ratios the same as healthy liver tissue (Cox *et al*., 1992b; Menon *et al*., 1995). Secondary metastatic tumours such as colonic adenocarcinomas have elevated PME/ATP and PME/PDE ratios, but normal PDE/ATP and Pi/ATP ratios (Bell *et al*., 1993; Cox *et al*., 1992b).

A unique feature of the liver is its ability to regenerate after a portion of tissue has been removed, such as during a partial hepatectomy. ^{31}P-MRS of regenerating liver has shown that immediately following the removal of up to 70% of a rat's liver, there is an immediate decrease in the NTP and PDE resonance and a concurrent increase in the Pi and PME (Campbell *et al*., 1990; Corbin *et al*., 2002; Farghali *et al*., 1994; Kooby *et al*., 2000; Mann *et al*., 2001). The decrease in NTP resonance is due to the high energy demands and turnover for cellular proliferation, membrane synthesis and DNA replication. Elevated Pi is due to the hydrolysis of γ-NTP to NDP as the NTP is required

for generating new hepatocytes. The elevated PME is due to increased cell membrane synthesis as the new hepatocytes are created to replace the missing tissue. As the tissue regenerates, these changes to the spectrum persist until the liver has fully regenerated and can maintain normal function. Once the liver has regenerated, all of the resonances in the ^{31}P-MRS spectrum have normalized to levels the same as before the partial hepatectomy (Campbell *et al*., 1990; Corbin *et al*., 2002; Farghali *et al*., 1994; Kooby *et al*., 2000; Mann *et al*., 2001).

Liver Disorder	PME	PDE	Pi	ATP
Alcoholic and Viral Cirrhosis	↑	↓	↓	NS
Regeneration (PHx)	↑	↓	↑	↓
HCC in woodchucks	↑	NS	NS	NS

Figure 4. Chart of distinct patterns seen of other liver disorders measured by ^{31}P-MRS. All liver disorders have significantly elevated PME, however cirrhosis and regeneration after partial hepatectomy also show decreases in PDE and alterations in Pi and ATP. These changes in PDE, Pi and ATP were not seen in woodchucks with HCC. (Bell et al. 1993; Dezortova et al. 2005; Jalan et al. 1996; Khan et al. 2005; Mann et al. 2002; Murphy et al. 1992; Taylor-Robinson et al. 1997; Zakian et al. 2005)

Two dimensional chemical shift imaging (2D-CSI) combines the biochemical information derived from magnetic resonance spectroscopy overlaid on an MR image. This allows for the correlation between the biochemical fingerprints of a disease with its anatomical position from the MR image (Figure 5a). The MR image of 2D-CSI is divided into a two dimensional grid. Each square of the grid, called a voxel (volume element), has a defined x and y position and has the same thickness (in the z-direction). In the experiments shown in Figure 5a, each voxel represented a total volume of $8cm^3$ (2cm x 2cm x 2cm). Smaller voxels provide a more accurate representation of the biochemistry of the tissue; however it requires longer data acquisition. 2D-CSI allows for the comparison of the spectra of two different voxels within the same organ (Skoch *et al*., 2008). The results of CSI can either be displayed by overlaying the spectrum onto the voxel(s) of interest (Figure 5a), or by displaying the molecule's distribution in a metabolite map (Skoch *et al*., 2008) (Figure 5c). When doing analysis, the PME peak (red arrow in Figure 5c) is selected from the voxel in the middle of the liver. The metabolite map adjusts to show the relative amount of PME in the rest of the 2D-CSI. White voxels have the highest concentration of PME, followed by red, yellow, green and finally blue and black having the lowest concentration of PME. The metabolite map shows that PME elevations are found only within a small region of the liver with very little PME found on the right lobes of the liver. A metabolite map can be created for any resonance in the phosphorus spectrum (Figure 5c).

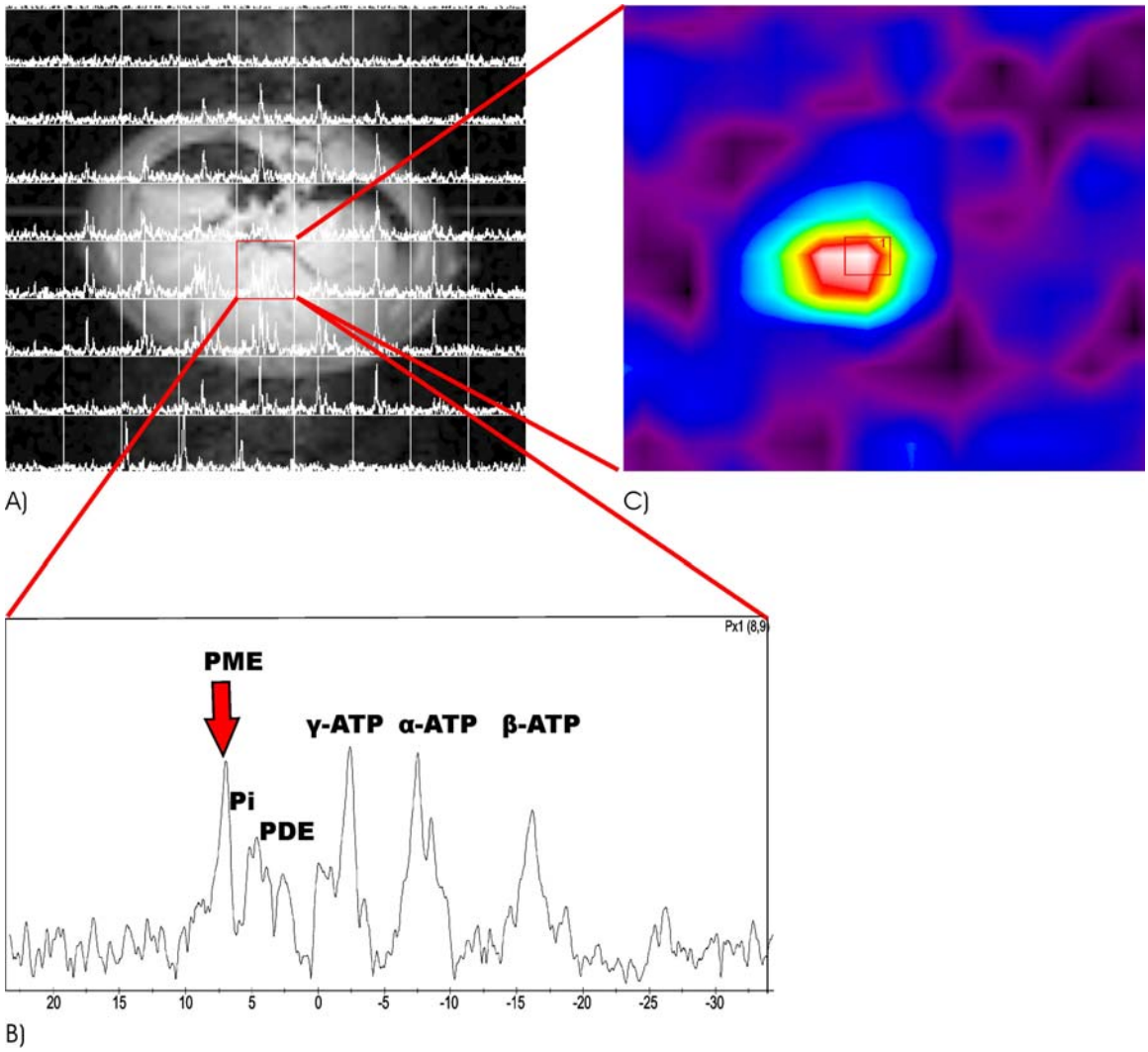
A)
C)
Px1 (8,9
PME
γ-ATP α-ATP β-ATP
Pi
PDE
20 15 10 5 0 -5 -10 -15 -20 -25 -30
B)

Figure 5a) 2D-CSI image with each ^{31}P-MRS spectrum overlayed on the scout axial image. The voxel of interest is highlighted by the red square and can be moved to different regions for comparison between two tissue types. The dimensions of each voxel were 2cm x 2cm x 2cm.

Figure 5b) Enlarged spectrum from the voxel highlighted in the scout image. The red arrow indicates which peak is selected for the metabolite map.

Figure 5c) Metabolite map showing the relative amounts of PME over the entire 2D-CSI dataset where the lowest concentrations are represented in blue and purple, and the highest concentration of PME is in red and white. Using the metabolite map, the region with the highest concentration of PME is limited to a small portion of the liver. Other voxels of the liver do not show elevated PME, indicating that cellular proliferation was limited to a distinct region of the liver, and not the entire liver (see Chapter 3). The red square in the metabolite map indicates the position of the voxel selected from the 2D-CSI image.

A complication with 2D-CSI is that the liver is not uniformly shaped. It is shaped like a triangle, with the left lobes above the stomach significantly smaller than the right lobes (Figure 6). The chemical shift data of each voxel represents the average of all the phosphorus signals contained within the voxel. All of the voxels have the same dimensions; therefore a 2cm thick voxel in the middle of the liver would be composed of the biochemical information of the liver and/or tumour. Voxels must be chosen from the middle of the liver to avoid signal contamination from the stomach and gall bladder. Voxels closest to the abdomen will contain signal contamination from PCr found in the muscles of the abdomen due to respiration. The gall bladder, located under the right lobes, has a different spectrum than the liver tissue due to the presence of bile within the gall bladder (Figure 7). Similarly, voxels chosen to the left side of the woodchuck would contain biochemical information from the stomach. Because of this, only the four voxels in the middle of the liver were used for spectroscopic analysis, regardless of where the HCC was developing. Voxels must be carefully chosen from the anatomical MR image so that the biochemical information contained in the spectrum accurately represents the disease condition and is not due to signals contributed from other organs. If an HCC is sufficiently large, that is, greater than $8cm^3$ in volume, then the phosphorus spectroscopy from the tumour can be analyzed using 2D-CSI regardless of position.

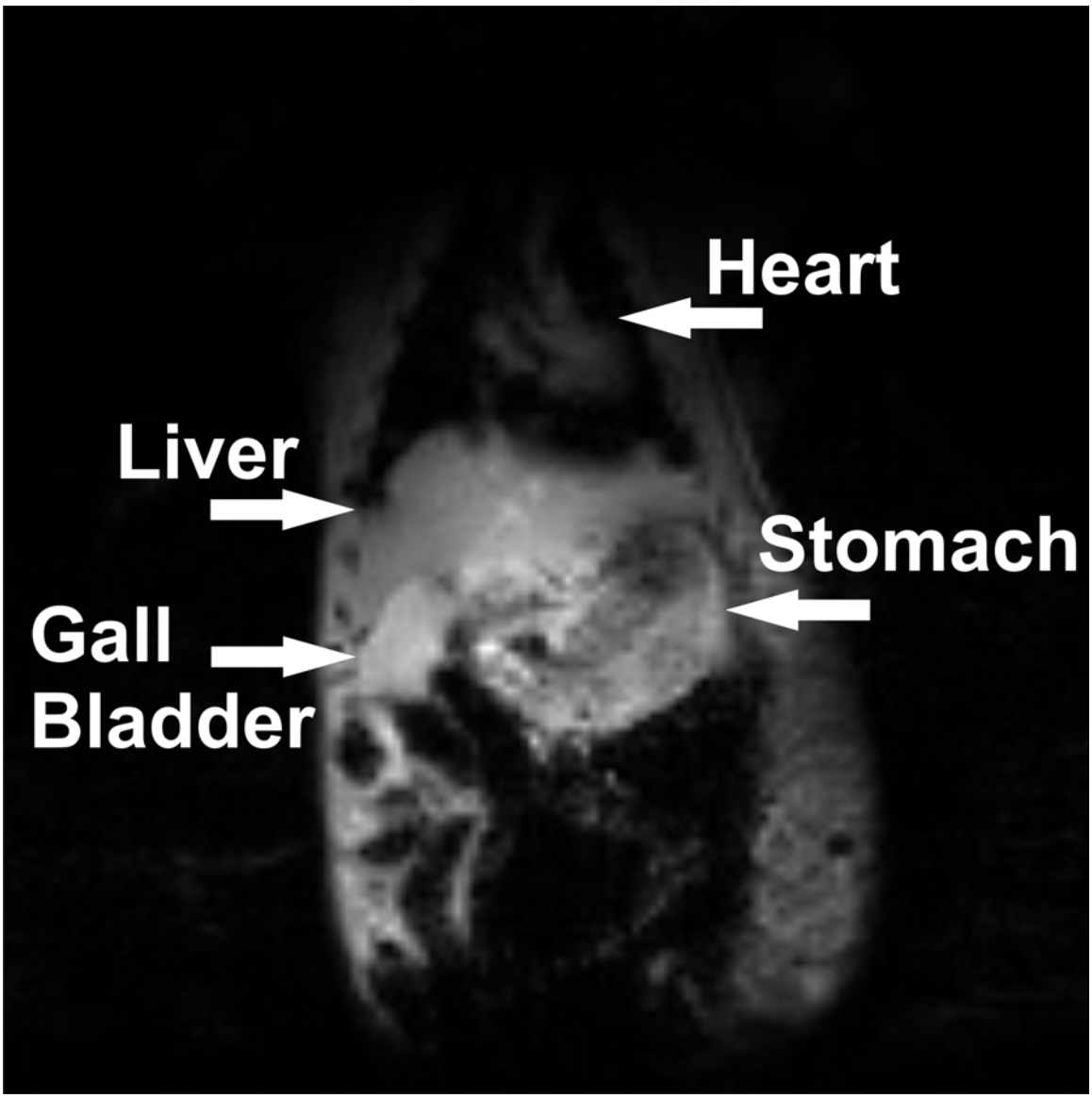
Heart
Liver
Stomach
Gall
Bladder

Figure 6. This coronal GEFI of a woodchuck demonstrating the shape of the liver and how the liver is considerably thicker on the right side of the animal than the left. An axial image along the horizontal plane, is must be accurately positioned to ensure that phosphorus spectrum represents only the liver and does not include signals from other organs.

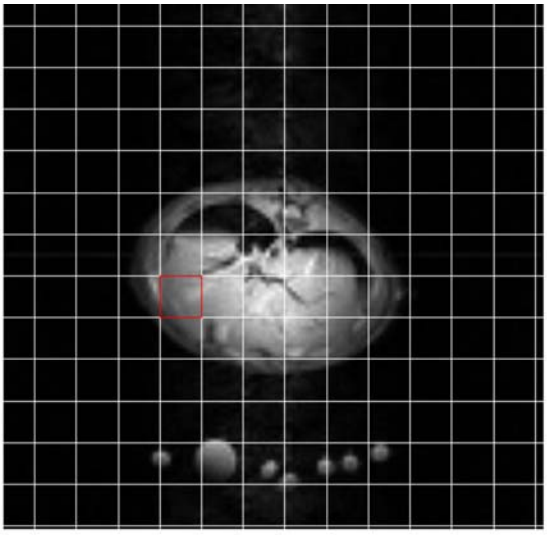

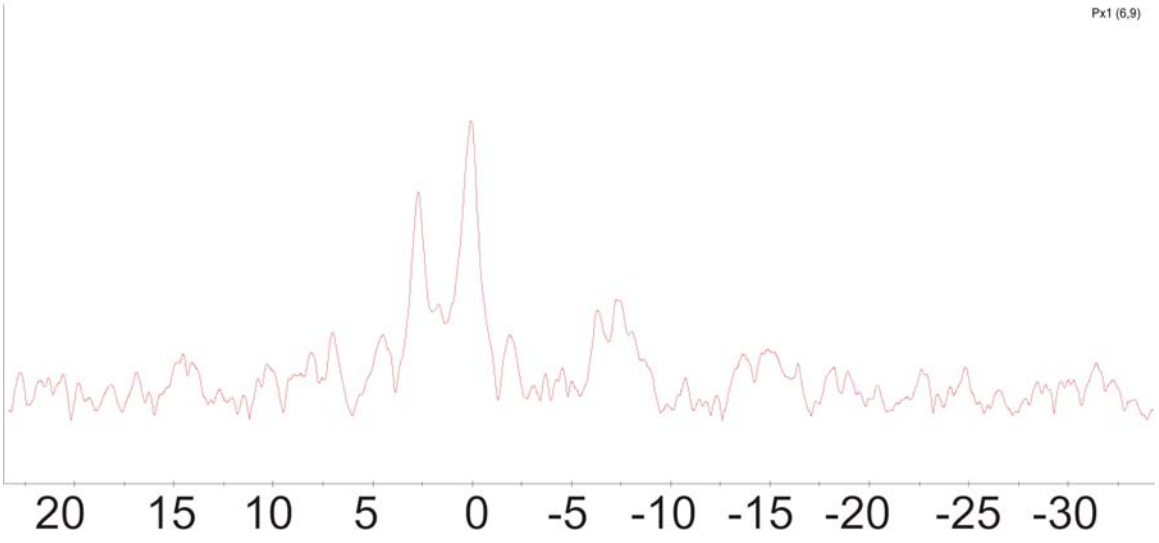
Px1 (6,9)
20
15
10
5
0
-5
-10
-15
-20
-25
-30

Figure 7. An example of the phosphorus spectrum of the gall bladder. This spectrum shows intense PDEs (at 2 ppm) resonances from the gall bladder, some PCr (at 0 ppm) from the abdominal wall. Phosphorus spectrum of the gall bladder is significantly different than of liver tissue (Figure 5b). Care must be taken when choosing voxels for spectroscopic analysis to minimize signal contamination from other organs. Voxels were chosen from four neighbouring voxels in the centre of the liver that did not include signal contributions from the gall bladder, stomach, and, if possible, from the abdominal muscle.

Although this may seem like a limiting factor in using 2D-CSI for tumour detection, four neighbouring voxels represents approximately half the total volume of the liver of a woodchuck because a woodchuck liver is only 8cm wide. Tumours can be greater than 5cm wide (personal measurement) (Popper *et al*., 1987; Reimer *et al*., 1991).

1.7 Choline and Cancer

A common trait amongst many types of cancerous tumours is a significant increase in intracellular concentrations of choline and phosphocholine (PC) detected by proton (^{1}H-) and phosphorus (^{31}P)-MRS respectively (Eliyahu *et al*., 2007; Glunde *et al*., 2006a). ^{1}H-MRS is a more sensitive technique to study alterations in choline concentration because it can detect three different forms of choline in cells: free choline, PC and glycerophosphocholine (GPC) (Glunde *et al*., 2006a). ^{1}H-MRS detects the nine protons in the $-N(CH_3)_3$ group in the three choline-containing molecule, while ^{31}P-MRS can only detect the phosphorus atoms in PC and GPC (Glunde *et al*., 2006a).

PC metabolism occurs in the Kennedy pathway to form phosphatidylcholine, which is found in cell membranes (Glunde *et al*., 2006b). Elevations in PC can be due to alterations in the expression or the activity levels of three different enzymes: 1) Choline kinase, which phosphorylates free choline into PC, 2) phosphatidylcholine-specific phospholipase C, which degrades phosphatidylcholine from cell membranes, releasing PC and 3) cytidylyltriphosphate:phosphocholine cytidylyltransferase, which synthesizes cytidylyldiphosphate-choline using PC as a substrate (Eliyahu *et al*., 2007; Glunde *et al*., 2006a; Glunde *et al*., 2006b; Payne *et al*., 2006). Phosphatidylcholine-specific phospholipase C upregulates oncogene signalling and its activity is correlated to the

extent of tumour invasion (Beloueche-Babari *et al*., 2006; Glunde *et al*., 2006a; Thomas *et al*., 1994). The rate of enzymatic activity of cytidylyltriphosphate:phosphocholine cytidylyltransferase is inversely proportional to intracellular concentrations of PC. An elevated concentration of phosphocholine has been shown to stimulate mitosis and promotes cells going into the S-phase of the cell cycle (Beloueche-Babari *et al*., 2006; Glunde *et al*., 2006a). Choline kinase inhibitors slow tumour growth by preventing cancerous cell's access to dietary choline, the main source of choline for the cell (Eliyahu *et al*., 2007; Glunde *et al*., 2006a). Decreases in PC and increases in GPC due to treatment with anti-cancer drugs like docetaxel (Taxotere™) and paclitaxel (Taxol™) are correlated to cellular necrosis, apoptosis and inhibition of tumour growth (Morse *et al*., 2007).

The choline resonance has been used to identify normal from cancerous tissues in multi-voxel magnetic resonance spectroscopy imaging (MRS) used in planning surgical resection of the tumour and predicting the outcome of treatment regimes (Glunde *et al*., 2006a). Breast and ovarian cancers that have converted from benign to malignant tumours demonstrate a change from high concentrations of GPC and low PC, to high concentrations of PC and low GPC (Eliyahu *et al*., 2007; Glunde *et al*., 2006a).

1.8 Current Clinical Diagnostic Criteria

The American Association for the Study of Liver Diseases recommends that the diagnosis of HCC can be made through combination of radiology, biopsy and α-fetoprotein (AFP) serology (Bruix *et al*., 2005). The sensitivity of MR to detect HCC is 81%, compared to computed tomography's 68% (Willatt *et al*., 2008). The sensitivity can

be increased through use of intravenous contrast agents like gadolinium (Magnovist™). If a patient has lesions greater than 2cm in diameter that shows arterial phase enhancement, venous phase wash-out during contrast enhanced MRI or computed tomography, and elevated α-fetoprotein (>200ng/mL), the positive predictive value of HCC increases to 95% (Bruix *et al*., 2005). Lesions smaller than 2cm are more difficult to diagnose as they may not have the typical wash-out characteristics of larger HCC, they may not cause an elevation in α-fetoprotein, and biopsy results may not be conclusive due to the small sample size of the biopsy relative to the size of the whole organ (Bruix *et al*., 2005). Patients with suspected tumours smaller than 2cm that lack the typical contrast enhancement patterns of HCC are recommended to undergo screening with ultrasound, CT or MRI regularly to ensure that the suspected lesion is not changing size (Bruix *et al*., 2005). Ultrasound guided biopsy of a suspected lesion smaller than 2cm may help improve the diagnosis of HCC, however, small and early HCC may lack some histological features that differentiate HCC from other lesions such as dysplastic nodules (Bruix *et al*., 2005). Combining imaging features already known to be specific to HCC, with the biochemical information specific to the growth of the tumour would improve diagnosis of HCC.

The diagnosis of HCC does not accurately predict the stage of the disease or the clinical outcome. Different methods of staging the disease have been developed (Okuda, Child-Pugh, MELD, BCLC) but they are more accurate in determining patients with end stage HCC and poor prognosis (Bruix *et al*., 2005). Patients with 1 isolated HCC or up to 3 tumours smaller than 3cm each, typically respond well to treatment (resection, transplant, or ablation) and have a 5-year survival rate between 50-75% (Bruix *et al*.,

2005). Having more than 3 tumours but without metastasis to other organs has a 3-year life expectancy of 50% (Bruix *et al*., 2005). Patients with metastasizing HCC have a 1-year life expectancy of 50% (Bruix *et al*., 2005).

Biopsies may cause patient discomfort (pain), possibility of bleeding, and may not sample from the lesion of interest because of difficulty in obtaining accurate images to use as a guide for the biopsy (Bruix *et al*., 2005). There is some concern that the biopsy may cause "seeding" or spreading cancerous tissue to new areas of the liver during the biopsy procedure (Bruix *et al*., 2005). Biopsies only sample 1/50,000 of the liver's total volume, which can not accurately represent the entire liver (Lim *et al*., 2007). Multi-voxel ^{31}P-MRS like 2D-CSI can sample larger areas non-invasively with less risk to the patient (Lim *et al*., 2007). Changes to the liver phosphorus spectrum are being correlated to liver disorders including HCC, steatosis, cirrhosis, hemachromatosis, regeneration after hepatectomy, transplant rejection and response to chemotherapy (Bell *et al*., 1998; Cox *et al*., 2006; Khan *et al*., 2005; Meyerhoff *et al*., 1992; Solga *et al*., 2005; Taylor-Robinson *et al*., 1997).

Unlike woodchucks who live in a controlled environment since birth, human studies are more complicated. Results from human studies of HCC depend on whether the patients have other liver disorders including cirrhosis (either alcoholic or viral in origin), fatty livers, chronic infection with other viruses, and inherited liver disorders. Data analysis is further complicated if the HCC is a primary malignancy or secondary due to metastasis from another tumour elsewhere in the body (Cox *et al*., 1992b).

1.9 Statement of Objectives

A better understanding of biochemical changes occurring in the liver preceding HCC development would improve patient diagnosis and outcome. The intent of this project is to develop and use the woodchuck model of HCC to detect differences in the phosphorus spectrum that correlate with tumour growth using ^{31}P-MRS to monitor tumour growth *in vivo*, and *ex vivo* with ^{31}P-NMR of the water-soluble metabolites extracted with perchorlic acid. Since the woodchucks are being group housed in identical rooms, the only difference between the groups is the infection. Therefore, any significant differences measured over time in the phosphorus spectra and serological samples between the two groups of woodchucks would be due to the development of HCC because of the infection. Tissue samples obtained from tumour and non-tumour tissue will be further analyzed by histology and light microscopy to confirm that the changes detected *in vivo* and *in vitro* were due to HCC growth and not from another liver disorder (e.g. parasites, exposure to hepatotoxins). Since the chronic infection is due to an insufficient immune response to the virus, chronically infected woodchucks will be treated with a novel immunostimulant designed to boost the Th1 response. By stimulating CTLs to viral antigen, the onset of HCC will be delayed as cells expressing viral antigens will be destroyed by a T-cell mediated immune response. The efficacy of the treatment will be determined by correlating serology to *in vivo* ^{31}P-MRS over time. Changes to the composition of the liver tissue were followed using ^{31}P-MRS and changes to the extent of infection and inflammation was followed by serology. If a significant reduction in PME, viral load, WHsAg expression, GGT and AST were detected, it would indicate that an immune response had been initiated, the woodchuck was recovering from the infection, and the tumour burden was reduced.

CHAPTER 2.

Chronic Care and Repeated MR Imaging of Woodchucks

The material presented in this chapter was originally published in Journal of the American Association for Lab Animal Science (JAALAS) in 2006. Reproduced with permission from the publisher The American Association for Laboratory Animal Science© 2006.

All experiments, data analysis and manuscript preparation was performed by me and the staff of NRC-IBD Animal Resources with supervision from Drs. M.L.H.Gruwel and M. Jackson. All MRS experiments, data analysis, and manuscript preparation was performed by me. RT-PCR was performed by Yvon Deschambault with supervision from Dr J. Cao. GGT and AST was determined by the Provincial Veterinary Lab. WHsAg was determined by Mrs. N. Churchill and Dr. T. Michalak.

Previously published papers using magnetic resonance imaging (MRI) of the woodchuck model of HCC were acute studies where the woodchucks were euthanized upon completion of the imaging (Ohtomo *et al*., 1991; Putzer *et al*., 2001; Reimer *et al*., 1991). Before developing the imaging techniques to detect HCC, our first important step was to establish a long-term housing and care strategy for the woodchucks at our facility. This ensured that the woodchucks' day-to-day care was sufficient to allow for repeated data acquisition over many months from the same animals. Secondly, collaborations had to be established with other laboratories to obtain the necessary serological information from the woodchucks due to a lack of equipment and expertise at our facility.

Using the imaging techniques that are described here, the development of HCC can be visualized using magnetic resonance imaging, correlated to serum tests, and compared with the results from uninfected control woodchucks. Chronic experimentation on the same woodchucks allows for better understanding of the disease process in individual animals over time, thereby reducing the total number of animals required in a long-term project.

Materials and Methods

All experiments were conducted with the approval of the National Research Council Institute for Biodiagnostics's Animal Care Committee, following the guidelines of the Canadian Council of Animal Care (CCAC).

Five 2-year old uninfected control woodchucks were purchased from the department of Molecular Virology and Hepatology Research (Faculty of Medicine, Memorial University, St. John's, Newfoundland, Canada). The average age of the woodchucks at delivery was 799 days +/-2.5 days. Five woodchucks chronically infected with WHV were purchased from NorthEastern Wildlife (South Plymouth, NY) when serum levels of WHsAg were consistently elevated, indicating chronic infection. The average age of the infected woodchucks at delivery was 853 days +/-5.4 days. Two different sources of woodchucks were required because of the limited availability of lab-raised woodchucks. Presently, there are two commercial sources of infected woodchucks (NorthEastern Wildlife and Marmotech). The colony at Memorial University is not a commercial business; rather, the woodchucks raised at Memorial University are for use of the Molecular Virology and Hepatology Research centre and their collaborators.

Uninfected woodchucks were purchased from Memorial University as part of a collaboration agreement for this phase of the project. Uninfected woodchucks were not available for purchase from NorthEastern Wildlife.

Infected woodchucks are only available at 1-yr post-infection. As previously described, not all woodchucks will develop a chronic infection after inoculation with the virus, therefore the commercial suppliers will only sell those woodchucks that are serologically positive for the virus. Purchasing woodchucks younger than 1-yr old has the risk that the woodchuck might recover from the infection and not develop HCC, or would develop the HCC much later than the chronically infected littermates would. Due to the high demand for the woodchucks and low availability, only five animals were available at the time of this experiment. The high cost of the woodchucks ($2000USD per animal) and the amount of space required to house the woodchucks limits the numbers that could be purchased. Female woodchucks go into heat once per year, typically in late January – early February producing one litter of six kits. New litters of woodchucks are typically born in late March; the earliest that chronically infected woodchucks are available for purchase is March of the following year.

Although in their natural habitat woodchucks are primarily asocial, territorial animals, in captivity they can be housed individually, in breeding pairs, or by gender. To avoid aggressive behaviour, breeding, and the spread of WHV, the woodchucks were separated among 4 CCAC-approved rooms (each 7.4 m^2 [3.7 m × 2.0 m]) according to gender and infection status; that is, control males, control females, infected males, and infected females were housed in separate rooms. The cement floor was covered with aspen shavings and shredded recycled paper, which was used by the woodchucks to hide

bodily wastes, typically in a corner or behind nest boxes (Bellezza *et. al*., 2002). Shavings were added as necessary; shredded paper was replaced every 3 to 4 d. The entire room was cleaned with a high temperature pressure washer as necessary.

A)

B)

Figure 8A). A typical woodchuck room that would house up to five woodchucks of the same gender and infection status. Aspen shavings and shredded paper were added to the room to protect the footpads of the woodchucks and to give the woodchucks bedding and nesting material, and to cover feces. Untreated wood planks were added for the woodchucks to gnaw on, preventing impaction of their teeth, as well as providing burrowing sites, mimicking nature behaviours.

Figure 8B) 1.5m high wall of 2cm thick clear plastic sheets were positioned in front of chain link fence to minimize the risk to the woodchucks from climbing the fencing and escaping, ripping out their nails on the links, and preventing the woodchucks from attacking animal care technicians from the top of the barrier. The plastic barrier can be seen more clearly in this image.

Large polyvinylchloride tubing (45 cm × 45 cm × 15 cm) and stainless steel nesting boxes (50 cm × 53 cm × 20 cm) were provided in each room as environmental enrichment, allowing a more natural burrow-like environment for the woodchucks. As woodchucks' incisors grow continuously, chemically untreated wooden benches constructed with wooden pegs were included for the woodchucks to gnaw on to avoid impaction of the teeth.

Room temperature was maintained at 20 to 22 °C. Humidity was maintained between 45% to 55% to prevent the drying and flaking of the woodchucks' skin, as well as cracking of the pads of the feet, which can become a source of infection (Bellezza *et. al*., 2002). Woodchucks eyes are sensitive to light, therefore, lighting in the rooms was set on 12-h timers with an incandescent bulb activated 30 min before the fluorescent lights turned on, and for 30 min after the fluorescent lights were turned off, to allow for acclimation to the change in luminosity.

Woodchucks were provided with filtered water and a mixture of rabbit and woodchuck pellets (Prolab Hi-Fiber Rabbit 5P25, Harlan Teklad Woodchuck Diet #7778 Madison, Wisconsin) *ad libitum*. Food and water were provided in multiple stainless steel food dishes to prevent aggressive competition between animals in the room. The food dishes had wide flat bases, which prevented the woodchucks from tipping the bowls over (Bellezza *et. al*., 2002; Young *et al*., 1979).

In group housing, individual animals were identified using unique shave patterns in the fur. As woodchucks only grow fur twice a year, patterns were reshaved in the spring and fall. The shave pattern was used for faster identification of the woodchuck by animal health technicians at a distance. Chest tattoos were not used because they are not

visible unless individual animals were caught, picked up and turned on their backs (Young *et al*., 1979). Ear tags originally used by the woodchucks' suppliers were removed because they potentially contained ferromagnetic metals that would interfere with the magnetic field of the MRI machine or could be ripped out during aggressive behaviour between animals.

Prior to imaging, each woodchuck was captured in an induction chamber, a heavy-gauge plastic box (48 cm × 21cm × 20 cm) with a locking lid. Isoflurane (Aerrane, Pharmaceutical Partners of Canada Richmond Hill, Ontario) was introduced into the induction chamber through tubing connected to the side of the box via an adaptor and pre-drilled holes. Exhaust was vented through a separate exhaust line on the other side of the container and connected to a passive vacuum. Deep-plane anaesthesia was achieved within 5 min (5% isoflurane, 5 l/min 100% O_2). The anesthetised woodchuck was removed from the induction chamber and positioned on its dorsal surface for physical examination and blood draws. Anaesthesia was maintained (3.5% isoflurane, 2 l/min O_2) during the physical examination by using a full facemask with a rubber diaphragm (inner diameter, 52 mm).

During the preimaging physical examinations, the abdomen of the anesthetised woodchuck was palpated to detect any abdominal firmness or tumours. The nails were clipped, and the feet were moisturized with Hibitane cream (1% chlorhexidine, Wyeth Ayerst Veterinary Laboratories, Zeneca Pharma Inc. Guelph, Ontario) preventing the pads drying due to the aspen shavings and cement floor. Eye lubricant was applied to prevent eye dryness during imaging. Nails were trimmed to reduce harm to other woodchucks during fights.

Blood was drawn prior to each imaging session by venipuncture of the tarsal vein of a hind foot by using a 21½-gauge, 1-in. needle (Bellezza *et. al*., 2002; Hornbuckle *et al*., 1985; Nada *et al*., 1997). The foot and inner leg was shaved, cleaned (Hibitane Scrub, Zeneca Pharma Inc. Guelph, Ontario) and rinsed with isopropyl alcohol. 2 -5 ml of blood was collected into phlebotomy tubes and centrifuged to separate the serum from the red blood cells. Pressure was applied to the puncture site to prevent the formation of a hematoma. The serum samples were tested for viral load, WHsAg, GGT, and AST to determine infection status and the extent of liver injury (Bellezza *et. al*., 2002; Hornbuckle *et al*., 1985).

At the Canadian Centre for Human and Animal Health, Division of Viral Hepatology, serum samples were tested for viral load using real time–polymerase chain reaction amplification (RT-PCR; Applied Biosystems 7500 Fast RT-PCR System). RT-PCR is a method to quantify the amount of viral DNA present in the serum obtained from the woodchucks. An oligonucleotide complementary to a section of WHV contains a 5' fluorescent reporter dye and a 3' quencher. During DNA amplification, the oligonucleotide is degraded by DNA polymerase, allowing the fluorescent reporter dye to emit light proportional to the amount of dye released which, in turn, is proportional to the amount of DNA produced. By using a standard curve created from known DNA concentrations, the amount of viral DNA present in the serum can be calculated.

Serum hepatic enzymes GGT and AST were measured at the provincial Veterinary Health Laboratory, using an automatic analyzer (Vitros 250, Ortho-Clinical Diagnostics Inc, Mississauga Ontario) using colourmetric analysis.

Memorial University quantitated WHsAg using sandwich enzyme-linked immunosorbent assays (ELISA). Monoclonal antibodies for WHsAg are not commercially available at this time and are required for accurate measurement of WHsAg. Memorial University has developed their own source of monoclonal antibodies and offered to provide the ELISA service for this experiment. Their system uses a solid substrate coated in anti-WHsAg antibodies. Serum from infected animals containing WHsAg is applied, followed by a secondary anti-WHsAg antibody conjugated with alkaline phosphatase. The absorbance of the alkaline phosphatase at 450 nm is proportional to the concentration of WHsAg in the serum tested. Results are reported as a ratio of the absorbance of infected serum to uninfected serum, where uninfected serum acts as a standard.

The anesthetised woodchuck was positioned on its ventral surface in a removable cradle (Figure 9). The cradle was inserted in the center of a custom-made doubly tunable quadrature volume coil for proton imaging and phosphorus spectroscopy (Tomanek *et al*., 2005). A volume coil was used in this experiment because it gives the greatest signal to noise, the largest field of view and the greatest depth of signal penetration verses a surface coil (Chakeres *et.al*.,1992; Hayes *et al*., 1985; Sank *et al*., 1986). Compared to a single surface coil, quadrature coils improve signal to noise by a factor of √2 (Sank *et al*., 1986; Tomanek *et al*., 2005). Because of the large size of the woodchuck and the fact that the liver is under a thick layer of fur and abdominal fat, a conventional surface coil would not be able to detect the liver in the middle of the abdomen without significant loss of signal to noise (Chakeres *et.al*.,1992). Using a volume coil, the region of highest signal homogeneity would be in the centre of the coil, where the woodchuck would be

positioned (Hayes *et al*., 1985). The volume coil, therefore, provided the best image and spectroscopic data (Hayes *et al*., 1985) and ensures uniform signal excitation over the entire woodchuck (Sank *et al*., 1986; Tomanek *et al*., 2005).

Anaesthesia was maintained at 2% to 3% isoflurane with a flow rate of 2 l/min O_2 via a flexible small-animal full facemask (Harvard Apparatus Holliston, Maine) and held in place with stockinette tubing (3M Health Care St Paul, Minnesota). Exhaust was vented via an active scavenging vacuum through an outlet on the side of the mask (Figure 8). Respiration and heart rate were monitored on a Grass recorder (Grass Instrument Co. Quincy Massachusetts) connected to a receiver coil positioned on the back of the animal. The coil detects minor fluctuations in the magnetic field due to motion from each breath. Outside the magnet, a stethoscope connected to extension tubing was attached to an esophageal tube positioned beneath the animal's chest. The esophageal tube was used to confirm the heart rate and respiration detected by the Grass recorder (McKenzie *et al*., 2005). The woodchuck's temperature was measured rectally with a thermocouple and maintained between 36.5 to 38.0 °C by using a circulating water bath connected to Tygon (Cole Parmer Instrument Co. Chicago, Illinois) tubing that lined the bottom of the cradle in a series of loops. The animal's body temperature was maintained by adjusting the temperature of the water bath. Anaesthesia was maintained at 2.5% and adjusted depending on respiratory rate and heart rate. The total anaesthesia time was 2.5 h.

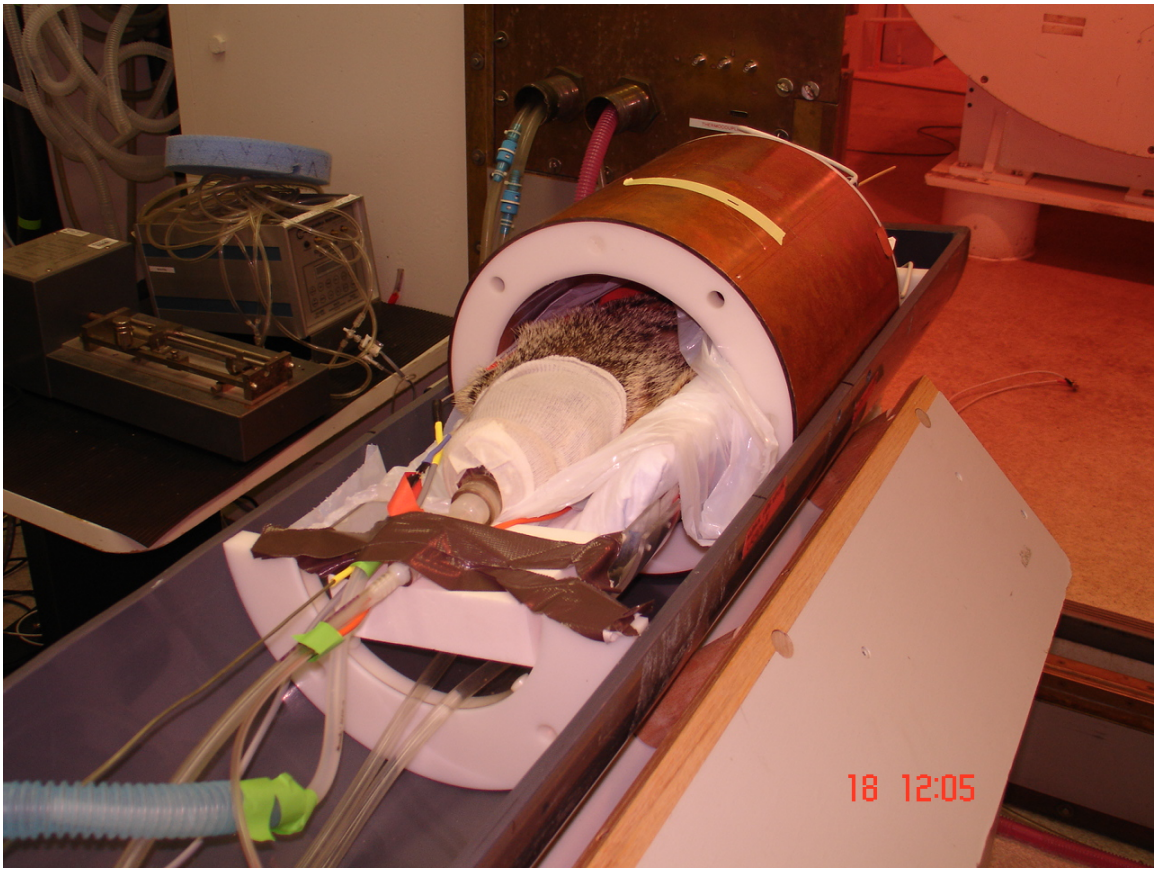
18 12:05

Figure 9. Woodchuck has been prepared for imaging and positioned tail first in the centre of the custom-built doubly tunable volume coil. The two clear Tygon™ tubes on the bottom of the cradle are connected to a circulating water bath and used to maintain the woodchuck's body temperature, measured rectally with a digital probe (not seen in photo). Heart rate was measured by an endotracheal balloon (orange tubing beneath woodchuck on the right of the photo). A small loop of wire is taped to the back of the woodchuck to detect respiration (red X on the back). Anaesthesia was introduced by full face mask held in place over the woodchuck's head, excess and expelled anaesthesia was removed via active scavenging (blue tubing in the bottom left of the photo). The plastic bag beneath the woodchuck was lined with absorbent padding. The absorbent padding was to collect waste expelled during imaging and acted as a thermal insulator for the woodchuck, minimizing fluctuations to body temperature over the course of the imaging. The entire unit is loaded into the centre of the 7T MRI where the coil is tuned and matched for signal optimization.

All MRI experiments were performed in a 7T horizontal bore magnet (Magnex, Yarnton Oxfordshire, UK) equipped with an Avance DRX Bruker console (Rheinstetten Germany). A sagittal fast low-angle shot (FLASH) scout proton image was acquired to determine the location of the liver. FLASH images are another type of gradient echo image (GEFI). From this sagittal image, a 2-cm axial slab was chosen that incorporated the largest portion of liver tissue without signal contamination from surrounding organs. An axial FLASH image was acquired in the middle of the slab to be used as the pilot image for 2D-CSI. Total imaging time was less than two hours; total anaesthesia time (from induction in the chamber to recovery) was less than three hours.

Upon completion of imaging, the animals were allowed to recover from anaesthesia by returning them to the induction chamber and manually stimulated by rubbing their bodies. The lid of the induction chamber was removed, allowing the animal to breathe room air. Two drops of eye lubrication were administered, and 20cc of sterile saline was injected subcutaneously to prevent dehydration. Once the woodchuck's righting reflex had recovered sufficiently and the woodchuck had accepted a food reward, it then was returned to group housing within an hour of being removed from anaesthesia.

Chronically infected woodchucks were euthanized with an intravenous injection of Euthanyl (Schering-Plough, Point Claire, Quebec) when a tumour could be palpated, when the animal reduced its food consumption, when it demonstrated social isolation, and serum GGT levels exceeded 200 U/l. Uninfected control woodchucks were euthanized using an intravenous injection of Euthanyl when all the approved imaging protocols expired.

The livers were removed at necropsy and divided into two portions. One portion was frozen in liquid nitrogen and the other portion was fixed in 10% buffered neutral formalin (Sigma-Aldrich, Oakville, ON, Canada). The fixed tissue was allowed to remain in formalin for a minimum of one month before being dehydrated through a series of ethanol changes (70%, 85%, 90%, three changes at 100%), two changes of xylene (100%) before being embedded in hot paraffin, preserving the tissue in paraffin blocks for histological analysis. 7μm thick sections of tissue were cut and floated on a warm water bath before being mounted on glass slides. After air drying for two days, the slides were dewaxed in two changes of xylene (100%), and rehydrated using decreasing concentration of ethanol (100%, 95%, 70%). The slides were immersed in hematoxylin for 2 minutes; the colour was developed in ammonia water and rinsed in tap water before submersion in eosin Y for 15 seconds. The slides were passed through an increasing ethanol series (70%, 95%, 100%) before two changes of 100% xylene and mounted using Permount (Sigma-Aldrich, Oakville, ON, Canada) and covered with a slipglass. After allowing the Permount to harden, the slides were reviewed by light microscopy. The nuclei of cells appear blue-purple while the cell walls appear pink. Fatty deposits do not stain.

MRS data was processed using Marevisi™ (Institute for Biodiagnostics, Winnipeg, Canada) and WinNMR6.0 (Bruker, Rheinstetten). Results represent the mean value from infected and control animals, and were considered significant with a p value less than 0.05 using a Student's t-test. (Statistica, Tulsa Oklahoma)

Results

During the examination before imaging, the abdomen was palpated to detect any tumour growth. Early changes in the liver of infected animals could be palpated as a non-specific firmness of the abdomen. Histological examination of tumours removed during necropsy showed fibrous encapsulation of the tumour from the surrounding parenchyma (Figure 10 A and B). Early HCC does not show this fibrotic encapsidation (Figure 9C) but does show a distinct difference between normal and pre-cancerous tissues (Popper *et al*., 1987).

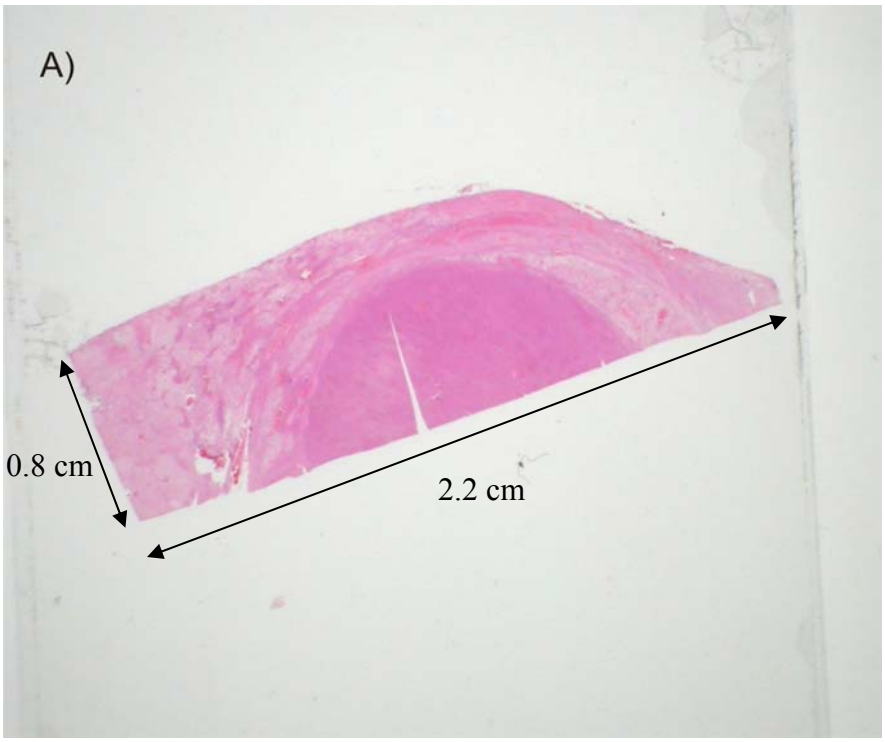
A)
0.8 cm
2.2 cm

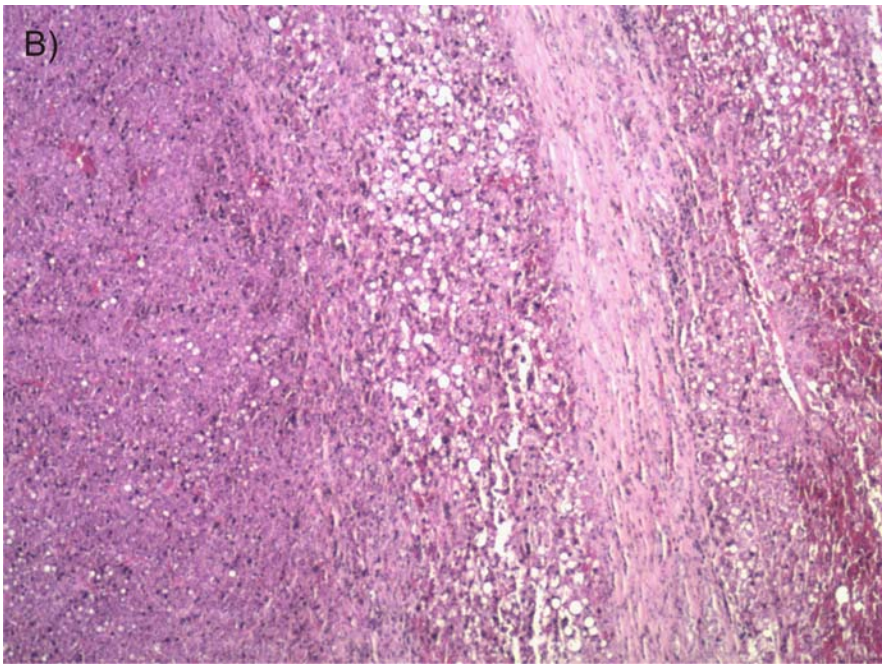
B)

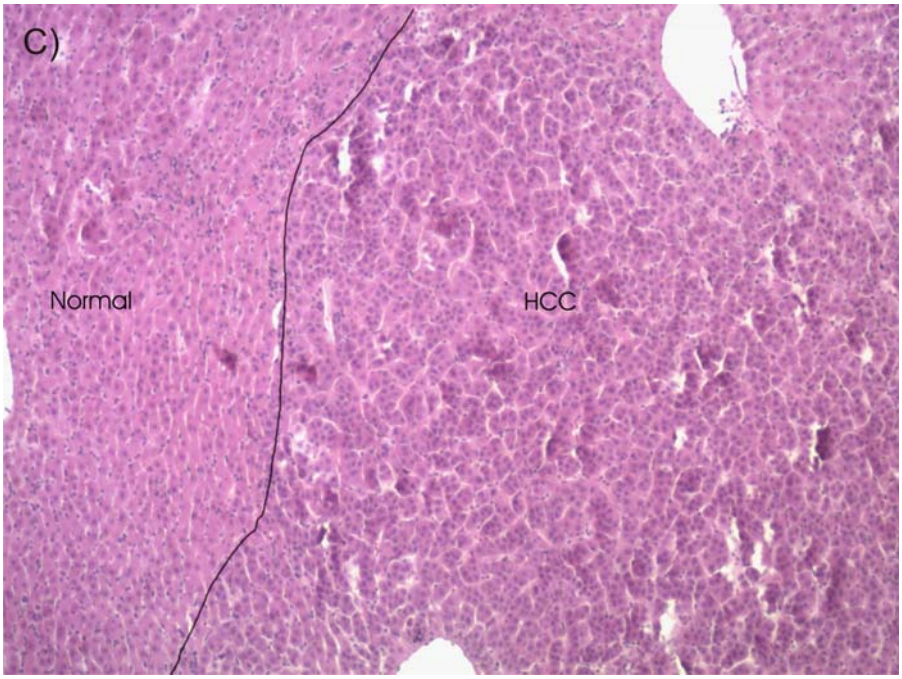
C)
Normal
HCC

Figure 10 A) 7μm hematoxylin and eosin Y stained portion of liver from chronically infected woodchuck. The circular region of tumour growth is clearly differentiated from surrounding tissue and encapsidated by fibrous tissue. Fat deposits and abnormal vasculature are typical of woodchuck HCC (Toshkov *et al*., 1990).

Figure 10 B) 8x magnification of the same tissue demonstrating changes to histology as a result of tumour formation. Note the fibrotic encapsidation along the edge of the tumour boundary, altered vasculature within the affected region and regions of fat deposits, typical of woodchuck HCC (Toshkov *et al*., 1990).

Figure 10 C) 20x magnification of an early HCC from a woodchuck that died before large HCC could develop. Notice the increased cell density, multinuclear hepatocytes, and irregular cellular architecture of the HCC compared to the adjacent normal tissue. Boundary between normal and HCC has been demarcated for clarity. The results are similar to published reports on early neoplastic changes to the livers of infected woodchucks (Popper *et al*., 1987).

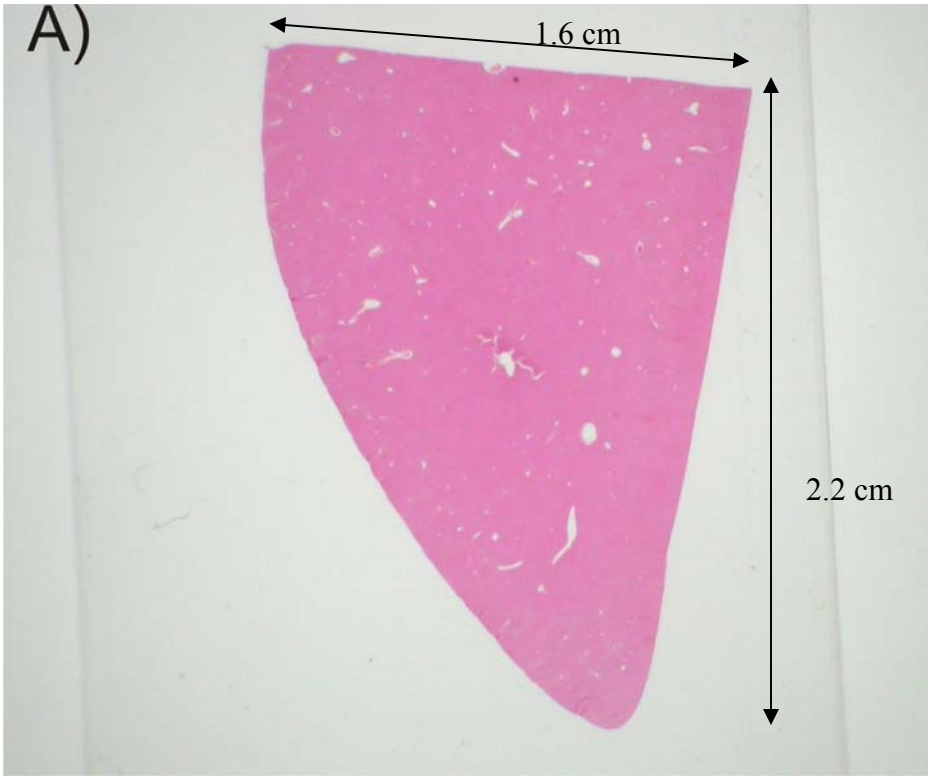
A)
1.6 cm
2.2 cm

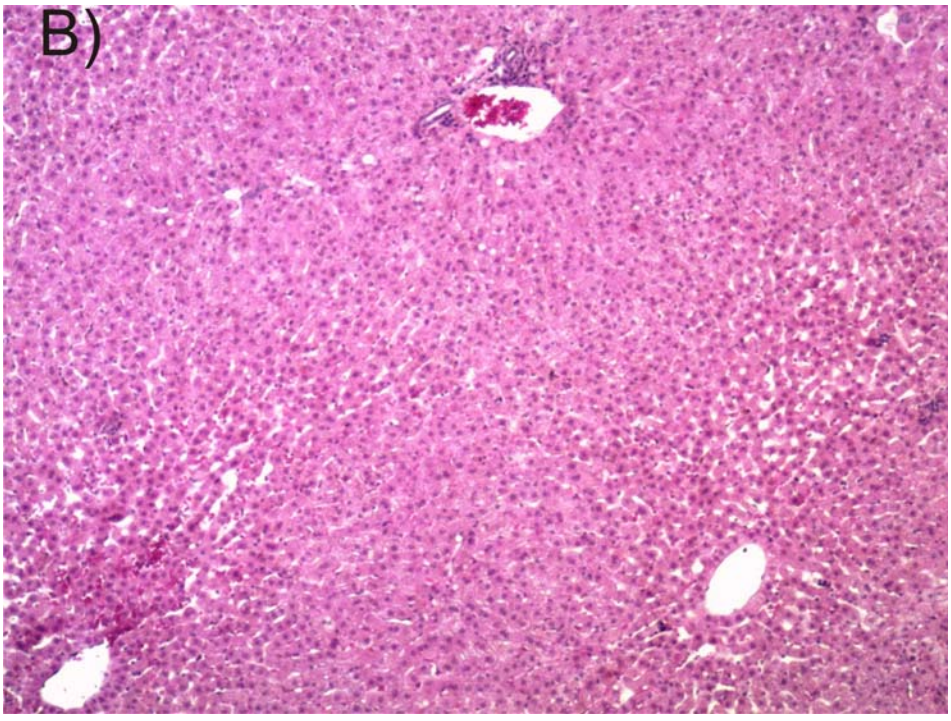
B)

Figure 11 A) Portion of normal tissue from uninfected woodchuck. In this section, note the regular distribution of blood vessels and arrangement of hepatocytes that is not seen in woodchucks with HCC (Figure 10A)

Figure 11 B) 8x magnification of the same slide, demonstrating the normal arrangement of hepatocytes and blood vessels, the lack of fibrous deposits, fat, or lymphocytes in the tissue.

The rate of isoflurane consumption depended on the season, with higher levels required during the summer months when respiration rates were higher. The average respiration rate during winter was 3 to 5 breaths per min; whereas during summer it was 8 to 10 breaths per min. The heart rate was maintained at 180 to 210 beats per min. Because of the animals' fluctuating respiration rates throughout the year, the levels of isoflurane were closely monitored and adjusted throughout the experiment to maintain a regular respiration rate. Unlike that of other animal species, the respiration of anesthetised woodchucks was irregular: during winter months, often 2 breaths occurred in quick succession, followed by a period as long as 20 s without breathing. During summer, when respiration rates are higher, breathing was more regular and predictable.

A)

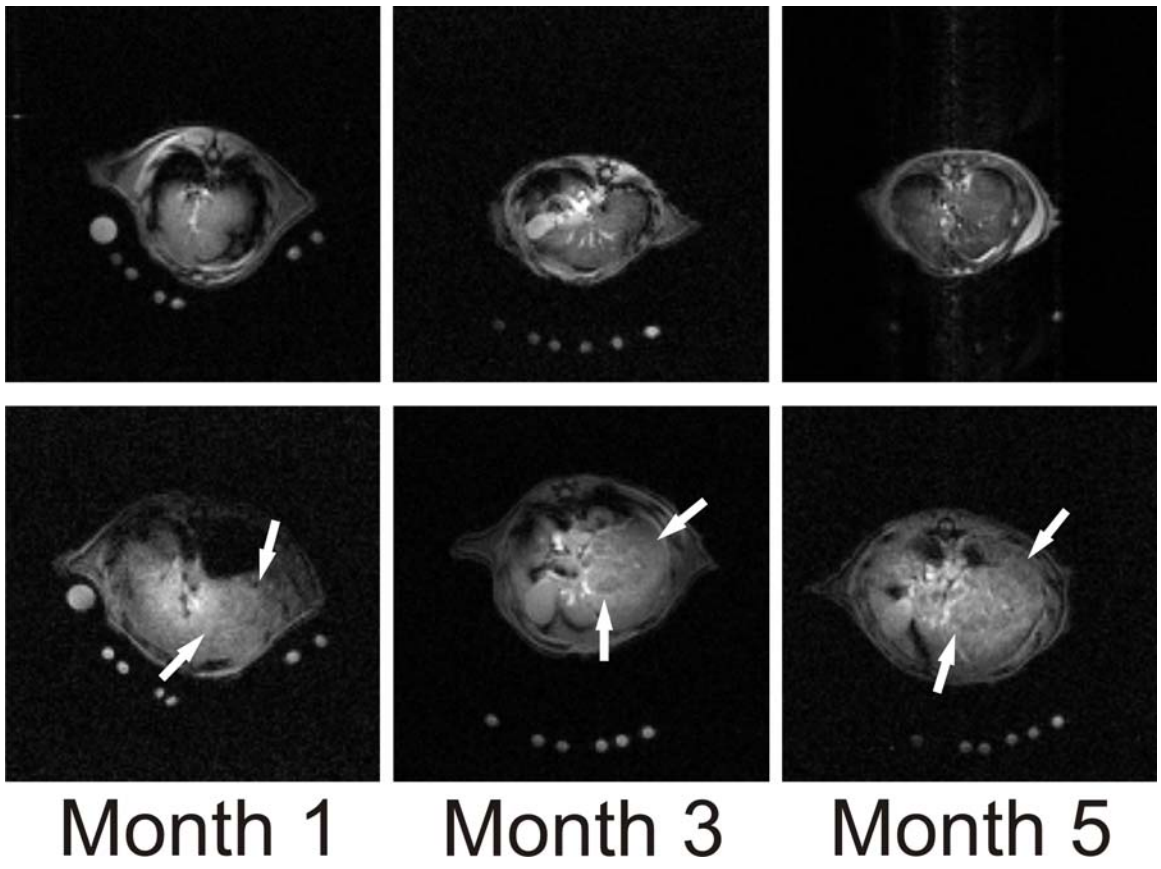

B)

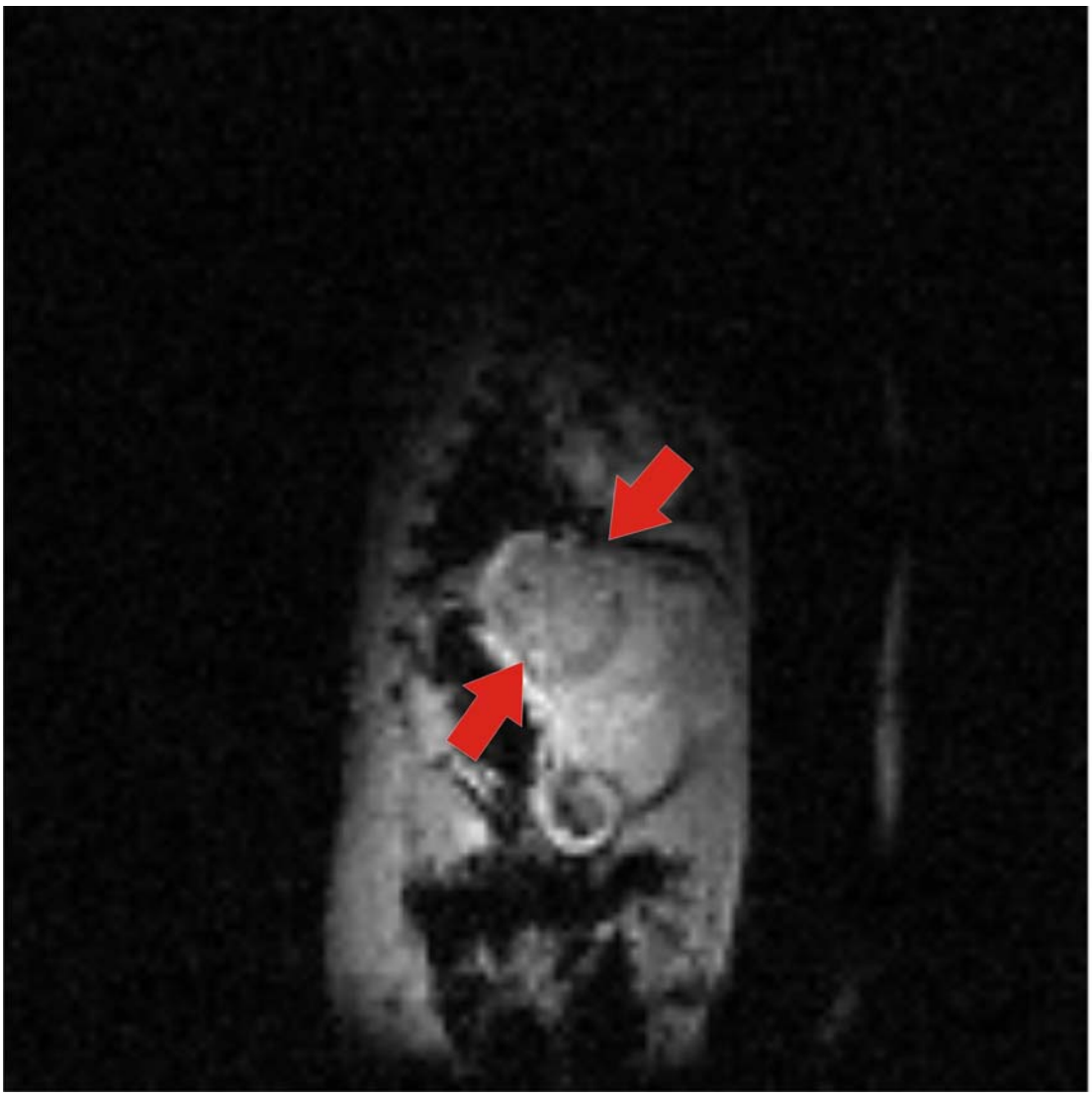

C)

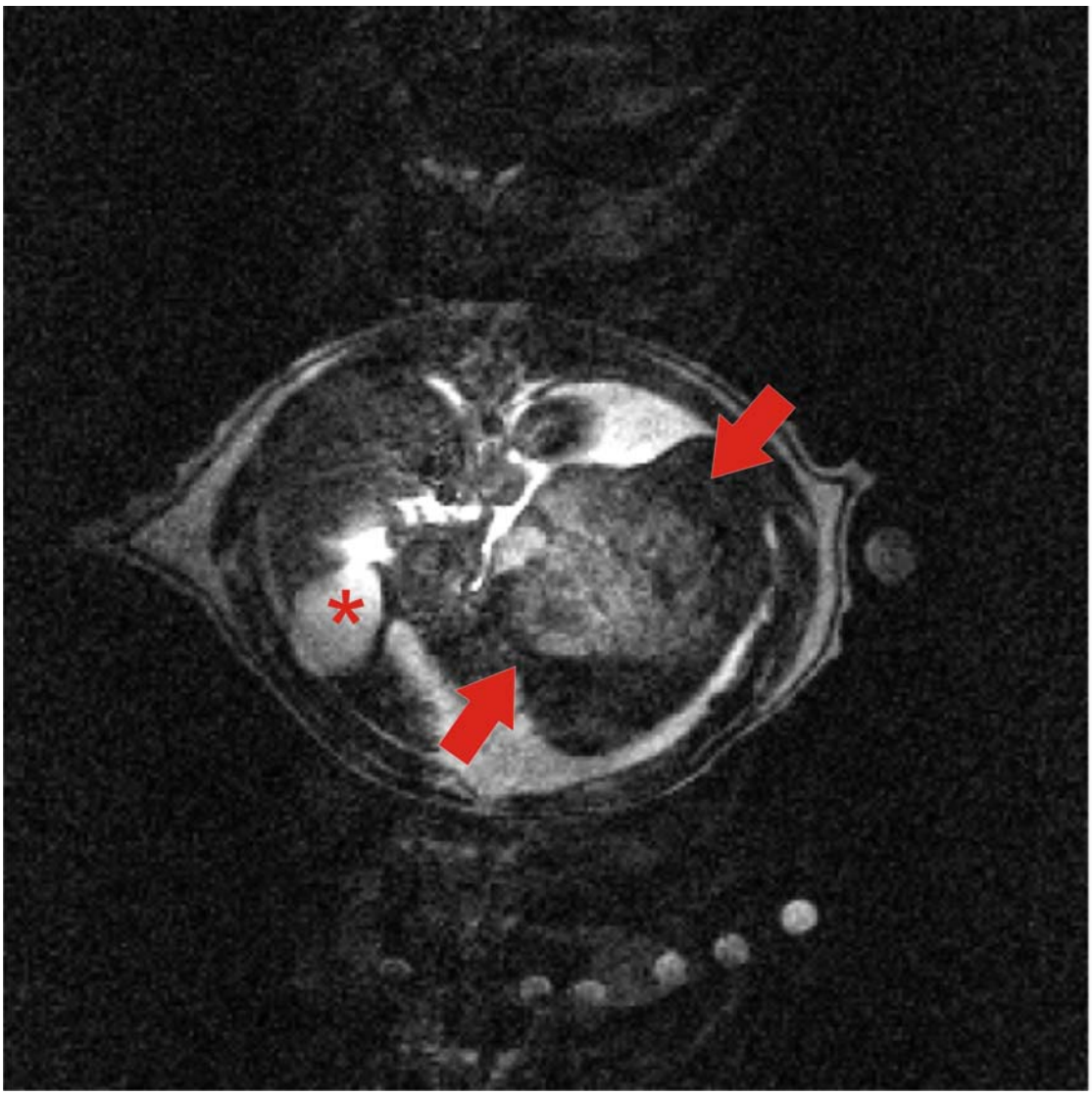

Figure 12 A. The liver of the same healthy uninfected woodchuck over a four month period imaged with GEFI images (top row) compared to the liver of an infected woodchuck imaged during the same period (bottom row). White arrows indicate the position of the HCC in the infected animal. Although the radiograph does not provide diagnostic quality images, it does demonstrate that significant alterations in the liver can be detected using GEFI imaging. These GEFI images were the scout images used to set up the 2D-CSI experiments. The infected woodchuck weighed approximately 1.5kg more than the healthy uninfected woodchucks, accounting for the difference in the size of the livers in the two images. The series of small white circles beneath each woodchuck are the Tygon tubes used to maintain the woodchuck's body temperature during imaging. The tubes were connected to a circulating water bath set to 37°C that was adjusted as necessary.

Figure 12 B. Coronal GEFI from the same woodchuck in the bottom row of Figure 12A at month 3. Red arrows indicate the edges of one HCC. This is an example of how large the tumours can grow in a woodchuck in proportion to the rest of the body.

Figure 12 C. T_2-weighted spin echo image of the same infected woodchuck in the bottom row of Figure 12A at month 3. This woodchuck was not intubated, causing motion artifacts visible above and below the animal as ghosting. The image quality is reduced compared to gated image acquisition. The edges of the tumour are indicated with red arrows. The gall bladder is marked with a red asterisk.

Despite the avoidance of hibernation, a woodchuck's weight will fluctuate throughout the year (Bellezza *et. al*., 2002). In our facility, we found that woodchucks consume food on a yearly cycle; this pattern occurred under *ad libitum* feeding, constant temperatures, and unvarying ratios of light and dark. Increases in activity, body temperature, vocalizations, food intake, and weight were seen during the months of April through October and decreased during the months of November through March (Figure 13). The weight gain from April to October of uninfected woodchucks was 9.96% ± 3.50% whereas the average weight loss during November to March was 10.27% ± 1.59% (mean ± standard error). A similar pattern was seen in the infected woodchucks, although there was a significant difference in weight between the two groups of animals. This difference is probably due to the woodchucks originating from two different suppliers and not related to the infection.

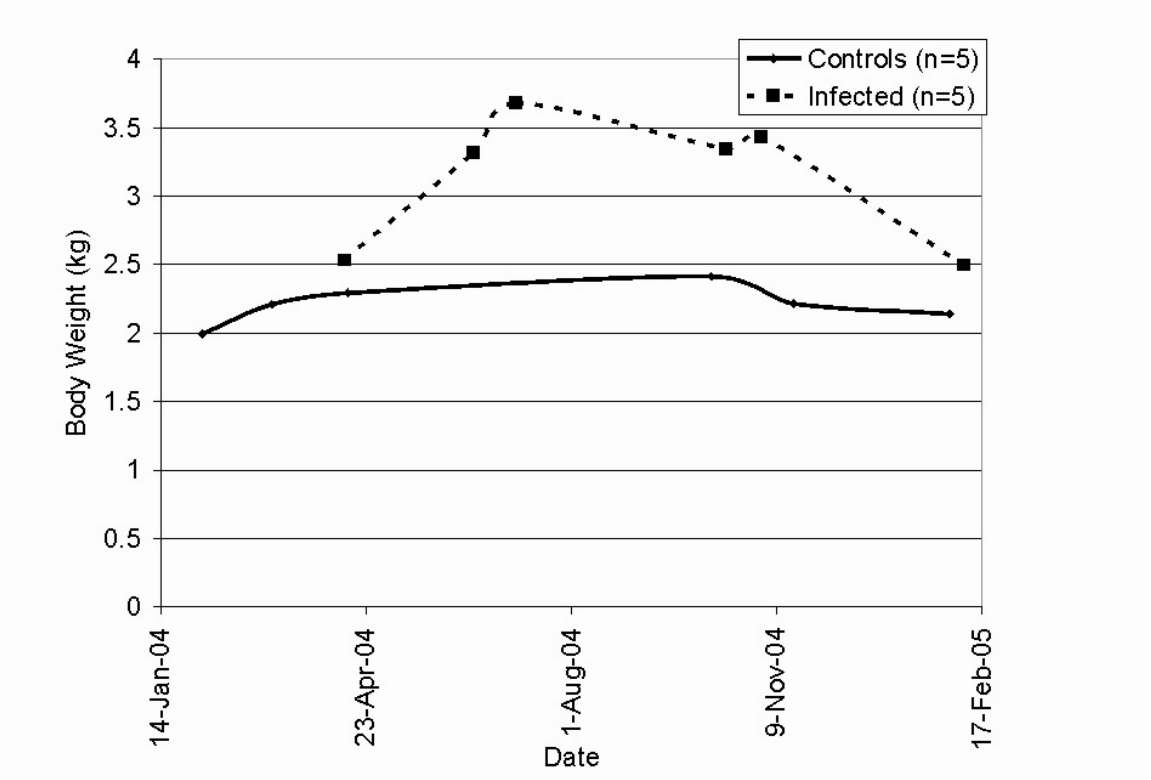
Controls (n=5)
Infected (n=5)
Body Weight (kg)
4
3.5
3
2.5
2
1.5
1
0.5
0
14-Jan-04
23-Apr-04
1-Aug-04
9-Nov-04
17-Feb-05
Date

Figure 13. Graph showing the change in weight of infected and uninfected woodchucks over time. The difference in the weights of the animals is probably due to the animals coming from different suppliers and is not related to the infection. During summer months, woodchucks consume significant amounts of food to build up a layer of fat, from which they will derive all energy to maintain themselves during hibernation. In the wild, male woodchucks can lose up to 47% of their body weight, while females may lose up to 37% of their pre-hibernation body weight (Bellezza *et. al*., 2002; Ferron, 1996.)

Using RT-PCR, the viral load of the infected and control woodchucks was calculated. Infected woodchucks had a significantly higher viral load (Figure 14). Uninfected control woodchucks had an average viral load of 171.77 copies/μL +/-100.03, whereas infected woodchucks had an average viral load of 7.33×10^6 copies/μL +/- $5.67x10^6$ ($p< 0.006$). The viral load of the uninfected woodchuck may not be due to the uninfected woodchucks testing positive for WHV DNA. Subsequent re-analysis of the backup vial of serum did not detect WHV DNA. The values (DNA detected and not detected) were averaged for that woodchuck's monthly viral load. The positive results in the control woodchucks were included in calculating the average viral load because there were not sufficient amounts of serum for a third test to determine which of the two tests was definitive. Having an average viral load of less than 171.77 copies//μL +/-100.03 also represents the very limits of detection by RT-PCR and may also be random sections of DNA that was being amplified but is not due to the presence of WHV DNA in the sample. It may also be due to contamination of the first sample because second sample tested negative for WHV DNA.

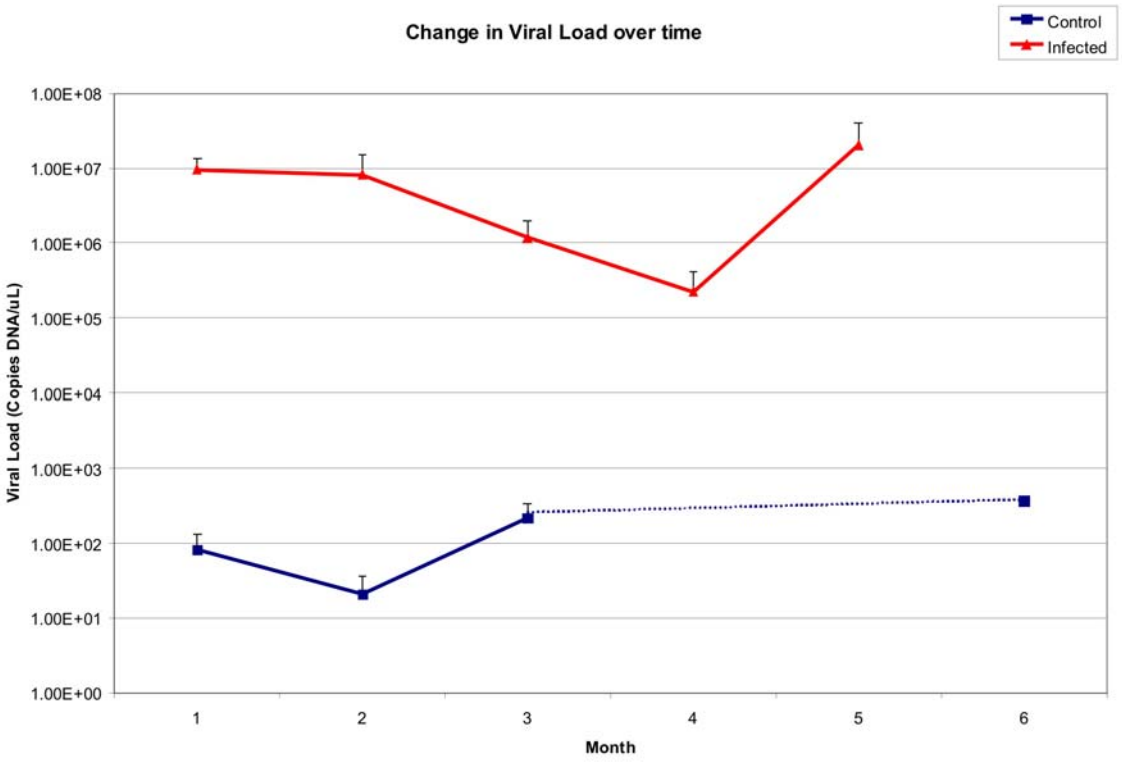
Change in Viral Load over time
Control
Infected
1.00E+08
1.00E+07
1.00E+06
1.00E+05
1.00E+04
1.00E+03
1.00E+02
1.00E+01
1.00E+00
Viral Load (Copies DNA/uL)
1
2
3
4
5
6
Month

Figure 14. Average viral load of infected (red, n=5) and uninfected (blue, n=4) woodchucks over time. Infected woodchucks had a significantly higher ($p<0.006$) viral load than uninfected woodchucks throughout the experiments. Values represent the mean +/- standard deviation. Uninfected woodchucks sometimes had detectable viral loads, subsequent retesting of the serum failed to find any viral DNA. The viral load of the uninfected woodchuck was recorded as the average of the two tests.

Infected woodchucks had an average WHsAg level of 6.72 ± 0.837 absorbance units as calculated by ELISA (Bio-Rad Mississauga, Ontario). Sample absorbance greater than 2.1 is considered positive.

Control woodchucks had an average serum AST level of 29.3 ± 2.99 IU/L, whereas that of infected woodchucks was 88.2 ± 19.2 IU/L ($p < 0.006$), confirming hepatocyte injury due to tumour growth. High levels of GGT indicated hepatocyte injury that could be correlated to the development of HCC in the chronically infected woodchucks (Bellezza *et. al*., 2002; Hornbuckle *et al*., 1985; Michalak,1998). Control woodchucks had GGT levels of 5.50 ± 0.5 IU/L (mean ± standard deviation), whereas those in infected animals were 208.8 ± 48.9 IU/L, confirming that chronically infected woodchucks with HCC have greater hepatocyte injury than uninfected control woodchucks ($p < 0.002$) (Figure 15). Chronically infected woodchucks lived for an average of 986 d ± 27 d after infection. Uninfected control woodchucks survived in excess of 1460 without development of HCC ($p<0.001$).

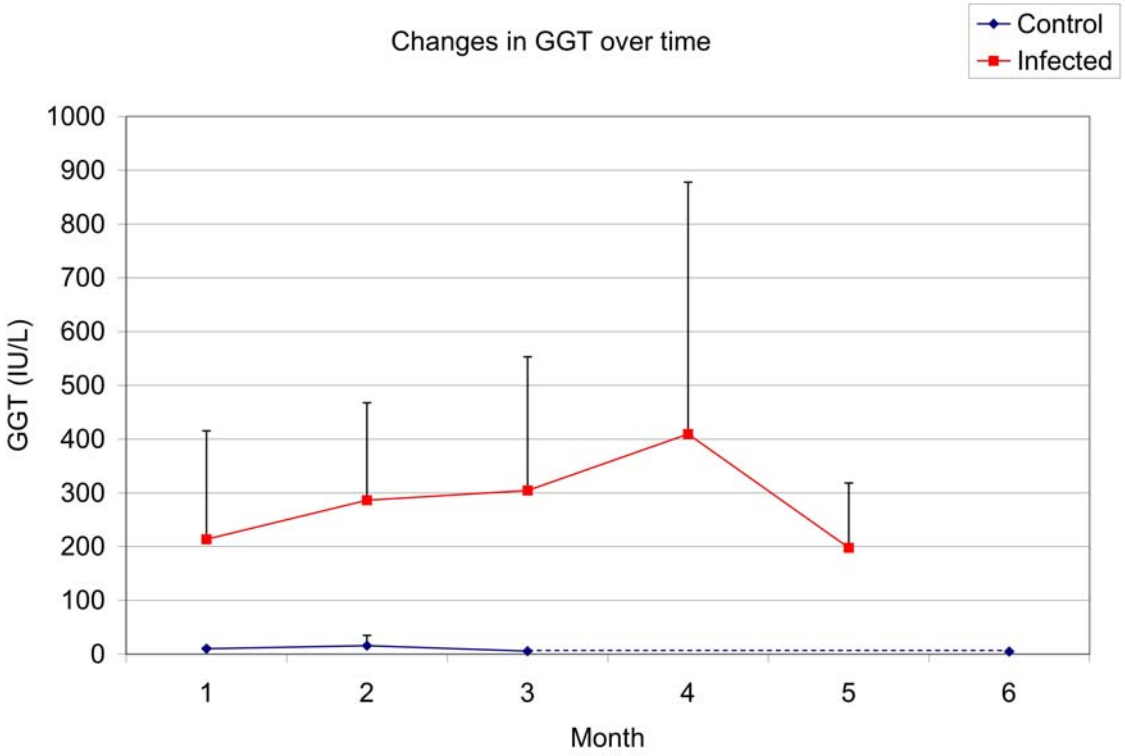
Changes in GGT over time
Control
Infected
GGT (IU/L)
1000
900
800
700
600
500
400
300
200
100
0
1
2
3
4
5
6
Month

Figure 15. Significant elevations in the serum GGT in the woodchucks with HCC (n=5) compared to uninfected woodchucks (n=4) over time. Results are reported as mean +/- standard deviation.

Discussion

All infected woodchucks developed hepatocellular carcinoma whilst uninfected woodchucks survived for greater than 3 years without the development of hepatocellular carcinoma, confirming previously published work that woodchucks not exposed to WHV do not develop tumours (Michalak,1998; Tennant,2001). Although GGT and AST levels do not correlate to the extent of tumour growth, it can be used as a serum marker for the degree of liver injury due to the tumour (Hornbuckle *et al*., 1985; Jacob *et al*., 2004). The extent of liver injury in humans is measured by α-fetoprotein, AST and ALT while in woodchucks, AST and GGT is used. α-Fetoprotein is not specific for HCC growth in woodchucks (personal communication, Dr. T. Michalak, Memorial University).

In clinical situations, human patients are instructed to breath-hold during imaging, reducing motion artifacts due to breathing. Because the woodchucks were not intubated due to irregular breathing, gradient echo images had to be acquired because they are a faster imaging sequence than conventional T_1 or T_2 -weighted high resolution images. Because image quality is poorer than with T_1 or T_2 –weighted images, only large tumours could be identified from surrounding normal tissue. In other experiments performed on woodchucks that were not part of this project, woodchucks were intubated and T_2 –weighted spin echo images were acquired (Figure 6, Figure 16). Intubation was considered too invasive a procedure to be performed on a monthly basis. Concerns about the development of scar tissue and the effect to the vocal cords prevented the use of intubation. Higher quality imaging like T_1 and T_2-weighted images typically used in clinical settings could not be obtained without intubation or breath-holding. The lower resolution GEFI images were used not as much for tumour detection as they were for

anatomical reference. The most important information for these experiments came from the 2D-CSI phosphorus spectroscopy, not the images.

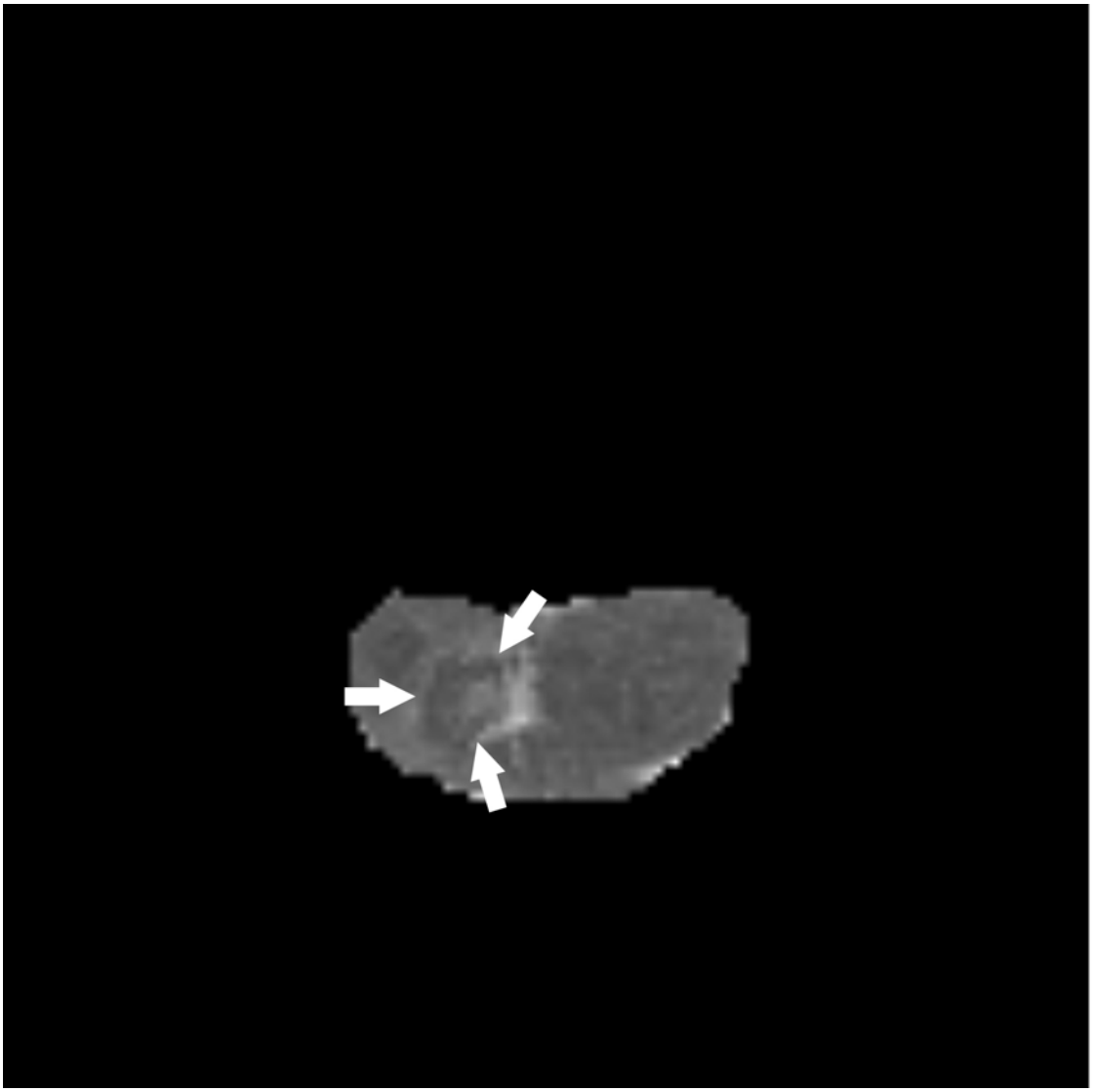

Figure 16. T_2-weighted spin echo image of an intubated woodchuck; image acquisition was gated to the respirator. White arrows indicate the edge of a large HCC towards the top right lobe of the liver. The tissue surrounding the liver has been removed by the software used for analysis because it interferes with the relative intensity of the image. Although T_2-weighted spin echo images provides better quality images than GEFI and are used in diagnostic imaging of humans, it could not be used for this project because of the invasiveness of intubation and the potential damage to the throats of the woodchucks with monthly insertion of the breathing tube. Fat has a higher T_2 value than tissues, therefore accumulations of abdominal fat appears a bright regions on either side of the woodchuck.

CHAPTER 3. Monitoring the development of HCC in woodchucks using 31P-MRS.

All experiments, data analysis and manuscript preparation was performed by me with supervision from Drs. M.L.H.Gruwel and M. Jackson.

After developing the techniques necessary to house and care for woodchucks over extended periods, and establishing the serology criteria to confirm both infection and degree of liver injury, the woodchucks could be imaged using ^{1}H-MRI and ^{31}P-MRS to determine whether there is a MR-detectable difference between woodchucks with HCC due to chronic infection, when compared to uninfected woodchucks without HCC. By using the techniques described in the previous chapter to take blood samples from an accessible vein, monthly serum samples could be obtained with minimal effect to the woodchuck. Using inhalation anaesthesia made imaging woodchucks possible without long-term effects to the animal and to the liver. Group housing of the woodchucks made handling the animals safer for the animal health technicians and benefited the woodchucks.

Materials and Methods

All animal experiments were conducted with approval from the National Research Council Institute for Biodiagnostics Animal Care Committee. All MRS experiments were performed in a 7T horizontal bore magnet (Magnex, UK) equipped with an Avance DRX

Bruker console. The animal was positioned in the centre of a doubly tunable quadrature volume coil tuned to 300MHz and 121.5MHz for proton imaging and phosphorus spectroscopy respectively (Tomanek *et al*., 2005). A fast low angle shot (FLASH) sagittal scout proton image (128x128, TR/TE=1000/4.1, slice thickness=5mm, FOV=25cm, 8 averages) was acquired to determine the location of the liver relative to the isocentre of the magnet (Figure 17).


seg
Date
FA
NA8
TE0
TR0.001
128*128
BW
SI1/1
E1/1
Pos0.0
TH-50.0
FOV250*250

Figure 17. Sagittal FLASH image of the woodchuck used to determine the position of the liver. A 2cm slab is positioned in the largest portion of the liver, trying to avoid signal contamination from the stomach (below the liver) or the heart/lungs (above the liver). The white streak to the right of the woodchuck is the Tygon™ tubing connected to a circulating water bath, used to keep the woodchuck warm. FLASH images are lower in resolution than the T_2-weighted spin echo image (Figure 16). The FLASH image, because it's a gradient echo image, was used because it was faster and can be acquired between respirations without requiring invasive intubation. The FLASH sagittal image was acquired to determine the location of the axial image and the 2D-CSI.

From this sagittal image, the position of a 20mm axial slab was determined which incorporates the largest portion of liver tissue without artifacts from the diaphragm and stomach. An axial FLASH image (128x128, TR/TE=1000/4.1, slice thickness=5mm, FOV=20cm, 8 averages*)* was acquired in the middle of the previously selected slab. This scout image was used as the pilot image for the 2D-CSI (Figure 18). Prior to ^{31}P- CSI-2D, the B_0 homogeneity of the selected slab was shimmed using the ^{1}H resonance signal. Using the position of the 20mm slab determined in the scout proton image, the ^{31}P MR spectra were acquired using a FOV 24cm x 24cm, a sweep width =7 kHz, a data matrix of 1024 spectroscopic points, a TR = 1000ms, and 16 averages. The total imaging time for 2D-CSI was 67 minutes (McKenzie *et al*., 2005).

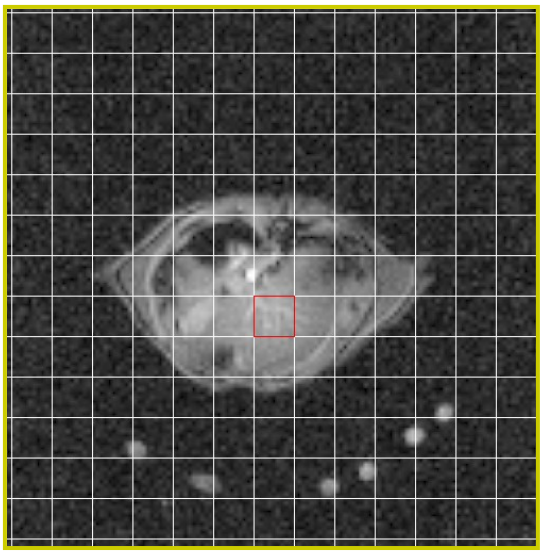

Figure 18. Scout axial 5mm thick GEFI image from the middle of the 2cm slab used for ^{31}P 2D-CSI experiment. This scout image will be used for 2D-CSI to determine the position of the voxels that contain the phosphorus data. The six white circles beneath the woodchuck are a cross-section of the Tygon™ tubing described previously.

Data processing was performed on a computer using Marevisi™ and WinNMR6.0 (Bruker Rheinstetten). In Marevisi™, the free induction decays (FID) from the 2D-CSI were reconstructed with a Hanning filter for the spectral dimension and exponential line broadening of 30Hz for the FID. Phosphocreatine (PCr) from the surrounding abdominal muscles was selected as the origin of the spectrum because it is found outside of the liver and would therefore be unaffected by alterations to the liver tissue as a result of tumour formation. A voxel with the least amount of PCr contamination from the abdominal walls and the highest phosphorus metabolite peaks was selected from the largest portion of the liver. By selecting a voxel with the least amount of PCr contamination, the signals for α-NTP, β-NTP, γ-NTP, PME and PDE originate exclusively from the liver, thus reduces the likelihood that these signals may have contributions from the abdominal wall. Manual phase correction was performed relative to the alpha adenosine triphosphate (α-NTP) peak at –7.5 ppm (Figure 19).

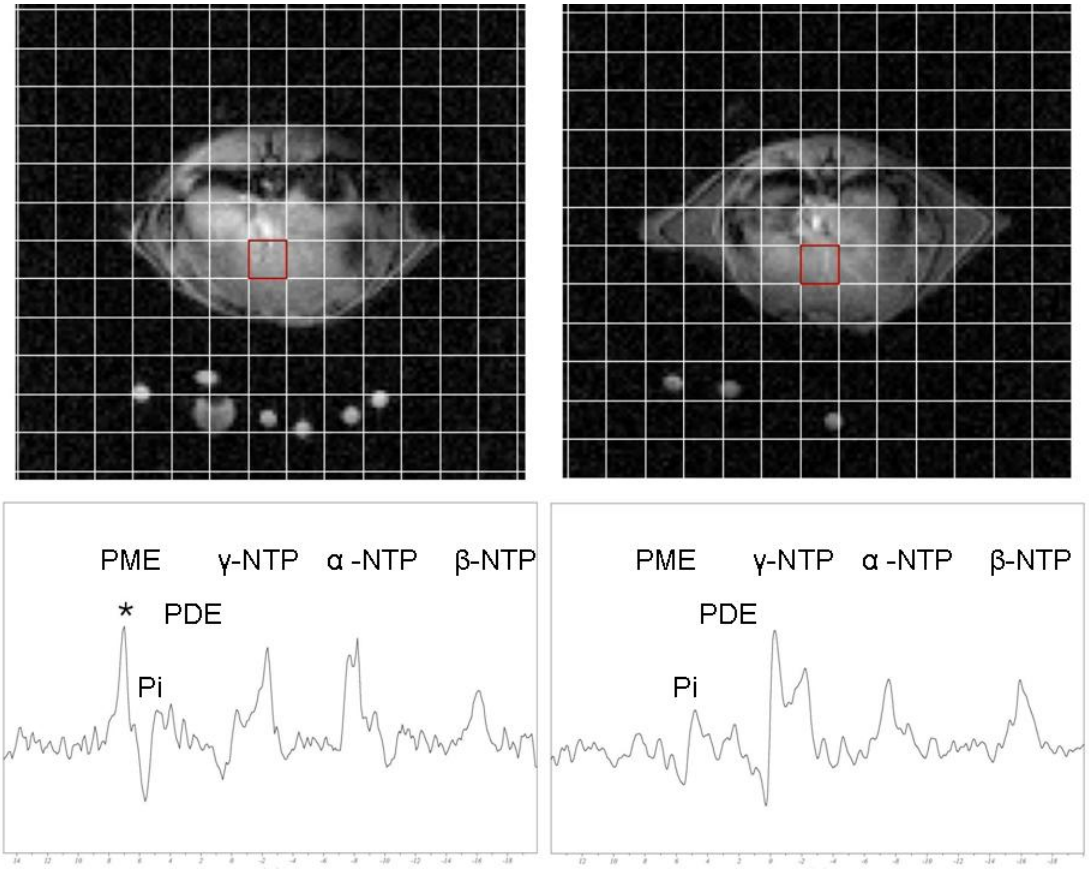
PME
γ-NTP
α -NTP
β-NTP
*
PDE
Pi
PME
γ-NTP
α -NTP
β-NTP
PDE
Pi

Figure 19. Axial FLASH MRI of woodchuck with HCC with corresponding ^{31}P 2D-CSI spectrum (left) and control woodchuck with HCC (right). Resonances in the spectrum include PME (7.5 ppm), Pi (4.8 ppm), PDE (2.2 ppm), PCr (0 ppm), γ-NTP (-2.2 ppm), α-NTP (-7.7 ppm), and β-NTP (-16.1 ppm)

Using WinNMR (Bruker Rheinstetten), the baseline was manually corrected prior to calculating the integrals of peak height by a Lorentzian curve. To reduce operator bias, the Lorentzian curve of each signal was calculated automatically. All signals were treated as singlets. The sum of the phosphorus signal (TotP) was calculated from the integrals of each phosphorus biomolecule (TotP=PME + Pi + PDE+ γ-NTP + α-NTP + β-NTP). Ratios of the integrals of peak height of PME, Pi, PDE, (α)-NTP, (γ)-NTP and β–NTP to TotP were calculated. This allowed for direct comparison of the ratios between woodchuck groups. PCr from the abdominal voxel directly below the liver was selected as the origin (at 0 ppm) as an internal standard because its chemical shift is not affected by pH, and the peak height is not affected by other phosphorus containing metabolites. All results are reported as the mean +/- standard error. Because of the small n value, standard error was used instead of standard deviation because five woodchucks do not accurately reflect a Normal distribution. Differences in relative concentrations between uninfected and chronically infected woodchucks were considered significant with a $p<0.05$ using a Mann-Whitney U test.

Results

Unlike in human hepatitis, woodchuck hepatitis is rarely cirrhotic (Michalak,1998); consequently, the differences in the ^{31}P MR spectra were due to HCC development not due to fibrosis. Resonances from PME (7.1 ppm), Pi (4.7 ppm), PDE (2.5 ppm), and three resonances of α (-7.5 ppm), β (-16.0 ppm), and γ-NTP (-2.1 ppm) were detected in both spectra from control woodchucks and those with advanced HCC. Small amounts of PCr can be detected as signal contamination from surrounding

abdominal muscle and were not included in the analysis. Ratios of phosphorus-containing metabolites to TotP were calculated for each woodchuck in two consecutive monthly imaging sessions prior to euthanasia. The ^{31}P MR spectra of chronically infected woodchucks with advanced hepatocellular carcinoma had a statistically significant increase in PME:TotP compared to controls (Figure 20). Woodchucks with HCC had an average PME/TotP of 0.157 +/- 0.01 while control woodchucks had a PME/TotP of 0.086 +/- 0.003 ($p<0.03$). Other phosphorus containing molecules were not significantly different between control and HCC (Figure 21).

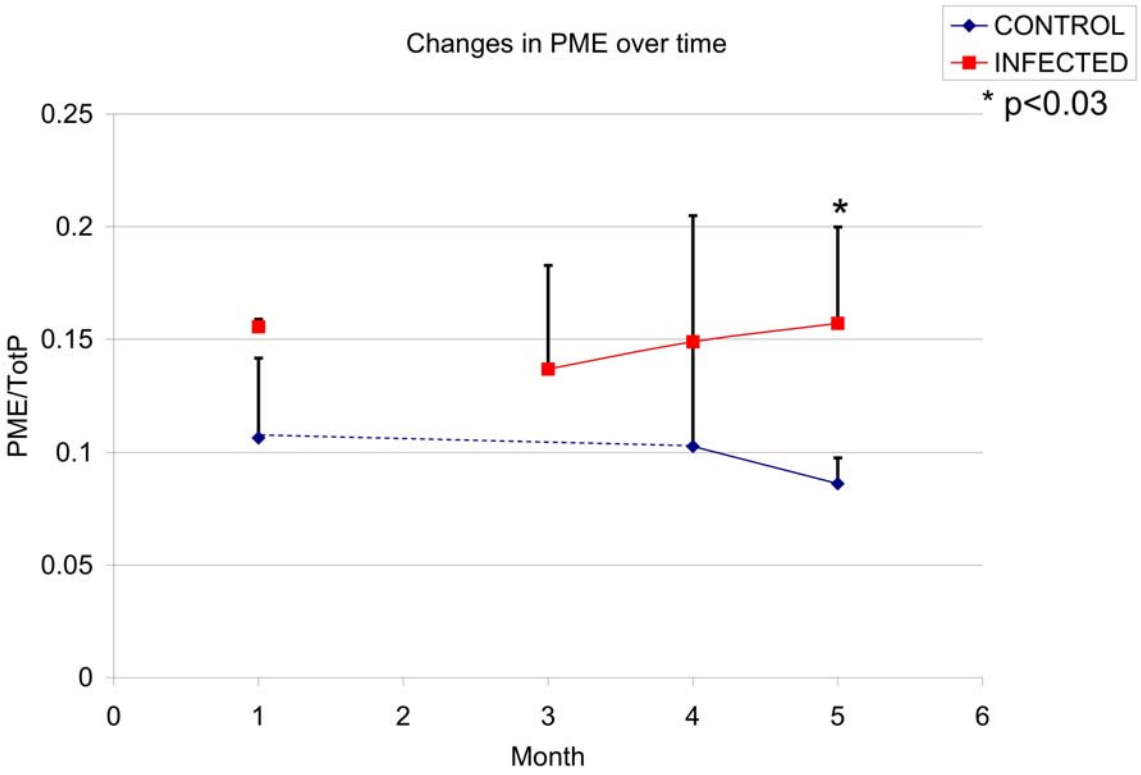
Changes in PME over time
CONTROL
INFECTED
* p<0.03
PME/TotP
0.25
0.2
0.15
0.1
0.05
0
0
1
2
3
4
5
6
Month
*

Figure 20. Changes in PME/TotP over time for infected woodchucks with HCC compared to uninfected woodchucks with healthy livers. The dashed line in the control data is extrapolated from data from the same control animals obtained from over three years of 2D-CSI. Uninfected woodchucks typically have a PME/TotP between 0.8-1.0, whereas woodchucks with HCC typically have PME/TotP greater than 0.14.

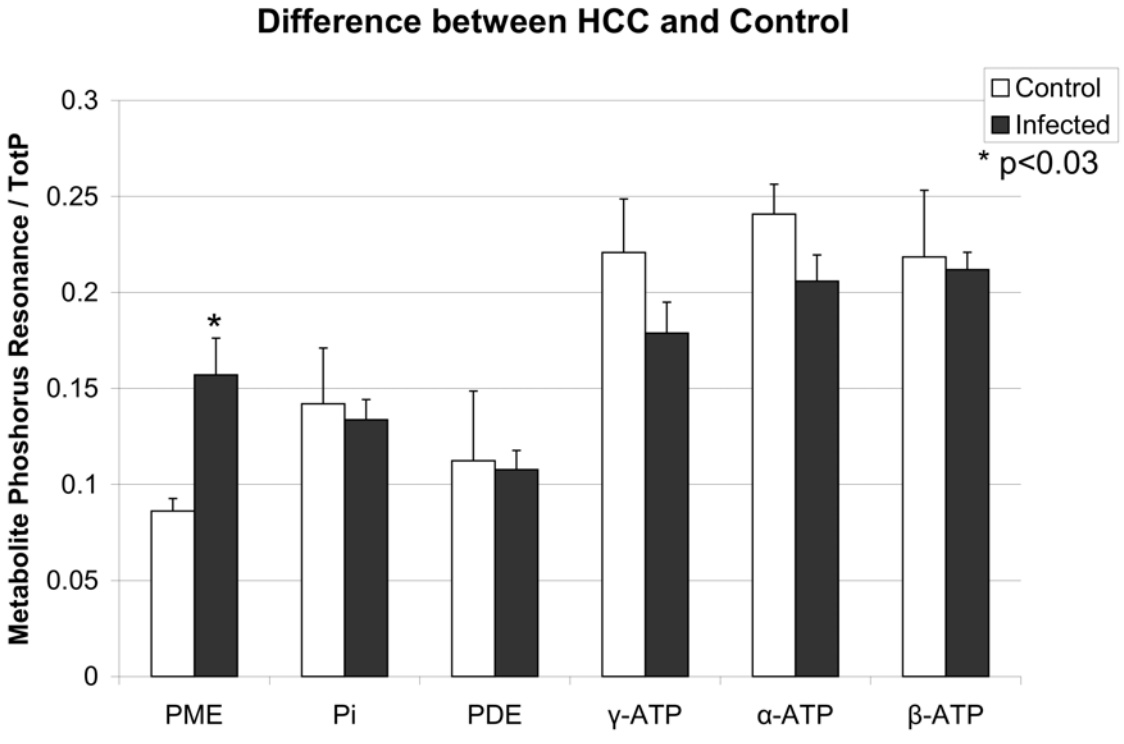
Difference between HCC and Control
Control
Infected
* p<0.03
Metabolite Phoshorus Resonance / TotP
0.3
0.25
0.2
0.15
0.1
0.05
0
*
PME
Pi
PDE
γ-ATP
α-ATP
β-ATP

Figure 21. PME is significantly elevated in the chronically infected woodchucks with HCC than in the uninfected woodchucks with normal livers. Other phosphorus containing molecules detected by ^{31}P-MRS were not significantly different between HCC and control livers.

Discussion

The PME signal contains resonances from adenosine monophosphate, phosphocholine (PC) and phosphoethanolamine (PE), the precursors to phosphatidylcholine and phosphatidylethanolamine used in the cell membranes (Corbin *et al*., 2002; Corbin *et al*., 2004; Cox *et al*., 1992a; Francis *et al*., 1991; Lim *et al*., 2003; Taylor-Robinson *et al*., 1998). GPC and GPE, along with adenosine diphosphate, contribute to the PDE signal (Glazer *et al*., 1989; Lim *et al*., 2003). In this study, the increase in the PME/TotP ratio in the livers of infected animal is similar to previously reported studies using ^{31}P-MRS to measure liver regeneration in partially hepatectomized rats (Campbell *et al*., 1990; Corbin *et al*., 2002) or comparing the ^{31}P spectrum of hepatocellular carcinoma in humans (Campbell *et al*., 1990; Francis *et al*., 1991; Glazer *et al*., 1989; Taylor-Robinson *et al*., 1998). An increase in PME/TotP is an indication of cellular proliferation and cell membrane synthesis.

Phosphorus spectroscopy has been shown as an effective method for non-invasive detection of a variety of different cancers including breast (Morse *et al*., 2007), pancreatic (Kaplan *et al*., 1997), and HCC (Cox *et al*., 1992b; Khan *et al*., 2005; McKenzie *et al*., 2005). The advantage to phosphorus spectroscopy is that it can simultaneously provide information about cellular growth and degradation, as well as tissue energetics. A characteristic feature of many solid tumours is the significant increase in phosphomonoester (PME) resonances, found between 7.2-8.0 ppm in the ^{31}P spectrum (Cox *et al*., 1992b; Khan *et al*., 2005; McKenzie *et al*., 2005). The PME peak is composed of signals from PC and PE that represent increased cell membrane synthesis, typical of the unregulated cellular proliferation found in cancer and liver regeneration

(Cox *et al*., 2006; Khan *et al*., 2005; Taylor-Robinson *et al*., 1998; Zakian *et al*., 2005). The resonances associated with the PDE peak, found between 3.0-3.5 ppm, result from the membrane degradation products GPC and GPE. The three resonances at -1.5 ppm, -6.5 ppm and -16 ppm represent the three phosphate groups of nucleotide triphosphate (γ, α, and β respectively) (McKenzie *et al*., 2005; Taylor-Robinson *et al*., 1998). Adenosine triphosphate represents the majority of the high energy triphosphate molecules; however there are still contributions to the resonance signals by other nucleotide triphosphates. The individual contributions from each nucleotide triphosphate can not be separated by phosphorus spectroscopy; therefore the NTP resonance represents the sum of all contributions from these molecules.

A reduction in PDE and an increase in Pi/β-NTP have been reported to be an indication of necrosis within a tumour (Campbell *et al*., 1990; Corbin *et al*., 2004; Cox *et al*., 1992a). The livers of infected woodchucks had similar levels of PDE/TotP and Pi/TotP to the control animals (Figure 21), which would infer that the tumour develops as a result of cellular proliferation without necrosis. There was also an increase in the amount of α-NTP/TotP in infected animals, especially in those animals with the highest GGT levels, however this increase was not statistically significant.

The pulse sequence used for 2D-CSI uses a repetition time of 1 second, which is less than the T_1 relaxation time of Pi (Malloy *et al*., 1986; Noseworthy *et al*., 1997). A TR greater than 4.2second would have allowed for complete relaxation of Pi, however, this would have significantly increased the total imaging time of the experiment and, by extension, the woodchuck's anaesthesia time. As a result of signal saturation, the peak height of Pi is less than the actual amount of Pi within the tissue. Because the same

sequence was used for every imaging session, the amount of signal saturation was assumed to be equal between groups, thus the Pi/TotP ratios are comparable; however no attempts were made to determine the pH of the liver tissue. It was expected that the pH of the tumour would be lower than normal tissue because regions in the centre of the tumour are poorly perfused and necrotic (Bhujwalla *et al*., 1999; Glazer *et al*., 1989; Malloy *et al*., 1986; Meyerhoff *et al*., 1992).

Chapter 4. Elevated phosphocholine detected by ^{31}P-NMR in the woodchuck model of HCC

All experiments, data analysis and manuscript preparation was performed by me with supervision from Dr. M.L.H.Gruwel.

Introduction

To confirm that increases in PME resonance detected *in vivo* is due to tumour growth, and not due to compensating regeneration, perchloric acid (PCA) extraction was performed on carefully selected frozen liver tissue samples excised at necropsy from the woodchucks that underwent 2D-CSI. The extracted samples were analyzed *ex vivo* using ^{31}P-NMR. *In vivo*, the PME resonance appears as a broad single peak at 6.9-7.2 ppm but is actually composed of resonances from PC and PE, which can only be differentiated *ex vivo* using high resolution ^{31}P-NMR spectroscopy. Similarly, PDE, a broad peak located at 3.0 ppm, is composed of resonances from glycerophosphocholine (GPC) and glycerophosphoethanolamine (GPE), which can be individually resolved using ^{31}P-NMR spectroscopy.

Material and Methods

Seronegative uninfected control and seropositive chronically infected woodchucks were purchased (Memorial University and Northeastern Wildlife respectively) and group housed in 9m x 13m Canadian Council of Animal Care approved rooms, as previously described (McKenzie *et al*., 2006).

Samples of the HCC were taken from the largest tumour of the chronically infected woodchucks (n=9). Samples of uninfected control woodchucks were taken from the largest lobe of the liver (n=5). The remaining portion of unused tissues were stored at -70°C until it was required for the replicate samples. All samples were prepared in triplicate from the same portion of frozen woodchuck liver. All chemicals used in this study were purchased from Sigma-Aldrich (Oakville, ON, Canada), unless mentioned otherwise.

Liver tissue was frozen at necropsy in liquid nitrogen and stored at -70°C prior to analysis. Portions of tissues (0.8g) were prepared for NMR analysis via PCA extraction by homogenizing with a mortar and pestle under liquid nitrogen (Le Belle *et al*., 2002; Thomas *et al*., 1994). The resulting powder was transferred to a ground glass homogenizer containing 3mL cold PCA (12%) and manually homogenized on ice. The slurry was centrifuged at 1200rpm (200g) for 10 minutes at 4°C (Daemon Clini-cool). The supernatant was collected and stored in a separate centrifuge tube while the pellet was resuspended with an additional 3mL of 12% PCA and centrifuged a second time. The two supernatants were combined and neutralized with 2M KOH to pH 7.4 on ice. After neutralization, the sample was centrifuged at 1200rpm for 10 minutes at 4°C to separate the water-soluble metabolites from the precipitate of potassium perchlorate ($KClO_4$) salt. Samples were frozen at -70°C for 24 hours prior to lyophilization.

The lyophilized powder was resuspended in 600µL of distilled water, shaken for 2 hours at room temperature, and the pH adjusted to 7.3 using 0.5M HCl. The solution was centrifuged at 3000rpm and stored at 4°C to allow further precipitation of potassium perchlorate salt. Using an Eppendorf pipette, 600µL of supernatant was transferred into

5mm NMR tubes (Wilmad™) containing an external reference of phenylphosphate (8.8mM) in D_2O within a sealed glass capillary tube. ^{31}P-NMR analysis was performed on an 8.4T Bruker Avance spectrometer using a one-pulse sequence with inverse gated decoupling (145.865MHz, a sweep width =11574.07Hz, number of scans=1024, a repetition time=5s, total acquisition time = 1hr 15minutes) using a 5mm multinuclear probehead.

The FID was reconstructed using a fast Fourier Transform (FFT) in XWinNMR (Bruker). A 1Hz line broadening was applied for exponential window function. Manual phase correction was performed relative to the PPA signal. Automatic baseline correction was applied before the integrals of peak heights were calculated. Peaks were assigned based on prior knowledge of the spectrum: PPA 18.5 ppm, PE 7.2 ppm, PC 6.8 ppm, inorganic phosphate (Pi) 5.8 ppm, GPE 4.0 ppm, GPC 3.4 ppm, α-NTP –7.3 ppm (Bell *et al*., 1993). All results are reported as the mean of the integrals from the three samples +/- standard deviation per gram of tissue (wet weight). All spectroscopic results were standardized relative to the wet weight of the tissue sample used to determine the integral of the resonance. Results were considered significant using a 2-tailed Student's t-test ($p<0.05$) with a Levene's test for variance (Statistica© 6.1, StatSoft Inc).

Results

All of the chronically infected woodchucks developed HCC that were confirmed histologically by pathologists (Drs. N. Pettigrew and J. Klein) unaware of the woodchucks' infectious status. Uninfected woodchucks did not have any significant liver disorders.

^{31}P-NMR of the PCA extracts contained resonances from PC, PE, Pi, GPC, GPE and small resonances α-NTP (Figure 22).

A)

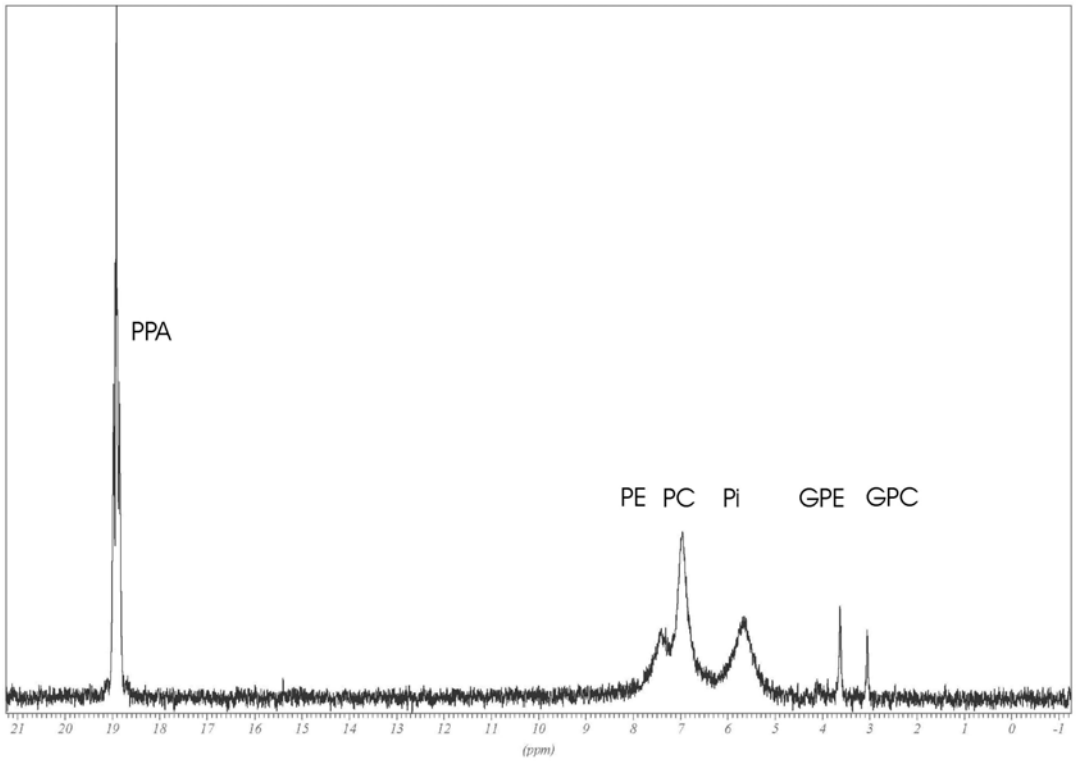
PPA
PE PC Pi GPE GPC
21 20 19 18 17 16 15 14 13 12 11 10 9 8 7 6 5 4 3 2 1 0 -1
(ppm)

B)

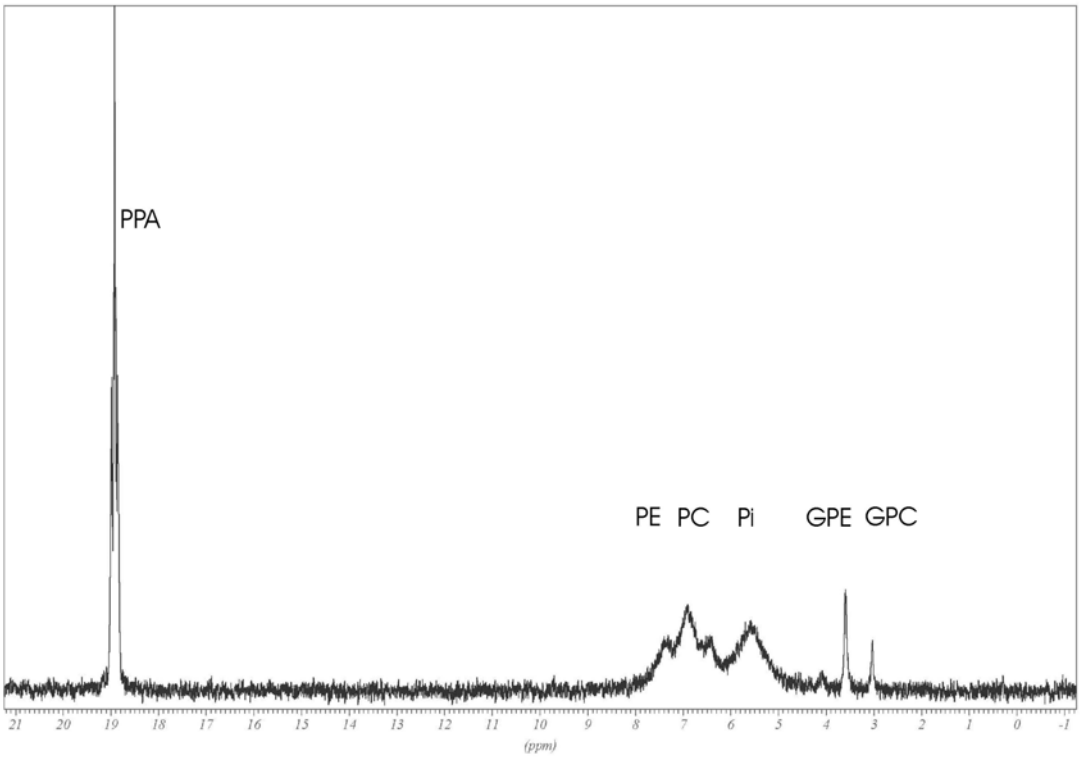
PPA
PE PC Pi GPE GPC
21 20 19 18 17 16 15 14 13 12 11 10 9 8 7 6 5 4 3 2 1 0 -1
(ppm)

Figure 22. Significant elevation in the PC resonance from HCC tissue (A) compared to uninfected control tissue (B). Other phosphorus containing molecules were not significantly different between HCC and control tissues. PPA (phenyl phosphoric acid) was used as an internal reference standard.

Samples obtained from HCC had significantly elevated PC (0.753+/-0.151 vs. 0.521+/-0.129, $p<0.01$) but not PE ($p=0.63$) (Figure 23). Elevations in PME, measured as the sum of PC and PE, approached significance in the HCC tissue compared to tissues from uninfected controls (1.19+/-0.246 vs. 0.919+/-0.211, $p=0.06$). Phosphodiesters, composed of resonances from glycerophosphoethanolamine (GPE) and glycerphosphocholine (GPC), represent cell membrane degradation typical of necrosis (Khan *et al*., 2005; Thomas *et al*., 1994). There was no significant difference in the concentration of GPE and GPC between HCC and control livers (0.313+/-0.239 vs. 0.212+/-0.08, $p=0.39$ and 0.128+/-0.065 vs. 0.101+/-0.04, $p=0.42$ respectively), indicating that there is not a significant amount of necrosis within the HCC.

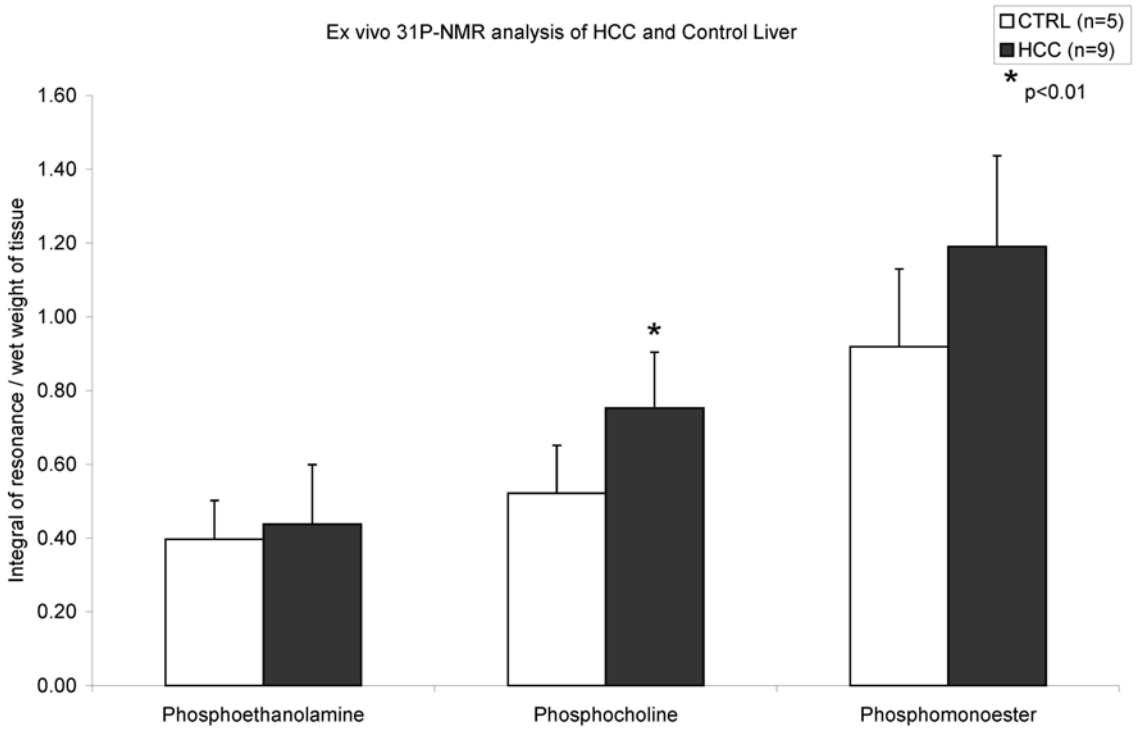
Ex vivo 31P-NMR analysis of HCC and Control Liver
CTRL (n=5)
HCC (n=9)
* p<0.01
Integral of resonance / wet weight of tissue
1.60
1.40
1.20
1.00
0.80
0.60
0.40
0.20
0.00
*
Phosphoethanolamine
Phosphocholine
Phosphomonoester

Figure 23. Significant elevations in PC but not PE were detected by ^{31}P-NMR. Elevations in PME, measured as the sum of PC+PE, approached significance ($p=0.06$).

Discussion

GPE and GPC were not significantly different between HCC and control, which is different than previously reported experiments of HCC and normal tissue where GPE and GPC were elevated in HCC, however this difference in results may be due to the area sampled from the HCC (Bell *et al*., 1998; Podo,1999). In this experiment, the exterior of the tumour at the interface with normal tissue was sampled for PCA extraction (Figure 9A). This region is still highly perfused with oxygen rich arterial blood and is not necrotic (Wang *et al*., 2005). Tissues within the core of the larger tumours are often necrotic due to diminished blood flow to the region. Had samples been taken from the core of the tumour, elevations in GPE and GPC may have been observed. Tumour tissue generally has a greater cellular density than surrounding normal tissue. Consequently, for similar tissue samples a general increase in signal amplitude for intracellular resonances could be observed. Our experiments clearly displayed an increase in the PC resonance in cancerous tissue with respect to other intracellular resonances (Figure 23)

The integral of the α-NTP resonance was analyzed and was not found to be significantly different between HCC and controls. Due to unavoidable delays in removal and sectioning of the organ during necropsy, post-mortem NTPase activity reduced the concentrations of β- and γ-NTP; consequently, γ- and β-NTP were not seen in significant quantities in the *ex vivo* ^{31}P-NMR spectrum. Had freeze-clamping been employed during necropsy, NTPase activity would have been minimal and total NTP concentrations would be more representative of *in vivo* conditions. Since tissue had to be carefully dissected for further analysis, it increased the time that the tissue was at room temperature and allowing enzymatic activity. The intent of this experiment was to determine which

phosphorylated biomolecule contributed to the increase in the phosphomonoester resonance, therefore the loss of NTP within the tissue was not considered consequential to the desired results.

CHAPTER 5.

Tumour growth continues despite positive immune response elicited by vaccinia-derived immunostimulant in the woodchuck model of HCC

All MRS experiments, data analysis, and manuscript preparation was performed by me with supervision from Dr. M.L.H.Gruwel. Preparation of the vaccinia construct and RT-PCR was performed by Yvon Deschambault with supervision from Dr. J. Cao.

Introduction

After developing a technique that can detect significant differences in the phosphorus spectrum of tumour tissue compared to uninfected healthy control livers, the efficacy of a therapeutic vaccine in the prevention of tumour formation was evaluated in chronically infected woodchucks over a six month period. Changes in liver enzymes, viral load and viral protein expression (WHsAg) were followed using serology. All results were compared to the same uninfected woodchucks from the first project (n=5).

The development of chronic viral hepatitis is a consequence of a deficient cytotoxic T-lymphocyte response against infected hepatocytes expressing viral antigens: core (WHcAg) and surface (WHsAg) proteins (Frank *et al*., 2007; Lu *et al*., 2001; Menne *et al*., 2002). The nucleocapsid is composed of WHc proteins. Although WHc are highly immunogenic, they are typically hidden from the immune system because the nucleocapsid is surrounded by host derived membranes which contain high concentrations of WHsAg. The nucleocapsid is exposed only once the virus has infected a cell, at which point, circulating immunoglobulins can not bind to it and initiate an immune response. Anti-WHc antibodies may develop if epitopes of WHc are presented to

the immune system by professional antigen presenting cells, such as B cells. WHc is highly immunogenic; however anti-WHc antibodies are non-neutralizing and do not prevent an infection (Zhang *et al*., 2006). Rather than an WHc-specific antibody-mediated response, a robust and multi-specific cytotoxic T-lymphocyte response against WHc is strongly associated with viral clearance and recovery from acute infection (Lu *et al*., 2001; Menne *et al*., 1997; Roos *et al*., 1989). Woodchucks vaccinated against WHc before being exposed to WHV had significantly higher concentration of WHc-specific cytotoxic T-lymphocytes in the blood if the infection was resolved than did woodchucks that developed chronic infection (Garcia-Navarro *et al*., 2001).

Heat shock proteins (HSPs) can chaperone a protein to the immune system, and initiate a cytotoxic T-lymphocyte-mediated immune response without the use of adjuvants (Suto *et. al*., 1996). By conjugating HSPs to WHc, T-lymphocytes would be primed to recognize and destroy those hepatocytes expressing WHc. Infected hepatocytes with the potential to initiate carcinogenesis would be eliminated. Intramuscular injections of plasmids expressing WHcAg DNA preferentially stimulate a Th1 immune response against the virus (Lu *et al*., 2005). Fusing WHcAg to another immunogen like cytotoxic T lymphocyte associated protein-4 elicits both a Th1 and a Th2 immune response, thereby creating both cytotoxic T lymphocytes that recognize and destroy virally infected cells, as well as antibodies against core antigen (Lu *et al*., 2005).

Replication deficient highly attenuated vaccinia virus (MVA) was used as an expression vector for an HSP70-WHc fusion protein by inserting the genes for both *M. tuberculosis* HSP70 and WHc in place of vaccinia's thymidine kinase genes. MVA was used because it can accommodate the insertion of large portions of foreign genes and

express the proteins encoded by the inserted genes. MVA acts as a vector by producing the immunotherapeutic (in this case, the conjugate protein HSP70-WHc) but the MVA is unable to reproduce. This reduces some of the safety concerns about handling vaccinia virus, especially with people who have not or are unable to receive the smallpox vaccine. The thymidine kinase region was chosen as the insertion site because that region is not necessary for MVA to replicate in a cell culture and it is a region that is genetically stable, that is, unlikely to mutate as the virus is passaged in culture (Scheiflinger *et al.*, 1996). HSP70 from *M. tuberculosis* was chosen because it contains both B and T cell epitopes to stimulate both arms of the immune system. Additionally, any protein can be fused to the amino terminus region of HSP70 and can elicit higher titres of antibodies to the fused protein (Suzue *et al.*, 1996). HSP70 would act as an adjuvant.

Materials and Methods

Similar to the infected woodchucks used in the first phase of this project, woodchucks (n=5) that had been infected within 7 days after birth with WHV were purchased and delivered (NorthEastern Wildlife, New York) when serological tests confirmed chronic infection. The male woodchucks were delivered to our facility at an average age of 595 days +/- 7.4. They were housed and cared for as previously described in Chapter 2. The same uninfected woodchucks from the first phase of this project were used for these experiments, despite being older than the infected woodchucks.

Using Clontech's Advantage HF PCR kit (Cat No. 639123) the *MycobacteriumTuberculosis* heat-shock protein 70 (HSP70) gene was amplified using primers HSP70_N (TAATCATATGGCTCGTGCGGTCGGGATC) and HSP70_C

(TTAACCCGGGTCACTTGGCCTCCCGGCCGT). HSP70 was subsequently cloned into Novagen's pT7blue2 perfectly blunt vector (Cat No. 70185). Positive colonies were sequenced in-house for sequence confirmation and orientation. The gene encoding WHV core protein (WHc) was amplified with the Advantage HF PCR kit and the following primers: WHc_N (TAATCTCGAGATGGACATAGATCCCTATAAAG), WHcCt (TATACCCGGGTCAGCAGTTGGCAGATGGAGATT) with the stop codon and WHcCNt (TGAGCATATGGCAGTTGGCAGATGGAGATT) without the stop codon. Both WHcCt and WHcCNt genes were cloned into Clontech's Topo 2.1 vector (Cat No. K4500-40) and sequenced. WHc (with stop codon) was digested out with XhoI/SmaI and ligated into pJS5 (NheI(blunt)/XhoI/CIP). WHc_Nt (without stop codon) was digested out with XhoI/NdeI and ligated into pT7blue2/HSP70 (XhoI/NdeI/CIP). Positive colonies were sequenced to ensure that both WHc and HSP70 genes were intact and in frame. WHc_HSP70 cassette was digested out with XhoI/NheI(blunt) and ligated into pJS5 (NheI(blunt)/XhoI/CIP). Positive pJS5/WHc_HSP70 constructs were transfected with Qiagen's Effectene reagent (Cat No. 301425) into BHK21 cells pre-infected with Modified Vaccinia Ankara (MVA). Utilising the thymidine kinase flanking regions of pJS5 for homologous recombination with guanine phosphoribosyl transferase, recombinant MVA expressing WHc and WHc_HSP70 proteins were selected. Western blot confirmed expression of both proteins.

Three chronically infected woodchucks were vaccinated once a month for four consecutive months through intramuscular injections of 0.2mL of MVA expressing the fusion protein HSP70-WHcAg. Two remaining chronically infected woodchucks were injected with vaccinia only. However, one woodchuck died during imaging early in the

experiment due to a failure of the anaesthesia equipment. The remaining woodchuck injected with vaccinia alone survived and developed HCC. However, the results of the remaining positive control woodchuck will not be discussed in this paper as no significant conclusion can be made from a single animal.

The woodchucks were imaged as previously described in Chapter 3. Serological samples were taken prior to monthly imaging and analyzed as described in Chapter 2.

Woodchucks were euthanized using an intravenous overdose of Euthanyl when liver tumours were palpable and GGT concentrations exceeded 100 IU/L. Previous studies showed that GGT elevations in excess of 100 IU/L was high enough to confirm HCC and that euthanizing the woodchucks at this GGT level was more humane to the woodchuck than waiting for additional liver damage to occur with larger HCC and GGT greater than 100 IU/L.

Upon necropsy, the liver was removed and portions were fixed in 10% buffered neutral formalin for paraffin embedding. The paraffin embedded tissues were sectioned at 7μm and stained with haematoxylin and eosin Y (Sigma-Aldrich, Oakville, ON, Canada) for further histological examination by light microscopy by a pathologist (Dr. N. Pettigrew).

All results are reported as the mean +/- standard error. Differences between uninfected and infected woodchucks were considered significant with a $p < 0.05$ using a Mann-Whitney U test (STATISTICA 6, StatSoft, Inc. Tulsa, USA).

Results

Prior to vaccination, chronically infected woodchucks had an average viral load of $8.93x10^7$ +/- $3.11x10^7$ copies/uL. After the final vaccination, the viral load of the treated woodchucks had decreased to $7.75x10^5$ +/-$6.85x10^5$ copies/uL (Figure 24). As was found in previous experiments, the uninfected woodchucks had an average viral load of 188.12 +/-196.0 copies/uL. Any serum from uninfected woodchucks that had detectable viral load was retested from a back-up vial of serum stored at -20°C. The results are reported as the average of the two tests because there was not enough serum to test a third time.

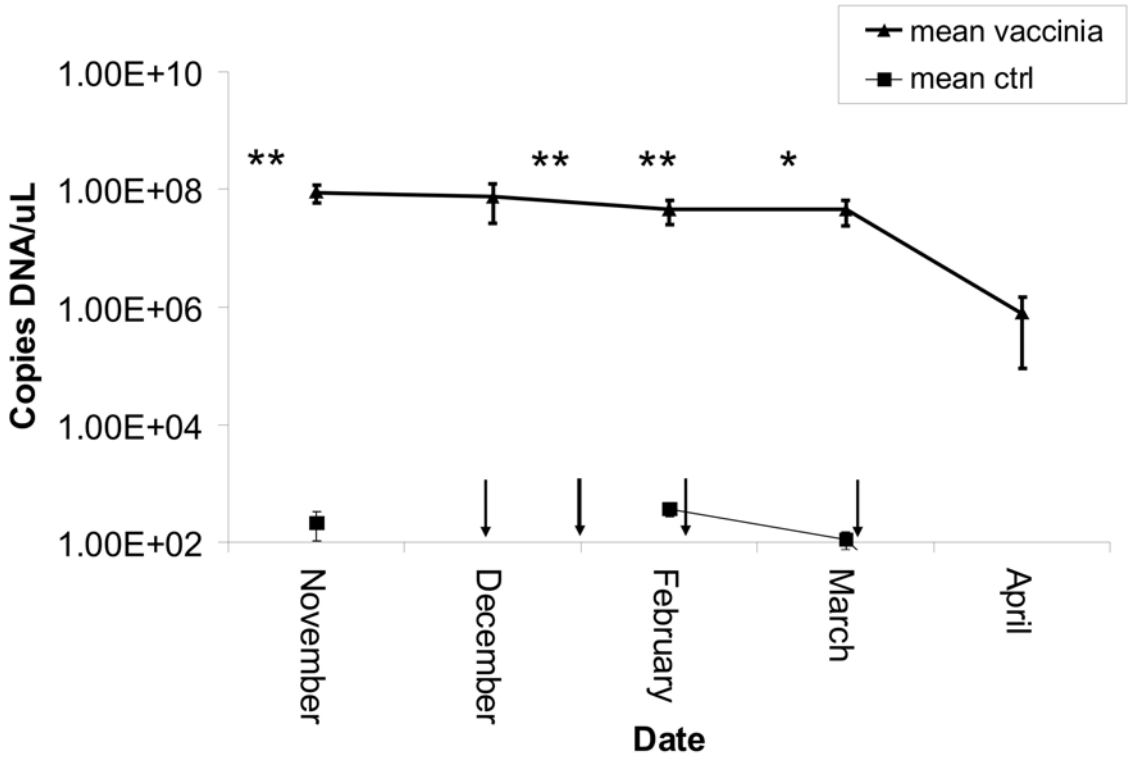
mean vaccinia
mean ctrl
1.00E+10
1.00E+08
1.00E+06
1.00E+04
1.00E+02
Copies DNA/uL
**
**
**
*
November
December
February
March
April
Date

Figure 24. Changes in viral load over time, as measured by RT-PCR, in the chronically infected woodchucks (n=5). Blood from uninfected woodchucks (n=4) was also analyzed for the presence of WHV but tested negative. Times of vaccinations are indicated with arrows. All calculated reported as mean +/- standard error. *$p<0.04$, *$p<0.008$.

A reduction in WHsAg expression from 10.58+/-3.31 to 4.71+/-0.16 was detected in the treated woodchucks during the vaccination period (Figure 25). One month after the final vaccination, slight increases in both viral load and WHsAg were detected in the treated woodchucks, but were not significant. The WHsAg expression increased to 6.40+/-0.40 after the final vaccination while the viral load increased to $1.01x10^6$ copies/μL $+/-8.00x10^5$ (data not included on Figure 24).

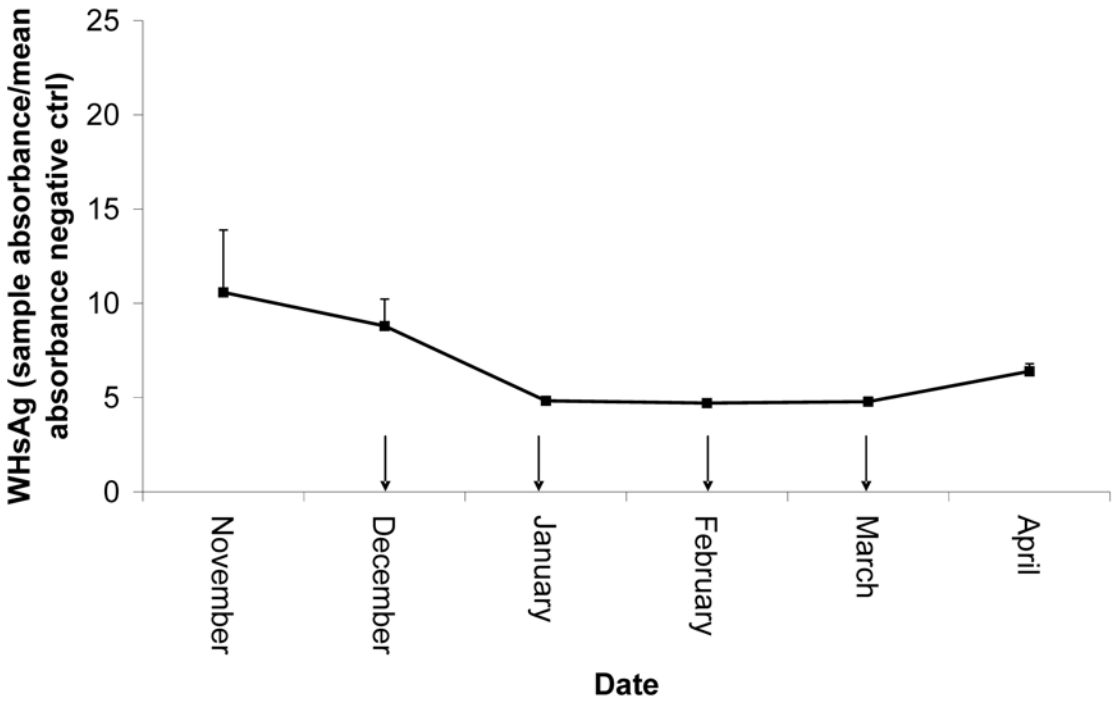
WHsAg (sample absorbance/mean absorbance negative ctrl)
25
20
15
10
5
0
November
December
January
February
March
April
Date

Figure 25. WHsAg measured by sandwich ELISA. Decreases in expression of viral surface proteins can be seen during the vaccination period. Times of vaccination are indicated with arrows. All calculations reported as mean +/- standard error. Error bars have been included but are too small to be visible.

Serum concentration of GGT prior to vaccination and throughout the experiment was significantly elevated in vaccinated woodchucks compared to uninfected woodchucks ($p < 0.02$). Chronically infected woodchucks had a serum GGT concentration of 31.83 +/- 7.59 IU/L prior to vaccination. After vaccination, infected woodchucks had a serum GGT concentration of 26.67 +/- 6.82 IU/L. The initial serum GGT concentration of uninfected woodchucks was 5.67 +/- 0.82 IU/L. At the end of the experiment, uninfected woodchucks had a serum GGT concentration of 5.00 +/- 0.0 IU/L. Serum was also tested for two other liver enzymes that indicate liver injury and inflammation: ALT and AST. Neither were significantly elevated in infected woodchucks compared to uninfected woodchucks throughout the entire experiment ($p < 0.057$ and $p < 0.125$ respectively).

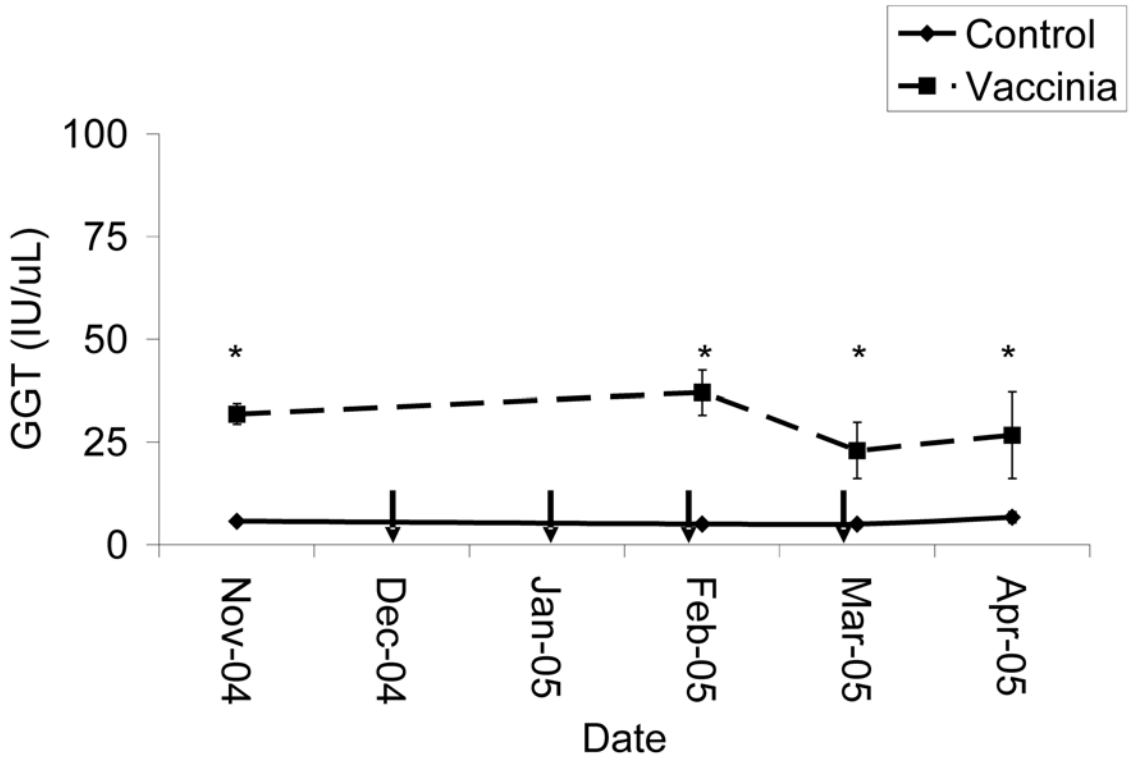
Control
Vaccinia
100
75
50
25
0
GGT (IU/uL)
*
*
*
*
Nov-04
Dec-04
Jan-05
Feb-05
Mar-05
Apr-05
Date

Figure 26. Change in GGT over time for woodchucks treated with WHc-HSP conjugate protein. Black arrows indicate when vaccinia treatments were administered.

Monthly ^{1}H imaging and ^{31}P spectroscopy of woodchuck livers indicated that PME resonances of infected woodchucks were significantly elevated throughout the vaccinations (Figure 28). Other biomolecules detected by phosphorus spectroscopy including Pi, γ-,α-, and β-NTP were not significantly different in the vaccinated woodchucks compared to the uninfected woodchucks (Figure 28).

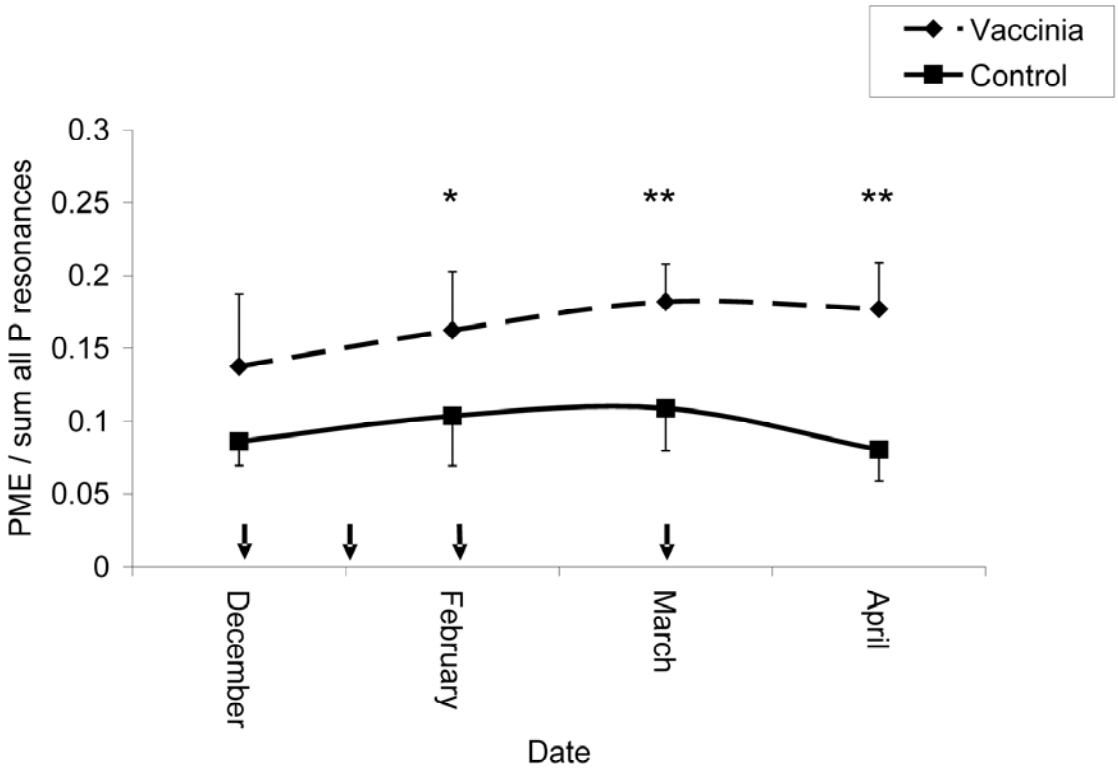
Vaccinia
Control
PME / sum all P resonances
0.3
0.25
0.2
0.15
0.1
0.05
0
*
**
**
December
February
March
April
Date

Figure 27. Average PME resonance for vaccinated woodchucks compared to uninfected. Times of vaccinations are indicated with arrows. All calculations reported as mean +/- standard error. *$p<0.04$ **$p<0.006$

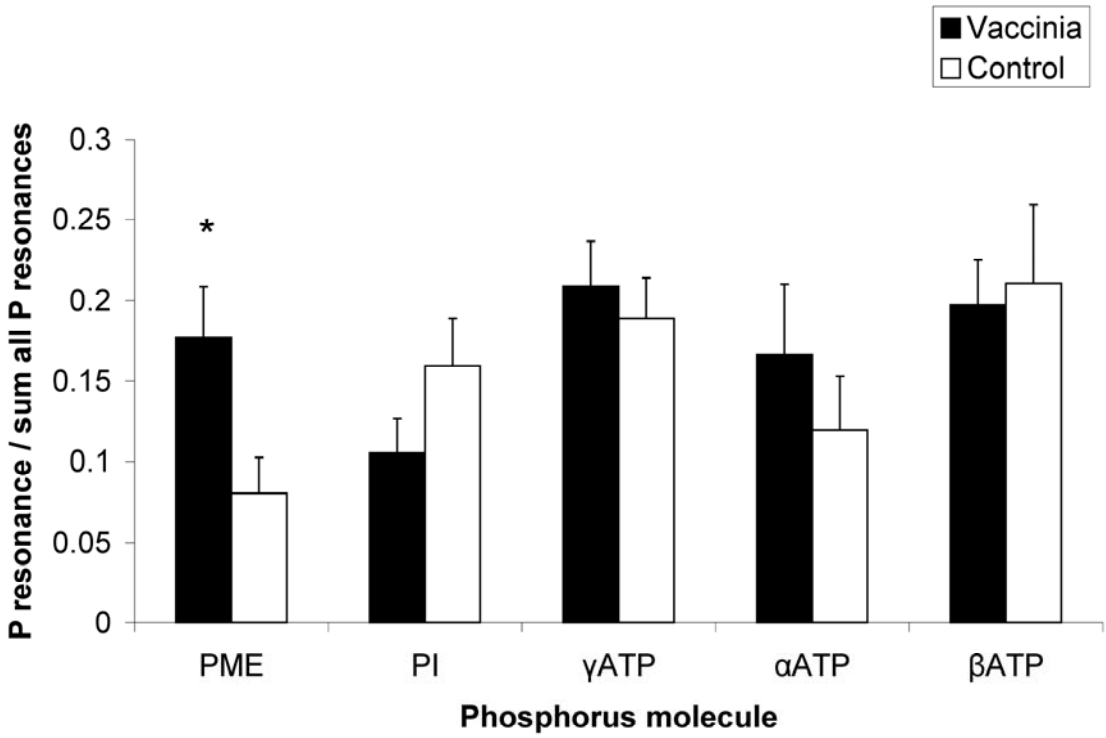
Vaccinia
Control
P resonance / sum all P resonances
0.3
0.25
0.2
0.15
0.1
0.05
0
*
PME
PI
γATP
αATP
βATP
Phosphorus molecule

Figure 28. Elevation in PME resonance was the only phosphorus-containing molecule which was significant different than the uninfected woodchucks (*$p<0.04$). Although α-ATP appears elevated, it did not reach significance ($p<0.06$). All calculations reported as mean +/- standard error.

The pathologist (Dr. N. Pettigrew) confirmed that HCC was found only in infected woodchucks after reviewing stained paraffin-embedded slides by light microscopy. HCC contained regions of hyper-vascularization, alterations to normal parenchyma arrangement, multinucleated hepatocytes, and lymphocytic infiltration typical of HCC. Uninfected woodchucks had normal liver histology.

Figure 29. Picture of HCC in a vaccinia-treated woodchuck at necropsy. Tumours have been highlighted with white arrows. The HCC seen in these woodchucks are similar in size and appearance to the HCC seen in published images (Salem *et al*., 2007).

Discussion

Despite the reduction in viral load, WHsAg and normal liver enzyme values in infected animals, carcinogenesis nevertheless progressed. The PME resonance and GGT were elevated prior to the initial vaccination, suggesting that small HCC may have been present in the livers of infected woodchucks. HCC growth could be detected by ^{31}P-MRS, as evidenced by the elevated PME resonances that remained elevated relative to uninfected woodchucks throughout the course of the vaccinations. PME in the vaccinated woodchucks is not significantly different than previously reported measurements in untreated, chronically infected woodchucks with HCC (McKenzie *et al*., 2005).

Post-exposure vaccinations of chronically infected woodchucks with MVA encoding for the fusion protein HSP70-WHcAg elicited an immune response as evidenced by a decrease in both WHsAg expression and viral load. The decrease in serum concentrations of WHsAg also suggests that viral replication was reduced. The serological data indicates that there was little inflammation and damage to the liver of vaccinated woodchucks suggesting that liver function was not significantly altered in the vaccinated woodchucks. Elevated serum concentrations of GGT has been reported as serum indicators of hepatocyte injury and HCC (Hornbuckle *et al*., 1985; McKenzie *et al*., 2005; McKenzie *et al*., 2006; Toshkov *et al*., 1990). GGT of treated woodchucks was elevated throughout the vaccination period relative to the uninfected woodchucks, but was lower than previously reported for chronically infected woodchucks (McKenzie *et al*., 2005). Viral load and WHsAg concentrations of the vaccinated woodchucks were also lower than previously reported for infected woodchucks, due to the younger age of woodchucks used in this experiment (McKenzie *et al*., 2005).

Chapter 6. Conclusion

These experiments were the first of their kind to use MRI and ^{31}P-MRS to image woodchucks on a monthly basis and to correlate the development of HCC to a specific biomarker in the ^{31}P spectrum. Previous MR studies were acute where the woodchucks were euthanized after imaging was completed (Putzer *et al*., 2001). By using the same woodchucks in longitudinal studies, results due to tumour growth can be correlated to an individual animal and serological test each time. Through the use of non-invasive techniques, the same animals can be imaged repeatedly allowing the natural progression of the malignant tumour to be followed regularly. Because MRI is noninvasive, fewer woodchucks are needed thus reducing the total number of animals required for a multiyear project. Repeated invasive surgical procedures and lengthy recovery times are unnecessary to monitor tumour growth, and with the model described in this work, tumour growth occurs as it would in nature. Changes in GGT, AST, viral load, tumour growth, weight, and behaviour can be monitored to better characterize the disease progress in individual animals. Compared with ultrasonography, ^{31}P-MRS allows for better characterization of tissues changes within the entire liver. Unlike computed tomography, MRI does not use x-rays to acquire images. Monthly computed tomography would pose a health risk to the animals from frequent exposure to radiation. To date, there has not been any permanent effect on the woodchucks due to repeated MRI or lengthy anaesthesia times. Control woodchucks survived for more than three years without HCC development.

The first set of experiments showed that woodchucks chronically infected with WHV develop HCC within 2 years post-infection. The development of HCC can be

monitored *in vivo* with ^{31}P-MRS by elevations in the PME/TotP resonance. Woodchucks with HCC had an average PME/TotP of 0.157 +/- 0.01 while control woodchucks had a PME/TotP of 0.086 +/- 0.003 ($p<0.04$).

In these experiments, only PME/TotP was elevated in the woodchucks with HCC. Spectroscopic features such as the elevated Pi and decreased NTP typical of liver regeneration and cirrhosis were not seen. What is being detected in the tumour-bearing woodchucks is cellular proliferation, because of the elevated PME, but this is not due to regeneration. There were no significant differences between the NTP and Pi resonances in the phosphorus spectrum of uninfected woodchucks and those with HCC. Histologically, there is evidence of fibrotic deposits within the tumours but this process is not the same as cirrhosis and can be confirmed by the different spectroscopic patterns seen both *in vivo* and *ex vivo* compared to published patterns of other liver diseases.

Elevated PME has been correlated to tumour growth *in vivo* in liver (Bell *et al*., 1993; Griffiths *et al*., 2002; Khan *et al*., 2005; McKenzie *et al*., 2005; Thomas *et al*., 1994), breast (Beloueche-Babari *et al*., 2006; Morse *et al*., 2007), and brain cancers (Payne *et al*., 2006). High rates of cellular replication are characteristic of the unregulated cellular proliferation within tumour tissue that is not present in normal tissue. The PME peak is composed of resonances from phosphoethanolamine (PE) and phosphocholine (PC), precursor metabolites of the membrane phospholipids phosphatidylcholine and phosphatidylethanolamine (Bell *et al*., 1993; Khan *et al*., 2005; Payne *et al*., 2006; Thomas *et al*., 1994). *Ex vivo* analysis of excised HCC tissues by perchloric acid extraction demonstrates that increases in PC cause the PME resonance elevations that were detected *in vivo* by ^{31}P-MRS. In the study described in Chapter 4, HCC has an

average relative PC resonance integral of 0.627 +/- 0.04 whereas control tissue has a significantly lower average relative PC resonance integral of 0.441 +/-0.05 ($p<0.02$). The analyzed samples were taken directly from HCC tissue, confirming that PC elevations occur as a result of malignant growth and not due to other hepatic lesions. PC is a component of the cell membrane and high concentrations within a cell can stimulate mitosis by simply increasing PC concentrations in a cell (Glunde *et al*., 2006b). Elevated PC in tumour tissue is due primarily to increased choline kinase activity via CDP-choline pathway (Glunde *et al*., 2006b; Payne *et al*., 2006), however other sources of PC are also due to degradation of membrane phosphatidylcholine to PC via phosphatidylcholine-specific phospholipase C (Glunde *et al*., 2006b), increased choline transport into cells, and/or the activity of CTP:PC cytidylyltransferase (Beloueche-Babari *et al*., 2006; Thomas *et al*., 1994).

Liver injury can be measured through serology with significant elevations in GGT and AST. Infected woodchucks with HCC had significantly higher serum concentrations of GGT and AST throughout the experimental period. Elevations in GGT and AST did not correlate to viral load or to changes in the PME resonance but they are serum markers of tumour growth. Significantly elevated viral load confirmed that the chronically infected woodchucks were infected with woodchuck hepatitis virus that they never recovered from.

The final experiment described in Chapter 5 confirmed that tumour growth can be detected in the earliest stages and that using a combination of serological monitoring and *in vivo* phosphorus spectroscopy of the liver during chronic infection to obtain the most accurate representation of liver damage and immune function as possible. Although an

immune response was elicited in the woodchucks treated with vaccinia-fusion protein, it was not sufficient to prevent the development of large HCC in the woodchucks. The immune response elicited by the MVA-based vaccine may have delayed further viral activity, but could not reverse pre-existing tumours present prior to vaccination. Hepatocytes within an HCC are typically WHcAg-negative while surrounding infected hepatocytes are WHcAg positive (Xu *et al*., 2006). These WHcAg-positive hepatocytes surrounding the HCC would be targeted by T-cells stimulated by the MVA-based vaccine, while WHcAg-negative hepatocytes would not. Localized proliferation of transformed WHcAg-negative hepatocytes can lead to tumourgenesis without interference from the immune system. An immune response against the virus was evident by the decrease in viral load and a decrease in serum WHsAg (Figures 25 & 26), however, tumour growth was still detected by elevations in PME and GGT. PME was elevated in the chronically infected woodchucks prior to the vaccinations, indicating that HCC was already present in these woodchucks. Tumour growth continued unchecked because the anti-viral immune response does not target cancerous cells, only those cells expressing WHcAg. Cancerous hepatocytes do not necessarily have to be infected with the virus; the transformed hepatocytes may be the progeny of previously infected hepatocytes. Consequently, the transformed hepatocytes will continue to proliferate in the HCC, but lack any infectious virus. This novel therapeutic would be better utilized in younger woodchucks without pre-existing HCC or be administered prior to exposure to the virus.

^{31}P-MRS was able to detect the growth of liver tumours, whilst serum analysis alone would have suggested that the vaccinations might have been effective in reducing

hepatitis, liver damage and viral load, and hence a reduced likelihood of developing HCCs. Our study shows the effectiveness of utilizing a dual approach to determine the efficacy of a novel therapeutic vaccine by simultaneously characterizing *in vivo* carcinogenesis in the liver in addition to monitoring changes to the viral load and WHsAg. This multi-model strategy can be used to follow changes in tissue growth, while simultaneously demonstrating a positive immune response to vaccination.

Further study into the effects of vaccinia-derived immunostimulation is warranted given the positive results seen in this study. Additional woodchucks would be required to determine vaccinia's efficacy. Two additional groups of woodchucks would be required: a positive control group receiving only vaccinia ensures that the immune response is due to the WHcAg-HSP70 and not to vaccinia, and a negative control group of age-matched chronically infected woodchucks to compare the changes in viral load, GGT, WHsAg and tumour development without treatment. It is recommended that all groups of woodchucks be obtained from the same source and be the same age. Antibody assays using woodchuck specific antibodies against WHc and WHs should be performed on the serum to determine any changes to antibody titres during treatment. As stated previously, commercially available cross-reactive antibodies are not specific enough for antibody-mediated assays like ELISA.

Isoflurane was used as an anaesthetic because it provides deep-plane anaesthesia with better control and faster recovery than injectable sedatives such as ketamine–xylazine(Abe *et al*., 1988; Bellezza *et. al*., 2002; Dahmen *et al*., 2002; Hornbuckle *et al*., 1985; Putzer *et al*., 2001; Reimer *et al*., 1991) and sodium pentobarbital.(Nada *et al*., 1997; Noyes *et al*., 1975; Putzer *et al*., 2001) Premedication prior to imaging was

unnecessary, due to the use of the induction chamber. Chronic experiments on the same animals would require monthly intramuscular injections of ketamine–xylazine, which can lead to permanent damage to muscle tissue and potential tolerance to the drugs used (Bellezza *et. al*., 2002). In addition, the woodchucks were placed in the center of a 4-m long MRI system for periods in excess of 2 hours; repeated intramuscular injections during imaging or 2 m of intravenous tubing would not be feasible. In light of the already decreased liver function of infected woodchucks, halothane was not used due to its toxicity to the liver. We found that bimonthly blood draws increase the likelihood of scar tissue in the hind paws, resulting in poor blood collection.

T_1- and T_2-weighted imaging requires that image acquisition occurs at fixed time intervals determined by the TR and the TE. Images of the liver are normally acquired when the patient is either breath-holding or when the patient is breathing predictably, so that the liver is in the same position in the magnet every time an image is taken. If an imaging sequence requires 16 averages, 16 images of the liver must be taken and the liver must be at the same place for every one of those 16 images. In the experiments presented in this work, the woodchucks were not ventilated and their breathing was irregular. Image acquisition could not be gated to the ventilation so T_1- and T_2- imaging that are standard to human diagnostic imaging could not be used with the woodchucks. Intubation of a woodchuck is too invasive a procedure to be done every month. Scar tissue formation in the throat, visibility of the vocal cords for intubation, the bite capacity of the woodchucks to severe the ventilation tube were all concerns that prevented the use of mechanical ventilation and image acquisition gated to the ventilation.

Contrast between two tissues can also be improved by using contrast agents, or paramagnetic substances like gadolinium (Magnavist™) which shortens T_1 and T_2. Contrast agents are usually administered through intravenous injections and can enhance vasculature by highlighting accumulations of blood, so called "blood-pool contrast agents". Contrast agents were not used with the woodchucks for a number of reasons. Primarily, repeated implantation of a venous catheter into the foot of the woodchuck represents a significantly invasive procedure with a high risk of developing scar tissue. Secondly, because of the difficulty in obtaining T_1- and T_2-imaging due to irregular breathing patterns of the woodchucks, contrast agents were not used because they would not significantly enhance the scout GEFI images that were acquired. The intent of this project was to use non-invasive means to follow tumour growth over time, therefore implanting a catheter each month would not fit with the intent of the project. Finally, the vasculature of the lower limbs does not allow for repeated implantation of a venous catheter. The largest and easily accessible veins are found within the muscles of the calves, between the lower paws and the knee. Exposing this vein is an acute surgical procedure and it would not be ethical to allow the woodchuck to recover from it.

Higher quality images could be obtained from the T_2 imaging that could follow tumour growth more effectively than with GEFI imaging. Phosphorus spectroscopy provides the best information about the biochemical changes of tumour growth over time. The imaging strategy that was employed for the phosphorus spectroscopy provided the average phosphorus spectrum contained within the $8cm^3$ volume of the voxel. Had smaller voxels been used, more information about where the HCC and normal tissues are located could have been determined; however, smaller voxels would have required longer

imaging time. This means that the woodchucks would have to be anaesthetised longer, potentially harming the animals. The protocol mandated that total anaesthesia time be less than 3 hours from the induction until recovery. Although smaller voxels would be more useful in determining HCC location, it would have increased the likelihood that the woodchuck may die during imaging from isoflurane overdose, especially during the winter months when rates of respiration are lowest.

The project demonstrates the importance of using the PME to determine cancerous growth in woodchucks and could be used to screen humans chronically infected with HBV who are at high risk for developing HCC. Phosphocholine represents a novel target for future therapeutics that may interfere with a cancerous cells' ability to utilize PC for replication, thereby limiting tumour growth and allowing for recovery.

Chapter 7. Future Directions

These experiments better represent screening that could be performed on humans. Serological testing is minimally invasive and ^{31}P-MRS is a completely non-invasive procedure that only requires a patient to remain motionless, with the exception of respiratory motion, during the scan. Both serological testing and ^{31}P-MRS can be performed on a regular basis to monitor changes to the biochemistry of the liver in people chronically infected with HBV who are at high risk for developing HCC. In combination with high resolution imaging, the diagnosis of HCC can be improved, and by extension, treatment regimes can be improved which will increase long-term survival rates. Guidelines for the diagnosis of HCCs greater than 2cm are already well established using contrast enhanced CT and MRI, looking for patterns in the uptake and wash-out patterns of the contrast agent within suspected nodules. The biochemical characteristics of HCC growth detected with ^{31}P-MRS by 2D-CSI can be used with other novel imaging techniques such as magnetic resonance elastography to investigate nodules smaller than 2cm that don't show the same imaging features as larger tumours. Magnetic resonance elastography uses shear waves to measure the stiffness of tissues and can differentiate between normal, cirrhotic and cancerous tissues. Patients with cirrhosis are more likely to develop HCC and must be monitored more closely than patients only infected with HBV. By using magnetic resonance elastography to identify potential tumours, then using ^{31}P-MRS 2D-CSI to look for elevations in PME can improve diagnosis of HCC in cirrhotic livers. Rather than scanning the entire liver to detect a tumour, smaller voxels positioned specifically in regions of interest can be used to investigate possible HCC and rule out other benign conditions without the use of contrast agents.

^{31}P-MRS 2D-CSI could be used in conjunction with standard clinical imaging modalities in lieu of contrast-enhanced imaging if a patient's renal function is limited and the use of gadolinium is contraindicated. ^{31}P-MRS 2D-CSI could be performed over a region where a suspected nodule is identified. Rather than using 2D-CSI to image the entire liver, using smaller voxels to get detailed information about the biochemistry of a particular region could improve diagnostic specificity and provide surgeons with precise information about which regions are cancerous and which regions are healthy.

Similarly, ^{31}P-MRS 2D-CSI can be used to monitor a tumour's response to image guided therapies like transarterial chemoembolization, or radiofrequency and percutaneous ethanol ablations of small tumours. A return to normal PME resonance would indicate that the tumour has stopped growing and the treatment was successful.

These projects were successful in using the woodchuck as a model for longitudinal studies of HCC. Although the results are significant between the two groups (infected and uninfected), statistical significance requires that additional animals be included in both groups. Larger groups of woodchucks were not possible because of the cost per animal ($2000USD) and the amount of housing required per cohort. There were neither the funds, nor the space available to have more than two groups of 5 woodchucks per group, to be studied simultaneously.

Repeating the experiments with younger woodchucks, ones less than a year old, would provide more information about the earliest stages of HCC formation and about serological markers that would indicate whether a woodchuck develops a chronic infection or an acute infection. It would also be beneficial to have younger woodchucks when testing a novel immunotherapy because HCCs are less likely to already exist,

therefore the immunotherapy may have a greater likelihood of success. Those infected hepatocytes would be destroyed before they could develop into an HCC.

References

Abe, K., Kurata, T., and Shikata, T. (1988). Localization of woodchuck hepatitis virus in the liver. *Hepatology* **8** (1): 88-92.

Alter, H. (12-27-1999). Discovery of non-A, non-B hepatitis and identification of its etiology. *Am.J Med.* **107** (6B): 16S-20S.

Beasley, R. P., Hwang, L. Y., Lin, C. C., and Chien, C. S. (1981). Hepatocellular carcinoma and hepatitis B virus. A prospective study of 22 707 men in Taiwan. *Lancet* **2** (8256): 1129-1133.

Bell, J. D. and Bhakoo, K. K. (1998). Metabolic changes underlying 31P MR spectral alterations in human hepatic tumours. *NMR Biomed* **11** (7): 354-359.

Bell, J. D., Cox, I. J., Sargentoni, J., Peden, C. J., Menon, D. K., Foster, C. S., Watanapa, P., Iles, R. A., and Urenjak, J. (1993). A 31P and 1H-NMR investigation in vitro of normal and abnormal human liver. *Biochim Biophys Acta* **1225** (1): 71-77.

Bellezza, C. A., Concannon, P. W., Hornbuckle, W. E., Roth, L., and Tennant, B. (2002). Woodchucks as Laboratory Animals. In *Laboratory Animal Medicine* (Fox, J. G., Anderson, L. C., Loew, F. M., and Quimby, F. W., ed.), pp.309-328.

Beloueche-Babari, M., Jackson, L. E., Al-Saffar, N. M., Eccles, S. A., Raynaud, F. I., Workman, P., Leach, M. O., and Ronen, S. M. (2006). Identification of magnetic

resonance detectable metabolic changes associated with inhibition of phosphoinositide 3-kinase signaling in human breast cancer cells. *Mol.Cancer Ther.* **5** (1): 187-196.

Bezuidenhout, A. J. and Evans, H. E. (2005). *Anatomy of the Woodchuck (Marmota monax)* , American Society of Mammalogists, Lawrence, KS

Bhujwalla, Z. M., Aboagye, E. O., Gillies, R. J., Chacko, V. P., Mendola, C. E., and Backer, J. M. (1999). Nm23-transfected MDA-MB-435 human breast carcinoma cells form tumors with altered phospholipid metabolism and pH: a 31P nuclear magnetic resonance study in vivo and in vitro. *Magn Reson Med.* **41** (5): 897-903.

Billaud, J. N., Peterson, D., Schodel, F., Chen, A., Sallberg, M., Garduno, F., Goldstein, P., McDowell, W., Hughes, J., Jones, J., and Milich, D. (2005). Comparative antigenicity and immunogenicity of hepadnavirus core proteins. *J Virol* **79** (21): 13641-13655.

Bruix, J. and Sherman, M. (2005). Management of hepatocellular carcinoma. *Hepatology* **42** (5): 1208-1236.

Bruni, R., Conti, I., Villano, U., Giuseppetti, R., Palmieri, G., and Rapicetta, M. (2006). Lack of WHV integration nearby N-myc2 and in the downstream b3n and win loci in a considerable fraction of liver tumors with activated N-myc2 from naturally infected wild woodchucks. *Virology* **345** (1): 258-269.

Buendia, M. A. (1994). Hepatitis B viruses and liver cancer: the woodchuck model. *Viruses and cancer: fifty-first symposium of the society for general microbiology* 173-189.

Campbell, K. A., Wu, Y. P., Chacko, V. P., and Sitzmann, J. V. (1990). In vivo 31P NMR spectroscopic changes during liver regeneration. *J Surg Res* **49** (3): 244-247.

Chakeres, D. W. and Schmalbrock, P. (1992). *Fundamentals of Magnetic Resonance Imaging* , Williams and Wilkins, Baltimore, MD

Chang, M. H. (2000). Natural history of hepatitis B virus infection in children. *J Gastroenterol Hepatol.* **15 Suppl** E16-E19.

Chang, M. H., Chen, C. J., Lai, M. S., Hsu, H. M., Wu, T. C., Kong, M. S., Liang, D. C., Shau, W. Y., and Chen, D. S. (1997a). Universal hepatitis B vaccination in Taiwan and the incidence of hepatocellular carcinoma in children. Taiwan Childhood Hepatoma Study Group. *N.Engl.J.Med.* **336** (26): 1855-1859.

Chang, M. H., Chen, C. J., Lai, M. S., Hsu, H. M., Wu, T. C., Kong, M. S., Liang, D. C., Shau, W. Y., and Chen, D. S. (1997b). Universal hepatitis B vaccination in Taiwan and the incidence of hepatocellular carcinoma in children. Taiwan Childhood Hepatoma Study Group. *N.Engl.J Med.* **336** (26): 1855-1859.

Chavhan, G. B. (2007). *MRI Made Easy* , Anshan Ltd, Kent

Chu, W. C., Lam, W. W., Lee, K. H., Yeung, D. K., Sihoe, J., and Yeung, C. K. (2005). Phosphorus-31 MR spectroscopy in pediatric liver transplant recipients: a noninvasive assessment of graft status with correlation with liver function tests and liver biopsy. *AJR Am J Roentgenol* **184** (5): 1624-1629.

Coffin, C. S. and Michalak, T. I. (1999). Persistence of infectious hepadnavirus in the offspring of woodchuck mothers recovered from viral hepatitis. *J Clin Invest* **104** (2): 203-212.

Coffin, C. S., Pham, T. N., Mulrooney, P. M., Churchill, N. D., and Michalak, T. I. (2004). Persistence of isolated antibodies to woodchuck hepatitis virus core antigen is indicative of occult infection. *Hepatology* **40** (5): 1053-1061.

Corbin, I. R., Buist, R., Volotovskyy, V., Peeling, J., Zhang, M., and Minuk, G. Y. (2002). Regenerative activity and liver function following partial hepatectomy in the rat using (31)P-MR spectroscopy. *Hepatology* **36** (2): 345-353.

Corbin, I. R., Ryner, L. N., Singh, H., and Minuk, G. Y. (2004). Quantitative hepatic phosphorus-31 magnetic resonance spectroscopy in compensated and decompensated cirrhosis. *Am J Physiol Gastrointest Liver Physiol* **287** (2): G379-G384.

Cote, P. J., Toshkov, I., Bellezza, C., Ascenzi, M., Roneker, C., Ann, Graham L., Baldwin, B. H., Gaye, K., Nakamura, I., Korba, B. E., Tennant, B. C., and Gerin, J. L. (2000). Temporal pathogenesis of experimental neonatal woodchuck hepatitis virus infection: increased initial viral load and decreased severity of acute hepatitis during the development of chronic viral infection. *Hepatology* **32** (4 Pt 1): 807-817.

Cox, I. J., Bell, J. D., Peden, C. J., Iles, R. A., Foster, C. S., Watanapa, P., and Williamson, R. C. (1992a). In vivo and in vitro 31P magnetic resonance spectroscopy of focal hepatic malignancies. *NMR Biomed* **5** (3): 114-120.

Cox, I. J., Menon, D. K., Sargentoni, J., Bryant, D. J., Collins, A. G., Coutts, G. A., Iles, R. A., Bell, J. D., Benjamin, I. S., and Gilbey, S. (1992b). Phosphorus-31 magnetic resonance spectroscopy of the human liver using chemical shift imaging techniques. *J Hepatol* **14** (2-3): 265-275.

Cox, I. J., Sharif, A., Cobbold, J. F., Thomas, H. C., and Taylor-Robinson, S. D. (2006). Current and future applications of in vitro magnetic resonance spectroscopy in hepatobiliary disease. *World J Gastroenterol.* **12** (30): 4773-4783.

Dahmen, U., Li, J., Dirsch, O., Fiedler, M., Lu, M., Roggendorf, M., and Broelsch, C. E. (2002). A new model of hepatitis B virus reinfection: liver transplantation in the woodchuck. *Transplantation* **74** (3): 373-380.

Dezortova, M., Taimr, P., Skoch, A., Spicak, J., and Hajek, M. (2005)Etiology and functional status of liver cirrhosis by 31P MR spectroscopy. *World J Gastroenterol.* **11**(44): 6926-6931.

El-Serag, H. B. and Mason, A. C. (1999). Rising incidence of hepatocellular carcinoma in the United States. *N.Engl.J Med.* **340** (10): 745-750.

Eliyahu, G., Kreizman, T., and Degani, H. (2007). Phosphocholine as a biomarker of breast cancer: molecular and biochemical studies. *Int.J Cancer* **120** (8): 1721-1730.

Fabregat, I., Roncero, C., and Fernandez, M. (2007). Survival and apoptosis: a dysregulated balance in liver cancer. *Liver Int* **27** (2): 155-162.

Farghali, H., Rilo, H., Zhang, W., Simplaceanu, V., Gavaler, J. S., Ho, C., and van Thiel, D. H. (1994). Liver regeneration after partial hepatectomy in the rat. Sequential events monitored by 31P-nuclear magnetic resonance spectroscopy and biochemical studies. *Lab Invest* **70** (3): 418-425.

Ferron, J. (1996) How does the woodchuck (Marmota monax) cope with harsh winter conditions? *J. Mammal.***77** (2): 412-416.

Francis, I. R., Chenevert, T. L., Gubin, B., Collomb, L., Ensminger, W., Walker-Andrews, S., and Glazer, G. M. (1991). Malignant hepatic tumors: P-31 MR

spectroscopy with one-dimensional chemical shift imaging. *Radiology* **180** (2): 341-344.

Frank, I., Budde, C., Fiedler, M., Dahmen, U., Viazov, S., Lu, M., Dittmer, U., and Roggendorf, M. (2007). Acute resolving woodchuck hepatitis virus (WHV) infection is associated with a strong cytotoxic T-lymphocyte response to a single WHV core peptide. *J Virol* **81** (13): 7156-7163.

Ganem, D. and Schneider, R. J. (2001). Hepadnaviridae: The viruses and their replication. In *Fundamental Virology* (Knipe, D. M. and Howley, P. M., ed.), pp.1285-1331. Lippincott William and Wilkins, Philadelphia.

Garcia-Navarro, R., Blanco-Urgoiti, B., Berraondo, P., Sanchez, de la Rosa, Vales, A., Hervas-Stubbs, S., Lasarte, J. J., Borras, F., Ruiz, J., and Prieto, J. (2001). Protection against woodchuck hepatitis virus (WHV) infection by gene gun coimmunization with WHV core and interleukin-12. *J Virol* **75** (19): 9068-9076.

Glazer, G. M., Smith, S. R., Chenevert, T. L., Martin, P. A., Stevens, A. N., and Edwards, R. H. (1989). Image localized 31P magnetic resonance spectroscopy of the human liver. *NMR Biomed* **1** (4): 184-189.

Glunde, K., Jacobs, M. A., and Bhujwalla, Z. M. (2006a). Choline metabolism in cancer: implications for diagnosis and therapy. *Expert.Rev.Mol.Diagn.* **6** (6): 821-829.

Glunde, K. and Serkova, N. J. (2006b). Therapeutic targets and biomarkers identified in cancer choline phospholipid metabolism. *Pharmacogenomics.* **7** (7): 1109-1123.

Griffiths, J. R., McSheehy, P. M., Robinson, S. P., Troy, H., Chung, Y. L., Leek, R. D., Williams, K. J., Stratford, I. J., Harris, A. L., and Stubbs, M. (2002). Metabolic changes detected by in vivo magnetic resonance studies of HEPA-1 wild-type tumors and tumors deficient in hypoxia-inducible factor-1beta (HIF-1beta): evidence of an anabolic role for the HIF-1 pathway. *Cancer Res.* **62** (3): 688-695.

Hann, H. W., Lee, J., Bussard, A., Liu, C., Jin, Y. R., Guha, K., Clayton, M. M., Ardlie, K., Pellini, M. J., and Feitelson, M. A. (2004). Preneoplastic markers of hepatitis B virus-associated hepatocellular carcinoma. *Cancer Res* **64** (20): 7329-7335.

Hayes, C., Edelstein, W. A., Schenck, J. F., Mueller, O. M., and Eash, M. (1985). An efficient, highly homogeneous radiofrequency coil for whole-body NMR imaging at 1.5T. *Journal of Magnetic Resonance* **63:** 622-628.

Hornbuckle, W. E., Graham, E. S., Roth, L., Baldwin, B. H., Wickenden, C., and Tennant, B. C. (1985). Laboratory assessment of hepatic injury in the woodchuck (Marmota monax). *Lab Anim Sci* **35** (4): 376-381.

Jacob, J. R., Sterczer, A., Toshkov, I. A., Yeager, A. E., Korba, B. E., Cote, P. J., Buendia, M. A., Gerin, J. L., and Tennant, B. C. (2004). Integration of

woodchuck hepatitis and N-myc rearrangement determine size and histologic grade of hepatic tumors. *Hepatology* **39** (4): 1008-1016.

Jalan, R., Sargentoni, J., Coutts, G.A., Bell, J.D., Rolles, K., Burroughs, A.K., and Taylor, R.S. (1996)Hepatic phosphorus-31 magnetic resonance spectroscopy in primary biliary cirrhosis and its relation to prognostic models. *Gut* **39**(1): 141-146.

Kaplan, O., Kushnir, T., Askenazy, N., Knubovets, T., and Navon, G. (1997). Role of nuclear magnetic resonance spectroscopy (MRS) in cancer diagnosis and treatment: 31P, 23Na, and 1H MRS studies of three models of pancreatic cancer. *Cancer Res* **57** (8): 1452-1459.

Khan, S. A., Cox, I. J., Hamilton, G., Thomas, H. C., and Taylor-Robinson, S. D. (2005). In vivo and in vitro nuclear magnetic resonance spectroscopy as a tool for investigating hepatobiliary disease: a review of H and P MRS applications. *Liver Int* **25** (2): 273-281.

Kiyono, K., Shibata, A., Sone, S., Watanabe, T., Oguchi, M., Shikama, N., Ichijo, T., Kiyosawa, K., and Sodeyama, T. (1998). Relationship of 31P MR spectroscopy to the histopathological grading of chronic hepatitis and response to therapy. *Acta Radiol* **39** (3): 309-314.

Kooby, D. A., Zakian, K. L., Challa, S. N., Matei, C., Petrowsky, H., Yoo, H. H., Koutcher, J. A., and Fong, Y. (2000). Use of phosphorous-31 nuclear magnetic

resonance spectroscopy to determine safe timing of chemotherapy after hepatic resection. *Cancer Res* **60** (14): 3800-3806.

Korba, B. E., Cote, P., Hornbuckle, W., Tennant, B. C., and Gerin, J. L. (2000). Treatment of chronic woodchuck hepatitis virus infection in the Eastern woodchuck (Marmota monax) with nucleoside analogues is predictive of therapy for chronic hepatitis B virus infection in humans. *Hepatology* **31** (5): 1165-1175.

Le Belle, J. E., Harris, N. G., Williams, S. R., and Bhakoo, K. K. (2002). A comparison of cell and tissue extraction techniques using high-resolution 1H-NMR spectroscopy. *NMR Biomed* **15** (1): 37-44.

Lee, W. M. (1997). Hepatitis B virus infection. *N.Engl.J Med.* **337** (24): 1733-1745.

Li, Y., Hacker, H. J., Kopp-Schneider, A., Bannasch, P., and Protzer, U. (2002). Woodchuck hepatitis virus replication and antigen expression gradually decrease in preneoplastic hepatocellular lineages. *J Hepatol* **37** (4): 478-485.

Lim, A. K., Patel, N., Hamilton, G., Hajnal, J. V., Goldin, R. D., and Taylor-Robinson, S. D. (2003). The relationship of in vivo 31P MR spectroscopy to histology in chronic hepatitis C. *Hepatology* **37** (4): 788-794.

Lim, A. K., Patel, N., Hamilton, G., Mylvahan, K., Kuo, Y. T., Goldin, R. D., and Taylor-Robinson, S. D. (2007). 31P MR spectroscopy in assessment of response

to antiviral therapy for hepatitis C virus-related liver disease. *AJR Am.J Roentgenol.* **189** (4): 819-823.

Lisi, D., Kondili, L. A., Ramieri, M. T., Giuseppetti, R., Bruni, R., Della, Rocca C., De, Santis A., and Rapicetta, M. (2003). Ultrasonography in the study of hepatocellular carcinoma in woodchucks chronically infected with WHV. *Lab Anim* **37** (3): 233-240.

Liu, C. J., Kao, J. H., and Chen, D. S. (2005). Therapeutic implications of hepatitis B virus genotypes. *Liver Int.* **25** (6): 1097-1107.

Lu, M., Hilken, G., Kruppenbacher, J., Kemper, T., Schirmbeck, R., Reimann, J., and Roggendorf, M. (1999). Immunization of woodchucks with plasmids expressing woodchuck hepatitis virus (WHV) core antigen and surface antigen suppresses WHV infection. *J Virol* **73** (1): 281-289.

Lu, M., Isogawa, M., Xu, Y., and Hilken, G. (2005). Immunization with the gene expressing woodchuck hepatitis virus nucleocapsid protein fused to cytotoxic-T-lymphocyte-associated antigen 4 leads to enhanced specific immune responses in mice and woodchucks. *J Virol* **79** (10): 6368-6376.

Lu, M. and Roggendorf, M. (2001). Evaluation of new approaches to prophylactic and therapeutic vaccinations against hepatitis B viruses in the woodchuck model. *Intervirology* **44** (2-3): 124-131.

Macomber, R. S. (1988). *NMR Spectroscopy Basic Principles and Applications* , Harcourt Brace Jovanovich College Outline Series, San Diego

Malloy, C. R., Cunningham, C. C., and Radda, G. K. (1986). The metabolic state of the rat liver in vivo measured by 31P-NMR spectroscopy. *Biochim.Biophys.Acta* **885** (1): 1-11.

Mann, D. V., Lam, W. W., Hjelm, N. M., So, N. M., Yeung, D. K., Metreweli, C., and Lau, W. Y. (2001). Human liver regeneration: hepatic energy economy is less efficient when the organ is diseased. *Hepatology* **34** (3): 557-565.

McKenzie, E. J., Jackson, M., Sun, J., Volotovskyy, V., and Gruwel, M. L. (2005). Monitoring the development of hepatocellular carcinoma in woodchucks using 31P-MRS. *Magn Reson Mater Phys* **18** (4): 201-205.

McKenzie, E. J., Jackson, M., Turner, A., Gregorash, L., and Harapiak, L. (2006). Chronic care and monitoring of woodchucks (Marmota monax) during repeated magnetic resonance imaging of the liver. *J Am Assoc Lab Anim Sci* **45** (2): 26-30.

McMahon, B. J., Alward, W. L., Hall, D. B., Heyward, W. L., Bender, T. R., Francis, D. P., and Maynard, J. E. (1985). Acute hepatitis B virus infection: relation of age to the clinical expression of disease and subsequent development of the carrier state. *J Infect.Dis* **151** (4): 599-603.

McRobbie, D. W., Moore, E. A., Graves, M. J., and Prince, M. R. (2003). *MRI from picture to proton* , Cambridge University Press, Cambridge UK

Menne, S. and Cote, P. J. (2007). The woodchuck as an animal model for pathogenesis and therapy of chronic hepatitis B virus infection. *World J Gastroenterol* **13** (1): 104-124.

Menne, S., Maschke, J., Tolle, T. K., Lu, M., and Roggendorf, M. (1997). Characterization of T-cell response to woodchuck hepatitis virus core protein and protection of woodchucks from infection by immunization with peptides containing a T-cell epitope. *J Virol* **71** (1): 65-74.

Menne, S., Roneker, C. A., Tennant, B. C., Korba, B. E., Gerin, J. L., and Cote, P. J. (2002). Immunogenic effects of woodchuck hepatitis virus surface antigen vaccine in combination with antiviral therapy: breaking of humoral and cellular immune tolerance in chronic woodchuck hepatitis virus infection. *Intervirology* **45** (4-6): 237-250.

Menon, D. K., Sargentoni, J., Taylor-Robinson, S. D., Bell, J. D., Cox, I. J., Bryant, D. J., Coutts, G. A., Rolles, K., Burroughs, A. K., and Morgan, M. Y. (1995). Effect of functional grade and etiology on in vivo hepatic phosphorus-31 magnetic resonance spectroscopy in cirrhosis: biochemical basis of spectral appearances. *Hepatology* **21** (2): 417-427.

Meyerhoff, D. J., Karczmar, G. S., Valone, F., Venook, A., Matson, G. B., and Weiner, M. W. (1992). Hepatic cancers and their response to chemoembolization therapy. Quantitative image-guided 31P magnetic resonance spectroscopy. *Invest Radiol* **27** (6): 456-464.

Michalak, T. I. (1998). The Woodchuck Animal Model of Hepatitis B. *Viral Hepatitis Reviews* **4** (3): 139-165.

Michalak, T. I. (2000). Occult persistence and lymphotropism of hepadnaviral infection: insights from the woodchuck viral hepatitis model. *Immunol Rev* **174** (Apr): 98-111.

Morse, D. L., Raghunand, N., Sadarangani, P., Murthi, S., Job, C., Day, S., Howison, C., and Gillies, R. J. (2007). Response of choline metabolites to docetaxel therapy is quantified in vivo by localized (31)P MRS of human breast cancer xenografts and in vitro by high-resolution (31)P NMR spectroscopy of cell extracts. *Magn Reson.Med.* **58** (2): 270-280.

Murphy, E.J., Brindle, K.M., Rorison, C.J., Dixon, R.M., Rajagopalan, B., and Radda, G.K. (1992)Changes in phosphatidylethanolamine metabolism in regenerating rat liver as measured by 31P-NMR. *Biochim Biophys Acta* **1135**(1): 27-34.

Nada, T., Moriyasu, F., Kono, Y., Suginoshita, Y., Matsumura, T., Kobayashi, K., Nakamura, T., and Chiba, T. (1997). Sonographic detection of tumor blood flow

using a new contrast agent in woodchuck hepatomas. *J Ultrasound Med* **16** (7): 485-491.

Ni, Y. H., Chang, M. H., Huang, L. M., Chen, H. L., Hsu, H. Y., Chiu, T. Y., Tsai, K. S., and Chen, D. S. (2001). Hepatitis B virus infection in children and adolescents in a hyperendemic area: 15 years after mass hepatitis B vaccination. *Ann Intern.Med.* **135** (9): 796-800.

Noseworthy, M. D., Janzen, E. G., Towner, R. A., and Yamashiro, S. (1997). In vivo study of halothane hepatotoxicity in the rat using magnetic resonance imaging and 31P spectroscopy. *J Biochem.Biophys.Methods* **34** (2): 107-122.

Noyes, D. H. and Siekierski, D. M. (1975). Anesthesia of marmots with sodium pentobarbital, ketamine hydrochloride, and a combination of droperidol and fentanyl. *Laboratory Animal Science* **25** (5): 557-562.

Ohtomo, K., Shiga, J., Sasaki, Y., and Itai, Y. (1991). [Iron oxide-enhanced MR imaging of hepatocellular carcinoma of woodchuck]. *Nippon Igaku Hoshasen Gakkai Zasshi* **51** (4): 433-435.

Payne, G. S., Troy, H., Vaidya, S. J., Griffiths, J. R., Leach, M. O., and Chung, Y. L. (2006). Evaluation of 31P high-resolution magic angle spinning of intact tissue samples. *NMR Biomed.* **19** (5): 593-598.

Peek, S. F., Cote, P. J., Jacob, J. R., Toshkov, I. A., Hornbuckle, W. E., Baldwin, B. H., Wells, F. V., Chu, C. K., Gerin, J. L., Tennant, B. C., and Korba, B. E. (2001). Antiviral activity of clevudine [L-FMAU, (1-(2-fluoro-5-methyl-beta, L-arabinofuranosyl) uracil)] against woodchuck hepatitis virus replication and gene expression in chronically infected woodchucks (Marmota monax). *Hepatology* **33** (1): 254-266.

Pisani, P., Parkin, D. M., Bray, F., and Ferlay, J. (1999). Estimates of the worldwide mortality from 25 cancers in 1990. *Int.J Cancer* **83** (1): 18-29.

Podo, F. (1999). Tumour phospholipid metabolism. *NMR Biomed* **12** (7): 413-439.

Popper, H., Roth, L., Purcell, R. H., Tennant, B., and Gerin, J. (1987). Hepatocarcinogenicity of the woodchuck hepatitis virus. *Proc Natl Acad Sci U S A* **84** : 866-870.

Putzer, B. M., Stiewe, T., Rodicker, F., Schildgen, O., Ruhm, S., Dirsch, O., Fiedler, M., Damen, U., Tennant, B., Scherer, C., Graham, F. L., and Roggendorf, M. (2001). Large nontransplanted hepatocellular carcinoma in woodchucks: treatment with adenovirus-mediated delivery of interleukin 12/B7.1 genes. *J Natl Cancer Inst* **93** (6): 472-479.

Radaeva, S., Li, Y., Hacker, H. J., Burger, V., Kopp-Schneider, A., and Bannasch, P. (2000). Hepadnaviral hepatocarcinogenesis: in situ visualization of viral antigens,

cytoplasmic compartmentation, enzymic patterns, and cellular proliferation in preneoplastic hepatocellular lineages in woodchucks. *J Hepatol* **33** (4): 580-600.

Reimer, P., Weissleder, R., Brady, T. J., Yeager, A. E., Baldwin, B. H., Tennant, B. C., and Wittenberg, J. (1991). Experimental hepatocellular carcinoma: MR receptor imaging. *Radiology* **180** (3): 641-645.

Roos, S., Fuchs, K., and Roggendorf, M. (1989). Protection of woodchucks from infection with woodchuck hepatitis virus by immunization with recombinant core protein. *J Gen.Virol* **70 (Pt 8)** : 2087-2095.

Salem, N., MacLennan, G. T., Kuang, Y., Anderson, P. W., Schomisch, S. J., Tochkov, I. A., Tennant, B. C., and Lee, Z. (2007). Quantitative evaluation of 2-deoxy-2[F-18]fluoro-D-glucose-positron emission tomography imaging on the woodchuck model of hepatocellular carcinoma with histological correlation. *Mol.Imaging Biol.* **9** (3): 135-143.

Sank, V. J., Chen, C. N., and Hoult, D. I. (1986). A quadrature coil for the adult human head. *Journal of Magnetic Resonance* **69** : 236-242.

Scheiflinger, F., Falkner, F.G., and Dorner, F. (1996). Evaluation of the thymidine kinase (TK) locus as an insertion site in the highly attenuated vaccinia MVA strain. *Archives of Virology* **141**: 663-669.

Schild, H. H. (1990). *MRI Made Easy....Well Almost* , Berlex Laboratories, Berlin

Schiller, J. and Arnold, K. (2002). Application of high resolution 31P NMR spectroscopy to the characterization of the phospholipid composition of tissues and body fluids - a methodological review. *Med Sci Monit* **8** (11): MT205-MT222.

Schlemmer, H. P., Sawatzki, T., Sammet, S., Dornacher, I., Bachert, P., van Kaick, G., Waldherr, R., and Seitz, H. K. (2005). Hepatic phospholipids in alcoholic liver disease assessed by proton-decoupled 31P magnetic resonance spectroscopy. *J Hepatol* **42** (5): 752-759.

Schodel, F., Neckermann, G., Peterson, D., Fuchs, K., Fuller, S., Will, H., and Roggendorf, M. (1993). Immunization with recombinant woodchuck hepatitis virus nucleocapsid antigen or hepatitis B virus nucleocapsid antigen protects woodchucks from woodchuck hepatitis virus infection. *Vaccine* **11** (6): 624-628.

Skoch, A., Jiru, F., and Bunke, J. (2008). Spectroscopic imaging: Basic principles. *Eur J Radiol.*

Solga, S. F., Horska, A., Clark, J. M., and Diehl, A. M. (2005). Hepatic 31P magnetic resonance spectroscopy: a hepatologist's user guide. *Liver Int* **25** (3): 490-500.

Suzue, K, and Young, R.A. Adjuvant-free HSP70 fusion protein system elicits humoral and cellular responses to HIV-1 p24. *Journal of Immunology* **156**(2): 873-879.

Suto, R. and Srivastava, P. K. (1996). Heat shock protein-peptide complexes: pan-valent vaccines against cancers and infectious diseases. In *Tumor immunology: Immunotherapy and cancer vaccines* (Dalgleish, A. G. and Browning, M. J., ed.), pp.287-299. Cambridge University Press, New York, N.Y.

Tassopoulos, N. C., Papaevangelou, G. J., Sjogren, M. H., Roumeliotou-Karayannis, A., Gerin, J. L., and Purcell, R. H. (1987). Natural history of acute hepatitis B surface antigen-positive hepatitis in Greek adults. *Gastroenterology* **92** (6): 1844-1850.

Taylor-Robinson, S. D., Sargentoni, J., Bell, J. D., Saeed, N., Changani, K. K., Davidson, B. R., Rolles, K., Burroughs, A. K., Hodgson, H. J., Foster, C. S., and Cox, I. J. (1997). In vivo and in vitro hepatic 31P magnetic resonance spectroscopy and electron microscopy of the cirrhotic liver. *Liver* **17** (4): 198-209.

Taylor-Robinson, S. D., Sargentoni, J., Bell, J. D., Thomas, E. L., Marcus, C. D., Changani, K. K., Saeed, N., Hodgson, H. J., Davidson, B. R., Burroughs, A. K., Rolles, K., Foster, C. S., and Cox, I. J. (1998). In vivo and in vitro hepatic phosphorus-31 magnetic resonance spectroscopy and electron microscopy in chronic ductopenic rejection of human liver allografts. *Gut* **42** (5): 735-743.

Tennant, B. C. (1999). Woodchuck model of hepatitis B virus infection. In *Handbook of animal models of infection: Experimental models in antimicrobial chemotherapy* (Zak, O. and Sande, M. A., ed.), pp.1033-1039. Academic Press, London, U.K.

Tennant, B. C. (2001). Animal models of hepadnavirus-associated hepatocellular carcinoma. *Clin Liver Dis* **5** (1): 43-68.

Tennant, B. C., Toshkov, I. A., Peek, S. F., Jacob, J. R., Menne, S., Hornbuckle, W. E., Schinazi, R. D., Korba, B. E., Cote, P. J., and Gerin, J. L. (2004). Hepatocellular carcinoma in the woodchuck model of hepatitis B virus infection. *Gastroenterology* **127** (5 Suppl 1): S283-S293.

Thomas, C. P., Dixon, R. M., Tian, M., Butler, S. A., Counsell, C. J., Bradley, J. K., Adams, G. E., and Radda, G. K. (1994). Phosphorus metabolism during growth of lymphoma in mouse liver: a comparison of 31P magnetic resonance spectroscopy in vivo and in vitro. *Br.J Cancer* **69** (4): 633-640.

Tomanek, B., Volotovskyy, V., Gruwel, M. L. H., McKenzie, E., and King, S. B. (2005). Double-Frequency Birdcage Volume Coils for 4.7T and 7T. *Concepts in Magnetic Resonance Part B, Magnetic Resonanace Engineering* **26B** (1): 16-22.

Toshkov, I., Hacker, H. J., Roggendorf, M., and Bannasch, P. (1990). Phenotypic patterns of preneoplastic and neoplastic hepatic lesions in woodchucks infected with woodchuck hepatitis virus. *J Cancer Res Clin Oncol* **116** (6): 581-590.

Vejchapipat, P., Eaton, S., Fukumoto, K., Parkes, H. G., Spitz, L., and Pierro, A. (2002). Hepatic glutamine metabolism during endotoxemia in neonatal rats. *Nutrition* **18** (4): 293-297.

Wang, B., Gao, Z. Q., and Yan, X. (2005). Correlative study of angiogenesis and dynamic contrast-enhanced magnetic resonance imaging features of hepatocellular carcinoma. *Acta Radiol* **46** (4): 353-358.

Wang, Y., Menne, S., Baldwin, B. H., Tennant, B. C., Gerin, J. L., and Cote, P. J. (2004). Kinetics of viremia and acute liver injury in relation to outcome of neonatal woodchuck hepatitis virus infection. *J Med Virol* **72** (3): 406-415.

Wang, Y., Menne, S., Jacob, J. R., Tennant, B. C., Gerin, J. L., and Cote, P. J. (2003). Role of type 1 versus type 2 immune responses in liver during the onset of chronic woodchuck hepatitis virus infection. *Hepatology* **37** (4): 771-780.

Willatt, J. M., Hussain, H. K., Adusumilli, S., and Marrero, J. A. (2008). MR Imaging of hepatocellular carcinoma in the cirrhotic liver: challenges and controversies. *Radiology* **247** (2): 311-330.

Wong, D. K., Yuen, M. F., Poon, R. T., Yuen, J. C., Fung, J., and Lai, C. L. (2006). Quantification of hepatitis B virus covalently closed circular DNA in patients with hepatocellular carcinoma. *J Hepatol* **45** (4): 553-559.

Xu, C., Yamamoto, T., Zhou, T., Aldrich, C. E., Frank, K., Cullen, J. M., Jilbert, A. R., and Mason, W. S. (2006). The liver of woodchucks chronically infected with the woodchuck hepatitis virus contains foci of virus core antigen-negative hepatocytes with both altered and normal morphology. *Virology* **359** (2): 283-294.

Young, R. A. and Sims, E. A. (1979). The woodchuck, Marmota monax, as a laboratory animal. *Lab Anim Sci* **29** (6): 770-780.

Zakian, K. L., Koutcher, J. A., Malhotra, S., Thaler, H., Jarnagin, W., Schwartz, L., and Fong, Y. (2005). Liver regeneration in humans is characterized by significant changes in cellular phosphorus metabolism: assessment using proton-decoupled 31P-magnetic resonance spectroscopic imaging. *Magn Reson Med* **54** (2): 264-271.

Zhang, Z., Tian, Y., Li, L., Fiedler, M., Schmid, E., Roggendorf, M., Xu, Y., Lu, M., and Yang, D. (2006). A conserved linear B-cell epitope at the N-terminal region of woodchuck hepatitis virus core protein (WHcAg). *J Virol Methods* **135** (1): 17-25.